PEOPLE`S DEMOCRATIC REPUBLIC OF ALGERIA

MINISTRY OF HIGHER EDUCATION AND SCIENTIFIC RESEARCH

20 AUGUST 1955 UNIVERSITY OF SKIKDA

FACULTY OF SCIENCES

DEPARTMENT OF PHYSICS

THESIS

PRESENTED FOR THE PURPOSE OF OBTAINING THE DOCTORATE DEGREE IN SCIENCES

SPECIALTY

ENERGETICS PHYSICS

THEME:

STUDY OF HEAT TRANSFER IN A MULTILAYER WALL UNDERGOING PHASE CHANGE BY SOLIDIFICATION. APPLICATION TO THERMAL STORAGE.

PRESENTED BY:

OUALID ARFI

DIRECTOR: PROF. EL HACENE MEZAACHE (UNIVERSITY OF SKIKDA)

Thesis defense held on: 28/02/2024

THESIS COMMITTEE:

Dr: Aicha Bouhezza	M.C.A	University of Skikda	Chairperson
Prof: El Hacene Mezaache	Professor	University of Skikda	Director
Prof: Nadir Attaf	Professor	University of Constantine 1	Examiner
Prof: Mohamed Teggar	Professor	University of Laghouat	Examiner
Dr: Abdelghani Laouer	M.C.A	University of Jijel	Invited

Acknowledgements

First and foremost, I would like to express the deepest appreciation to my PhD thesis supervisor, Prof. EL HACENE MEZAACHE, for his invaluable advice, continuous support, and patience during my PhD study.

I would like to thanks Prof. Luisa F. Cabeza and Dr. Gabriel Zsembinszki, for all what they have done for me since I was enrolled in GREA research group.

I would like to express my gratitude to the Algerian ministry of higher education and scientific research/D-GRSDT for the funding during my research fellowship at University of Lleida.

I would like to extend a special mention to both my friends and colleagues at the University of Skikda, as well as at the Research Center of Semi-Conductor Technology for Energy (CRTSE). Especially to those who are more than colleagues.

Last but not least, I extend my heartfelt gratitude to my family for their unwavering encouragement and support. Their sacrifices are beyond words, and I am profoundly thankful for their dedication. The successful completion of my doctoral degree would not have been possible without their steadfast devotion and motivation. I wholeheartedly dedicate my dissertation to my family.

Dedication

“To my dearest father, who instilled in me the values of hard work and perseverance. Your memory continues to be my guiding light in this journey.

To my beloved mother, the pillar of strength in our family, who has unwaveringly supported and believed in me. Your love and sacrifices have been my greatest inspiration.

To my dear nephew, 'Nounou,' whose brief presence left a lasting impact on our lives. Your innocence and joy brought light to our family, and you will forever hold a special place in our hearts.

To my brothers, sisters and my entire family, who have stood by me through the challenges and triumphs. Your collective love and encouragement have been the foundation of my achievements.

This thesis is a tribute to all of you. Your memory and support have been the driving force behind my dedication and perseverance. I hope to make you all proud. In loving memory and deep gratitude.”

Oualid

Abstract

The goal of this thesis is to carry out a detailed study in order to overcome situations where the PCM double layer building envelope is not efficient, taking into account numerous melting temperatures and latent heats for single PCM layer configurations, as well as several combinations of melting temperatures (θ_{m1}, θ_{m2}), and latent heat (Ste_1, Ste_2) for double PCM layer building envelope during charging cycle in summer by solidification. Furthermore, this work aims to numerically investigate the performance of mobile PCM layers in a building wall for different seasons (summer and winter). This study takes into account numerous combinations of PCM melting temperature (θ_{m1}, θ_{m2}), based on examining numerous parameters, through studying the processes of phase change solidification/fusion, by exhibiting the kinetics of phase change fronts, the duration of charging /discharging cycles, as well as the operating PCM fraction and the average heat flux gained/lost over one cycle. The finite volume approach is used to solve numerically the mathematical model that governs the configuration. the study examined the performance of a building envelope incorporating a single PCM layer during various seasons, including summer and winter, indicate that the cases where the melting temperatures are situated within the range of outside temperature fluctuations and are in proximity to the indoor comfort temperature (depending on the season) result in optimal yearly performance of the PCM wall. This optimal performance is manifested in the smoothing of instantaneous heat flux and the reduction of its amplitude. Conversely, instances where melting temperatures are aligned with the farthest temperature values from the outside fluctuations (one near the maximum temperature in summer and the other close to the minimum temperature in winter) contribute to minimizing energy consumption by the HVAC system. While, the obtained results among the part that focuses only on examining the double PCM layers wall during charging cycle show that, the melting temperature of outer PCM layer is the main controlling parameter of the heat lost amount, where increasing θ_{m1} increases the heat lost, such as, combination (θ_{m1}=0.7, θ_{m2}=0.5) releases the ratio of 18% as extra heat more than the reference case (without PCM). While, for the combination (θ_{m1}=0.5, θ_{m2}=0.7) it achieves 13%. Moreover, it is better for the latent heat of the inner layer to be lower than the latent heat of the outer layer, which leads to a strong solidification process, then, a high amount of released heat could be achieved. As well as, combination (Ste_1=0.1, Ste_2=0.01) the extra heat released ratio was 15%, while for (Ste_1=0.1,

Ste$_2$=0.5) it was 8%. However, the results depicts the dynamic double PCM layers configuration, showed that combinations $(\theta_{m1} = 2.4, \theta_{m2} = 2.4)$ and $(\theta_{m1} = 1, \theta_{m2} = 1)$ are the best in terms of smoothing the amplitude of heat flux fluctuation throughout their appropriate season, summer and winter, with ratios of 13% and 15%, respectively. Furthermore, using mobile layers design, the combination $((\theta_{m1} = 1, \theta_{m2} = 2.4)$ for summer, $(\theta_{m1} = 2.4, \theta_{m2} = 1)$ for winter) has the best annual performance, where it provides the highest annual average operating PCM fraction (35%), with the longest yearly average length of discharging. Combinations with melting temperatures close to the outside fluctuating temperature and close to the inside comfort temperature (according to the season), ensure the best annual performance of the building envelope, in terms of smoothing the instantaneous heat flux and diminishing the fluctuating amplitude, which reduces the required power of heating, ventilation, and air conditioning (HVAC) system (it could reach 6.5%). However, combinations with melting temperatures include in the field of the outside temperature fluctuating, one close to the maximum temperature in summer and the other one close to the minimum temperature in winter; ensure minimizing the energy consumed by the HVAC system by around 12%.

Keywords: Phase change material; double PCM layer; mobile layers; charging/discharging cycles; enthalpy method; building envelope.

Résumé

L'objectif de cette thèse est d'effectuer une étude détaillée afin de surmonter les situations où l'enveloppe d'un bâtiment à double couches PCM n'est pas efficace, en tenant compte de nombreuses températures de fusion et de chaleurs latentes pour les configurations à couche PCM simple, ainsi que de plusieurs combinaisons de températures de fusion (θ_{m1}, θ_{m2}) et de chaleur latente (Ste_1, Ste_2) pour l'enveloppe du bâtiment à double couches PCM, pendant le cycle de charge en été par solidification. De plus, ce travail vise également à étudier numériquement comment les couches PCM mobiles fonctionnent dans un mur de bâtiment pendant différentes saisons (été et hiver). Cette étude prend en considération de nombreuses combinaisons de températures de fusion du PCM (θ_{m1}, θ_{m2}). Elle examine de nombreux paramètres, étudie les processus de changement de phase solidification/fusion, analyse la cinétique des fronts de changement de phase, mesure la durée des cycles de charge/décharge, évalue la fraction de PCM en fonctionnement, ainsi que le flux de chaleur moyen gagné ou perdu au cours d'un cycle. L'approche des volumes finis est utilisée pour résoudre numériquement le modèle mathématique qui régit la configuration. L'étude a examiné les performances d'une enveloppe de bâtiment incorporant une seule couche de PCM pendant différentes saisons, notamment l'été et l'hiver, indiquant que les cas où les températures de fusion sont situées dans la plage des fluctuations de température extérieure et sont proches de la température de confort intérieur (selon la saison) donnent des performances annuelles optimales du mur PCM. Cette performance optimale se manifeste par l'atténuation du flux de chaleur instantané et la réduction de son amplitude. En revanche, les cas où les températures de fusion sont alignées sur les valeurs de température les plus éloignées des fluctuations extérieures (l'une proche de la température maximale en été et l'autre proche de la température minimale en hiver) contribuent à minimiser la consommation d'énergie du système HVAC. Cependant, les résultats obtenus pour la partie qui se concentre uniquement sur l'examen de la paroi à double couche PCM pendant le cycle de charge montrent que la température de fusion de la couche externe de PCM est le principal paramètre de contrôle de la quantité de chaleur perdue, où l'augmentation de θ_{m1} augmente la chaleur perdue, par exemple, la combinaison (θ_{m1}=0.7, θ_{m2}=0.5) libère un ratio de 18% de chaleur supplémentaire par rapport au cas de référence (sans PCM). En revanche, pour la combinaison (θ_{m1}=0.5, θ_{m2}=0.7), elle atteint 13%. De plus, il est préférable que la chaleur latente de la couche intérieure soit inférieure à la chaleur latente de la couche extérieure, ce qui entraîne un processus de solidification solide,

puis une grande quantité de chaleur libérée pourrait être obtenue. Ainsi, la combinaison (Ste_1=0.1, Ste_2=0.01) a libéré chaleur supplémentaire de 15%, tandis que pour (Ste_1=0.1, Ste_2=0.5), il était de 8%. Cependant, les résultats montrent que la configuration dynamique à double couches PCM, les combinaisons $(\theta_{m1} = 2.4, \theta_{m2} = 2.4)$ et $(\theta_{m1} = 1, \theta_{m2} = 1)$ sont les meilleures en termes d'atténuation de l'amplitude des fluctuations du flux de chaleur tout au long de leur saison appropriée, été et hiver, avec des fractions de 13% et 15% respectivement. De plus, en utilisant la conception de couches mobiles, la combinaison ($(\theta_{m1} = 1, \theta_{m2} = 2.4)$ pour l'été, $(\theta_{m1} = 2.4, \theta_{m2} = 1)$ pour l'hiver) présente les meilleures performances annuelles, avec la plus haute fraction de PCM en fonctionnement en moyenne annuelle (35%), avec la plus longue période moyenne annuelle de décharge. Les combinaisons avec des températures de fusion proches de la température extérieure fluctuante et proches de la température de confort intérieur (selon la saison) assurent la meilleure performance annuelle de l'enveloppe du bâtiment, en termes d'atténuation du flux de chaleur instantané et de réduction de l'amplitude des fluctuations, ce qui réduit la puissance requise du système de chauffage, de ventilation et de climatisation (HVAC) (elle peut atteindre 6,5%). Cependant, les combinaisons avec des températures de fusion incluses dans le champ des fluctuations de température extérieure, une proche de la température maximale en été et l'autre proche de la température minimale en hiver, garantissent une réduction de la consommation d'énergie du système HVAC d'environ 12%.

Mots-clés : Matériau à changement de phase ; double couches de PCM ; couches mobiles ; cycles de charge/décharge ; méthode enthalpique ; enveloppe du bâtiment

ملخص

تهدف هذه الرسالة الى اجراء دراسة مفصلة تساعد على تجاوز الحالات التي يكون فيها غلاف البناء الذي يحتوي على طبقتين من المواد متغيرة الطور غير فعال، و هذا بداية بالأخذ بعين الاعتبار تأثير درجة حرارة الانصهار (θ_m) والحرارة الكامنة الممثلة بالعدد اللابعدي ستيفان (Ste) ، في حالة غلاف بناء يحتوي على طبقة واحدة من المواد متغيرة الطور. بينما في حالة جدار يحتوي على طبقتين من المواد متغيرة الطور خلال مرحلة الشحن في فصل الصيف عن طريق التجمد, تم التركيز على تأثير عدد معتبر من ثنائيات درجة حرارة الانصهار (θ_{m1}, θ_{m2}) و الحرارة الكامنة لكلتا الطبقتين (Ste_1, Ste_2).اضافة لهذا يهدف هذا العمل الى دراسة عددية لسلوك غلاف بناء يحتوي على طبقتين من المواد متغيرة الطور قابلتين لتغيير موضعيهما فيما بينها حسب الفصل المناسب (صيف او شتاء)، و هذا من خلال تحليل مختلف المقادير الفيزيائية المؤثرة على عملية تغير الطور (انصهار / تجمد)، عبر توضيح مسار تحرك الحد الفاصل بين المنطقتين السائلة والصلبة، المدة الزمنية اللازمة لإكمال دورة من التخزين و التفريغ الحراري باستعمال تغير الطور، ايضا نسبة المواد متغيرة الطور الفعالة المساهمة في عملية التخزين و التفريغ الحراري في كل حالة، اضافة الى التدفق الحراري المكتسب / الضائع خلال دورة واحدة. تم الاعتماد على الطريقة العددية المسماة بالأحجام المنتهية من اجل الدراسة العددية للنموذج الرياضي الذي يمثل التركيبة الفيزيائية في كل حالة. فيما يخص الدراسة التي تعنى بالجدار ذو طبقة متغيرة الطور واحدة خلال فصلي الصيف و الشتاء، وضحت النتائج ان الحالات التي تكون فيها درجة حرارة الانصهار ضمن مجال تغير درجة الحرارة الخارجية و قريبة من درجة حرارة الوسط الداخلي (حسب الفصل) تؤدي الى افضل اداء حراري سنوي لغلاف البناء و هذا يتجلى في تنعيم التدفق الحراري اللحظي بتقليص سعة اهتزازه، هذا و يلاحظ العكس في حالة درجات حرارة الانصهار القريبة من اعلى درجة حرارة خارجية في الصيف او من ادنى درجة حرارة خارجية في الشتاء، اين يكون تقليص الطاقة المستهلكة من نظام التبريد و التسخين في اعلى قيمه. فيما يتعلق بالغلاف ذو طبقتين من المواد متغيرة الطور يظهر ان درجة حرارة الانصهار للطبقة الخارجية هي المقدار الرئيسي المتحكم في كمية الحرارة الضائعة الى الخارج، بحيث الزيادة في هذا المقدار تؤدي الى زيادة الطاقة الضائعة للوسط الخارجي، مثلا التركيبة (θ_{m1}=0.7, θ_{m2}=0.5)تؤدي الى تفريغ كمية حرارة مقدارها 18% بزيادة على التركيبة المرجعية (غلاف بناء لا يحتوي على مواد متغيرة الطور PSM)، بينما قد تبلغ هذه النسبة حوالي 13% في حالة التركيبة (θ_{m1}=0.5, θ_{m2}=0.7).اما بخصوص تأثير الحرارة الكامنة، يتضح انه من الافضل ان تكون الحرارة الكامنة للطبقة الداخلية اقل منها في الطبقة الخارجية، مما يؤدي الى عملية تجمد على نطاق اوسع، و منه كمية اكبر من الحرارة يتم تفريغها للوسط الخارجي، على غرار التركيبة (Ste_1=0.1, Ste_2=0.01)اين سجلت كمية حرارة ضائعة مقدرة ب 15% مقارنة بالحالة المرجعية، في حين باستعمال التركيبة (Ste_1=0.1, Ste_2=0.5) قدرت ب 8%. فيما يخص النتائج المتعلقة بالغلاف ذو طبقتين من مواد متغيرة الطور متحركة، تبين ان التركيبتين التاليتين $(\theta_{m1} = 2.4, \theta_{m2} = 2.4)$ و $(\theta_{m1} = 1, \theta_{m2} = 1)$ هما الافضل فيما يتعلق بتنعيم اهتزازات التدفق الحراري كل واحدة في الفصل المناسب لها (صيف ، شتاء) على الترتيب، بنسب تقدر ب 13% و 15%. في حين باعتماد تقنية تغيير موضع الطبقات ذات المواد متغيرة الطور فيما بينها، التركيبة (شتاء $(\theta_{m1} = 2.4, \theta_{m2} = 1)$و صيفا $(\theta_{m1} = 1, \theta_{m2} = 2.4)$)، تقدم افضل نتائج مقارنة بالبقية، اين يتم الوصول الى نسبة 35% من المواد المتغيرة الطور مساهمة في عملية الشحن و التفريغ (ذوبان / تجمد)، مع اكبر معدل سنوي للمدة الزمنية اللازمة لتفريغ الحرارة المخزنة. يظهر ايضا ان التركيبات التي تملك درجات حرارة انصهار مقاربة لدرجات

الحرارة الخارجية و في نفس الوقت قريبة من درجة حرارة الراحة للوسط الداخلي(حسب الفصل)، تعطي ايضا نتائج جيدة فيما يخص تنعيم اهتزازات التدفق الحراري بتقليل سعة الاهتزاز و منه تقليص استطاعة نظام التبريد و التسخين المطلوبة بحوالي 6.5%. بينما التركيبات التي تكون فيها درجات حرارة الانصهار ضمن مجال تغير درجة الحرارة الخارجية، بحيث احداهما قريبة من اعلى درجة حرارة خارجية في الصيف و الاخرى من ادنى درجة حرارة خارجية في الشتاء، تضمن تقليص كمية الطاقة المستهلكة من قبل نظام التسخين و التبريد بحوالي 12%.

الكلمات المفتاحية: مادة متغيرة الطور، طبقة مزدوجة المادة متغيرة الطور، الطبقات المتنقلة، دورات الشحن/التفريغ الحراري، الطريقة الاونثالبية، غلاف البناء.

List of Figures

List of Tables

Table of Contents

Nomenclature

Bi	Biot number
c	heat capacity [J/kg.K]
C	dimensionless heat capacity
f	average operating PCM fraction
h	convection heat transfer coefficients [W/m^2.K]
H	dimensionless enthalpy
$\hbar$	specific enthalpy [J/kg]
j	time increment
k	thermal conductivity [W/m.K]
K	dimensionless thermal conductivity
L	thickness [m]
N	nodes total number
Q	dimensionless heat gained/lost
$\bar{Q}$	dimensionless annual average heat gained/lost
q^*	dimensionless instantaneous heat flux
$\bar{q}$	dimensionless average heat flux
Ste	Stefan number
T	temperature [K]
t	time [s]
V	dimensionless volume
x	space coordinate [m]
X_f	dimensionless phase change front position

Greek symbols

α	thermal diffusivity [m^2/s]
$\Delta\tau$	dimensionless time step
Δx	space step
θ	dimensionless temperature
λ	latent heat [J/kg]
ρ	density [kg/m^3]

τ	dimensionless time
$\bar{\tau}$	average duration of charging/discharging
τ_{cycle}	phase change dimensionless operating duration of charging/discharging
τ_f	dimensionless duration of one cycle

Subscripts

c	cold
h	hot
i	initial
l	liquid
m	phase change
ref	reference
s	solid
1	first PCM layer placement
2	second PCM layer placement

Abbreviations

HVAC	heating, ventilation and air conditioning
FS	full solidification
PCM	phase change material
PCMW	phase change material wallboard
PC	phase change
PSM	phase stabilized material
SSPCM	shape-stabilized phase change material
TS	total solidification

General Introduction

The use of fossil fuels and reliance on non-renewable energy sources became a problem in the building industry during the last years of the 20th century. A variety of difficulties emerged in this area, including the need to reduce consumption, improve the effectiveness of energy production, and finally adopt sustainable resources. Notably, the construction industry has demonstrated a huge thirst for energy, accounting for about 33% of the world's energy consumption while also producing over 25% of the total emissions of greenhouse gases [1].

Innovative strategies are always being investigated to improve the thermal performance of building envelopes in the quest of sustainable and energy-efficient building designs. The incorporation of Phase Change Materials (PCMs) into building structures is one possible direction for this attempt. Due to their distinct capacity to store and release thermal energy during phase transitions, PCMs have drawn a lot of attention. This has helped to increase interior comfort and promote energy efficiency. The incorporation of PCMs has the potential to completely transform how we design, build, and run buildings as the globe struggles with issues of energy consumption and environmental impact.

This thesis embarks on a comprehensive exploration of the performance and potential of PCM-integrated building envelopes. Through a synthesis of theoretical foundations, computational modeling, and empirical analysis, this study aims to unravel the intricate dynamics of PCM behavior within building structures. By examining various aspects such as material properties, phase change kinetics, and system design, we seek to not only deepen our understanding of the underlying mechanisms but also uncover novel strategies for harnessing PCM technology to its fullest extent. It aims also to illustrate how different parameters effecting the phase change phenomena within a multilayered building envelope, under numerous inside/outside situations, in order to overcome the circumstances where the PCM wall is not well operating, where a single and double PCM layer building envelope are studied. Further, the impact of mobile PCM layers enhancing the building envelope via different seasons (summer and winter) was examined.

The first chapter provides an extensive exploration of the phase change phenomenon, covering its fundamental principles and a range of practical applications. Beginning with an

introductory context, subsequent sections delve into the mechanics of phase change and the factors influencing this process. The discussion then expands to encompass the various types of Phase Change Materials (PCMs), each with distinct characteristics. The versatility of PCMs in enhancing diverse applications is showcased, and their role in revolutionizing building techniques is illuminated. The subsequent chapters delve into specific aspects, including single and double PCM layers, dynamic insulation, and dynamic single PCM layers, offering a comprehensive understanding of PCM utilization within construction contexts.

The primary goal of the second chapter was to showcase and evaluate the effectiveness of the phase change process within a building envelope that incorporates a single layer of phase change material (PCM). This was achieved by demonstrating the diverse mechanisms employed for cold (or heat) storage, utilizing both sensible and latent heat methods, and by monitoring the advancement of phase change fronts. Additionally, the study conducted an in-depth analysis of the influence of variables such as melting temperature and latent heat. Furthermore, the investigation explored the time required to reach the point of solidification limit concerning the melting temperature or latent heat. Furthermore, the study delved into the assessment of heat loss during the charging cycle.

In this chapter (3), a comprehensive investigation is centered on addressing situations where the operational efficiency of a single PCM building envelope is suboptimal. This is achieved by delving into the processes of solidification and fusion, characterized by the illustration of phase change front kinetics, analysis of charging and discharging cycle durations, examination of the proportion of operational PCM, and the assessment of the average heat flux gained or lost during a complete cycle. This analysis is conducted across a range of varying melting temperatures to ensure a comprehensive examination of the subject.

The fundamental aim of next chapter (4) is to illustrate and evaluate the operational effectiveness of the phase change process within a building envelope that incorporates dual layers of Phase Change Material (PCM). This objective was accomplished by showcasing the ways in which cold (or heat) is stored using sensible or latent heat mechanisms, all while investigating the dynamics of phase change fronts. Furthermore, the study explored the implications of utilizing two distinct PCM layers, which differ in terms of either their melting temperatures or latent heats. Additionally, the investigation examined the outcomes resulting from variations in the melting temperatures $|\theta_{m1}-\theta_{m2}|$ and latent heats $|Ste_1- Ste_2|$ of the

two PCM layers, considering a wide array of combinations $(\theta_{m1}, \theta_{m2})$ and (Ste_1, Ste_2). Moreover, the study assessed the time required to reach the solidification limit point, taking into account the temperature and latent heat differences $|\theta_{m1}-\theta_{m2}|$ and $|Ste_1- Ste_2|$. Furthermore, the research scrutinized the heat loss experienced during the charging cycle.

The aim of this chapter (5) is to explore the impact of integrating two mobile Phase Change Material (PCM) layers into a building wall, each designed for specific seasons (either summer or winter). These layers can switch positions based on the most effective configuration for the given time of year. Several combinations of melting temperatures $(\theta_{m1}, \theta_{m2})$ are suggested, and the behavior of the wall is examined during both seasons. The analysis covers alterations in temperature and enthalpy, as well as the advancement of phase change fronts (either solidification or fusion) of the PCM. Furthermore, it evaluates the proportion of operational PCM for each season, the duration of PCM charging/discharging cycles, and the temporal fluctuation of heat flux.

Chapter 1: An overview of the phase change phenomenon

1.1 Introduction

Due to its exceptional capacity to store and release thermal energy during phase transitions, the use of Phase Change Materials (PCMs) has attracted considerable attention in a number of different sectors. The fundamental ideas underlying phase change processes and their consequences for improving many applications, notably in the field of construction approaches, are laid forth in this chapter.

1.2 Phase change process

1.2.1 Sensible Heat

Sensible heat storage involves the accumulation or release of thermal energy by manipulating the temperature of a solid or liquid storage substance through interactions with heat transfer. In a sensible heat storage process, the storage or release of thermal energy occurs across a temperature span without causing a change in the material's phase during the charging and discharging phases. The quantity of heat stored is determined by factors like the mass of the storage material, its specific heat capacity, and the degree of temperature alteration, as referenced by Abedin and Rosen [2], Zalba et al. [3], and Pielichowska and Pielichowski [4].

Hence, the equation for sensible heat storage can be formulated as follows:

$$Q = \int_{T_1}^{T_2} mC_p \, dT = mC_p(T_2 - T_1) \tag{1.1}$$

where Q is the sensible heat stored, m is the mass of storage material, C_p is the specific heat capacity at constant pressure, and $[T_1 \, ,T_2]$ are the temperature range [5].

1.2.2 Latent Heat

A latent heat storage presents an exceedingly effective way for the storage or release of thermal energy, owing to its elevated storage density maintained at a consistent temperature [4]. The efficiency of a latent heat storage relies on the capacity of the storage material to absorb or release heat while maintaining a constant temperature during the process of phase transition. In contrast to sensible heat storage, latent heat storage offers a greater storage density within a narrower temperature range. Moreover, materials used in

latent heat storage, such as Phase Change Materials (PCMs), are capable of storing 5-14 times more heat per unit volume compared to materials used in sensible heat storage, such as water, masonry, or rock [6].

A sensible heat storage throughout the complete temperature range should be taken into account together with a latent heat storage at a restricted temperature range during the phase transition in order to comprehend the storage density of a latent heat storage system. As a result, according to Pielichowska and Pielichowski [4], and Tao et al. [7], the total stored energy for the TES system with a PCM may be represented as:

$$Q = m \int_{T_i}^{T_m} C_{p,solid}\, dT + m\Delta h + m \int_{T_m}^{T_f} C_{p,liquid}\, dT \qquad 1.2)$$

Here, the initial and final expressions represent the sensible heat contained within the solid and liquid phases, respectively, while the intermediary element signifies the latent heat engaged in the process of phase transition.

m is the mass of a PCM, T_i is an initial temperature, T_m is a melting temperature, T_f is a finish temperature, and Δh is a latent heat of fusion.

1.3 Phase Change Materials (PCM)

These are materials that can change their physical state within limited ranges of temperature. The most typical phase change within this temperature range is melting/solidification.

The most effective way to store thermal energy is through phase change or latent heat storage materials. When a solid transform into a liquid and then freezes at a certain temperature, energy per unit mass is stored and released. The energy received by the substance enables the component atoms or molecules to vibrate at higher energy states[8]. Since the atomic bonds relax during melting, the substance transforms from a solid to a liquid. However, when the substance solidifies, energy is transferred, allowing the molecules to lose energy and arrange themselves into a solid form.

Phase change materials classification

The three main categories of phase change materials are: organic (paraffin and nonparaffin), inorganic (salt hydrates and metallic alloys), and eutectic (a combination of two or more organic, inorganic, or both PCM components). Fig. 1. [9]

Saline hydrates are substances formed by combining salt with a precisely determined amount of water. Take, for example, the one developed by combining sodium chloride and water and producing the hydrate (NaCl,2 H_2O), sodium sulphate deca hydrate (Glauber's salt Na_2SO_4,10H_2O), calcium chloride hexahydrate ($CaCl_2$,6H_2O), ...

Organic Paraffinic Compounds: Paraffins are organic materials, consisting of mixtures of saturated hydrocarbons, which are alkanes of the general formula CnH2n+2.

Non-paraffinic organic compounds are other compounds apart from paraffins, such as fatty acids, esters, alcohols, and glycols.

Eutectics are mixtures of two or more substances. They exhibit behavior similar to that of salt hydrates with congruent melting.

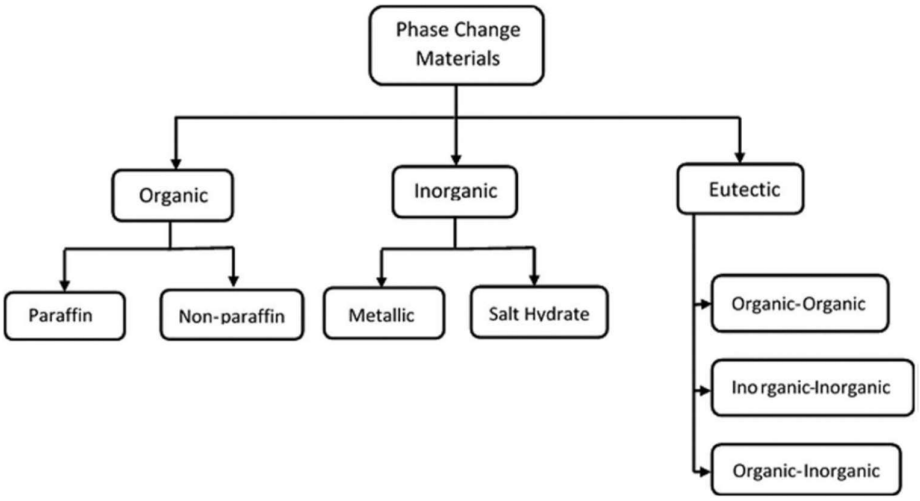

Figure 1.1 PCM Classification [9]

1.4 Literature review

Since the first use of Phase change materials, its importance has been improved significantly in widely fields. Numerous applications based on phase change materials in order to make it

more efficient, either for heat and cold storage [10,11], photovoltaic applications [12,13], as well as for cooling and heating systems, such as electronic devices [14,15] and building [16,17].

1.4.1 PCM enhancing numerous applications

1.4.1.1 Electronic devices

In the field of incorporating PCMs into electronic devices, such as, electric batteries, power electronic and portable device applications[18], the thermal management of electronic components is generally categorized into two types: active and passive systems [19,9]. Active cooling systems involve mechanical components such as fan-assisted cooling, spray cooling, and micro-channel systems with single or multi-phase flows[20]. These systems provide high heat removal capacity and offer a certain level of control over their operation. However, they can be associated with drawbacks such as increased maintenance requirements, noise generation, and vibration. On the other hand, passive cooling systems operate without the need for external components. Examples of passive cooling techniques include heat pipes[21] and heat sinks [22]. While passive systems may have lower heat removal capacity compared to active systems, they present several advantages for electronic applications. They are noise-free, have no parasitic power consumption, and incur lower operational and maintenance costs. Therefore, passive cooling techniques offer an appealing solution in many electronic applications.

Researchers have shown a significant interest in integrating phase change materials (PCMs) into heat sinks due to their advantageous characteristics such as high latent heat of fusion, low flammability, and safety. During device operation, PCMs absorb heat at a constant temperature while undergoing a phase change, typically from a solid to a liquid state. When the device is powered off, the PCM releases heat to the surrounding environment and initiates the reverse phase-change process, transitioning back from a liquid to a solid state. The primary motivation behind incorporating PCMs into electronic devices is to effectively reduce their operating temperature over a specific period while also enhancing the thermal response of the equipment[23].

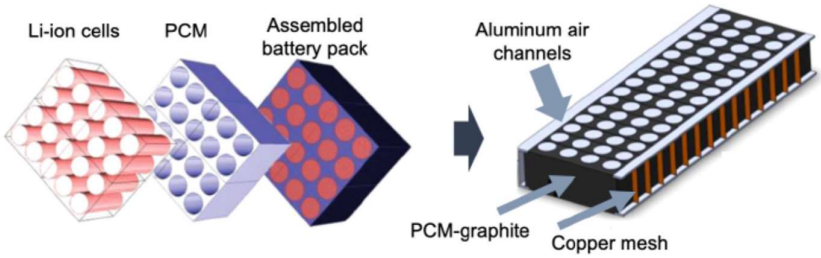

Figure 1.2 Example of PCM-based thermal management of electric battery [18]

The charge and discharge capabilities of a battery, represented by the charge/discharge current, are typically assessed using the C-rate. The C-rate refers to the rate at which the battery can be charged or discharged relative to its maximum capacity. For example, consider a battery with a nominal capacity of 100 Ah and a C-rate of 1C. This means the battery can deliver a current of 100 A for 1 hour. In contrast, if the C-rate is 0.5C, the same battery can provide 50 A of current for 1 hour. From a thermal management perspective, this parameter holds significant importance. Batteries with high charge and discharge rates experience an increased temperature rise due to internal losses. These losses can exceed the standard operating values, such as 60°C, as referenced in sources[24]. Therefore, monitoring the C-rate is crucial for effective thermal management of batteries to prevent excessive temperature increases. Within this context, researchers have proposed incorporating phase change materials (PCM) into thermal management systems for large battery packs and batteries with high charge/discharge rates. The aim is to enhance the heat removal system's performance and stabilize the batteries' operating temperature. Al Hallaj and Selman [25] conducted experimental demonstrations that showcased the effectiveness of this solution. Additionally, they delved into various aspects such as PCM thermal properties, configurations, PCM encapsulation, and potential techniques for enhancing heat transfer.

Arshad et al. [26] conducted an experimental investigation to enhance the thermal performance of portable electronics. They utilized n-eicosane as a phase change material (PCM) to fill pin-fin heat sinks. Four different configurations of pin-fin heat sinks were examined, each with varying volumetric fractions of n-eicosane. This was done to evaluate the effectiveness of pin-fins in cooling electronics, including a configuration without fins for comparison purposes. The results of the study indicated that incorporating n-eicosane into the pin-fin heat sink design yielded favorable performance, effectively maintaining the

temperature of mobile devices within a comfortable range. Under lower heat inputs and steady-state operating conditions, it was observed that achieving uniform charging of the PCM took a longer duration, resulting in a greater duration of latent heat release. The analysis of enhancement ratios revealed that a pin-fin heat sink with a thickness of 2 mm exhibited the highest thermal performance, making it a reliable choice for ensuring optimal performance of electronic packages.

1.4.1.2 Photovoltaic applications

The integration of phase change materials (PCM) with photovoltaic cells offers an enhancement in electrical conversion efficiency by utilizing latent heat storage. While crystalline silicon cells have dominated the photovoltaic industry, they exhibit a high temperature coefficient ranging from 0.4 to 0.5%. To address this issue, passive regulation of temperature increase during peak solar irradiation can be achieved by integrating PCM [27].

Naseer et al. [28] focuses on evaluating the performance of PV panels in the Taxila climate of Pakistan by varying the thickness of hybrid phase change materials (PCMs). Two PCMs with different melting points were utilized, separated by an aluminum plate and positioned on the rear side of the PV module. Three different configurations (B, C, D) of PV panels, each containing different thicknesses of hybrid PCMs, were compared to a reference configuration (A) that experienced natural cooling. The results revealed that the PV panel configuration with a higher proportion of low melting point PCM outperformed the others. Notably, configurations B, C, and D demonstrated average temperature reductions of 4.9°C, 6.5°C, and 8.1°C, respectively, compared to configuration A. Additionally, electrical efficiency improvements were observed in these three configurations, with enhancements of 5.0%, 6.1%, and 7.8% in electrical power output of the PV panels, respectively. Among the three configurations, configuration D, which featured the thickest layer of low melting PCM, exhibited the best results in terms of electrical power and efficiency, surpassing configurations B and C, which had high melting PCMs.

In this study conducted by Mahamudul et al. [29], the aim was to develop an efficient design for a temperature-regulated PV module suitable for the Malaysian weather conditions by integrating phase change materials (PCMs). The research involved a combination of numerical analysis and experimental investigations. The functioning of the system primarily

relies on the heat exchange properties between the phase change material and the PV module, Fig 2*. Excess heat absorbed by the PV module is transferred to the phase change materials. When the temperature of the PV module reaches the melting point of the PCM, the module's operating temperature remains constant during the phase transition, effectively regulating the temperature. The numerical analysis and experimental results demonstrate that incorporating phase change materials can regulate the PV module's temperature by approximately 10°C for approximately 6 hours in the Malaysian weather conditions. This reduction in operating temperature significantly enhances the conversion efficiency of the PV module, successfully achieving the fundamental objective of the study. However, challenges arise due to the issue of volume change of the PCM when integrated with the PV module. The authors suggest that using a shape-stabilized phase change material can resolve this problem, which serves as a potential future step for their work.

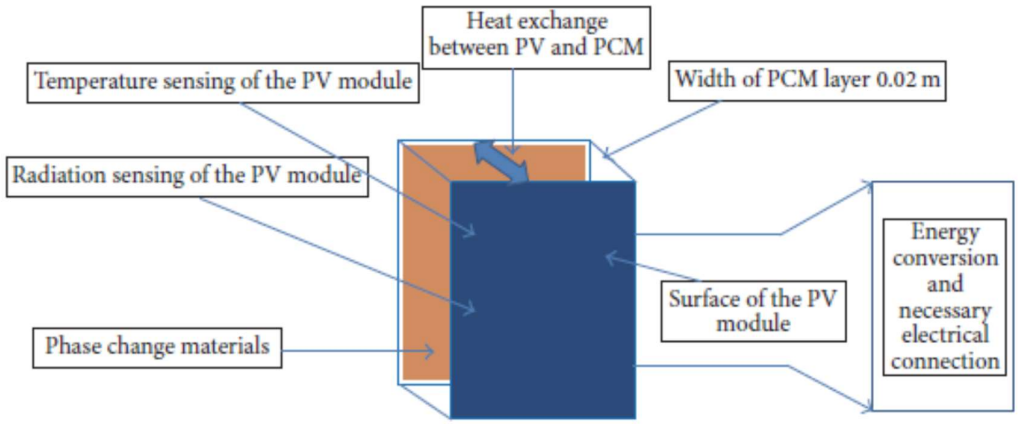

Figure 1.3 Diagram illustrating the arrangement of the PV-PCM system [29].

1.4.1.3 Heat and cold storage

Utilizing thermal energy storage (TES) has been demonstrated as a viable method to increase the integration of renewable energy into energy systems. Among various thermal storage technologies, latent heat thermal energy storage (LHTES) has garnered significant interest from researchers in the past decade. This is primarily due to its exceptional energy density and versatile range of applications [30].

To address the existing gap in the literature, Vérez et al. [31] conducted an experimental study to examine the influence of macro-encapsulation design on the performance of a

laboratory-scale thermal energy storage tank. The design of the storage material encapsulation was identified as a crucial parameter affecting heat transfer during the charging and discharging processes of the storage system. The study utilized two rectangular slabs filled with a commercial phase change material, having the same length and width but different thicknesses (35 mm and 17 mm). The results revealed that employing thinner slabs resulted in higher power output, leading to a reduction in both charging and discharging times by 14% and 30%, respectively, compared to the thicker slabs. Additionally, the variation in the flow rate of the heat transfer fluid had a more significant impact on temperature distribution and the amount of energy charged or released when thicker slabs were used. However, the macro-encapsulation design did not significantly influence the discharging efficiency of the tank, which remained at approximately 85% for the operating thresholds considered in this study.

Figure 1.4 Latent heat TES [31].

In a numerical investigation conducted by Arici et al. [32], the melting behavior of paraffin wax with Al_2O_3 nanoparticles in a partially heated and cooled square cavity was examined. The enclosure consisted of thermally active sections facing each other, maintained at different constant temperatures, while the remaining parts were thermally insulated. The study explored the influence of nanoparticle concentrations (Φ = 0 vol%, 1 vol%, 2 vol%, and 3 vol%), the orientation of the activated walls, and the temperature of the hot wall on the melting process and stored energy. The thermophysical properties of the nanocomposite phase change material (NEPCM) were considered to be temperature and phase dependent. The computational results revealed that the investigated parameters had a notable impact on both

the melting rate and stored energy. Specifically, the study found that the highest enhancement occurred when the enclosure was filled with a nanoparticle concentration of Φ = 1 vol% and heated from the bottom. However, beyond a nanoparticle concentration of Φ = 1 vol%, the purpose of enhancement was compromised, resulting in a decrease in overall performance.

In the context of heat and cold storage, PCM's low thermal conductivity has led to several studies exploring the integration of fins in latent heat storage systems to enhance the phase change response.

Tiji et al. [33] conducted a numerical investigation to examine the impact of T-shaped fins on enhancing PCM melting. Furthermore, Sun et al. [34] investigated the enhancement of solidification in a triple-tube latent heat energy storage system using twisted fins. Another study by Chatroudi et al. [35] evaluated the charging behavior of a double-tube latent heat storage device with circular fins.

To reduce energy consumption, Sheikholeslami [36] suggests combining thermal storage with solar concentrating devices in a numerical study. Additionally, an improved fin design and the dispersion of ZnO nano-powders are proposed to enhance the low conduction mode of pure paraffin. In another work by Sheikholeslami [37], the effect of using porous media on water solidification in the presence of hybrid nanoparticles is simulated. To expedite the process, a tree-shaped fin is employed, and radiation effects are taken into account. The introduction of radiation reduces solidification duration by approximately 56.28%, while the use of porous media further reduces it by 91.21%.

1.4.2 Integrating PCM in Building

1.4.2.1 Single PCM layer

Building is the main cause of energy consumption in many countries. Energy consumption is high in buildings due to the low thermal inertia of the building envelope. Thus, increasing the thermal inertia of the envelope can contribute to reduction in energy consumption and reduces hence the carbon footprint of buildings.

Thermal management through the incorporation of PCMs into building walls has gained significant interest among researchers. An array of building materials infused with PCM, including blocks, bricks, wallboards, panels, and plaster, have undergone extensive

production and testing. [38] [39]. In one example, Li et al. [40] Performed a numerical study to evaluate how the thermophysical properties of PCM impact the thermal performance of a double-glazing unit containing PCM. Subsequently, Liu et al. [41] validated the developed model experimentally to determine the thermal and optical performance of the same configuration. The study results indicated that when the refractive index of the PCM is below 1.95, its influence on the temperature decrement factor and other optical properties is comparatively limited.

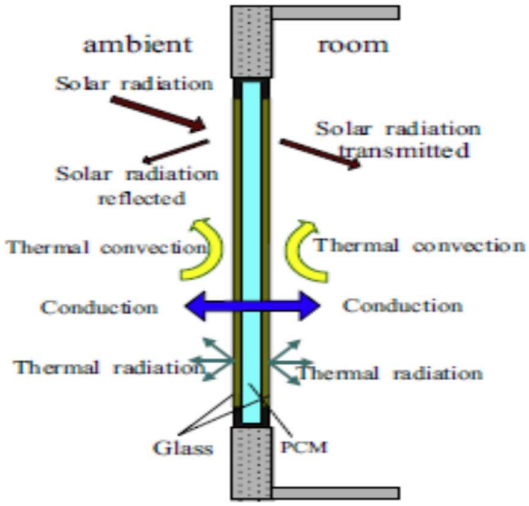

Figure 1.5 Double-glazing unit filled with PCM [40].

In Sheikholeslami's work [42], an air conditioning device incorporating a porous medium is proposed. The research incorporates the combination of paraffin (RT27) and nano-sized ZnO particles within numerous five-lobed cylinders within the duct to augment the material's conductivity. Utilizing porous media in this configuration results in a decrease in the necessary time by around 37.15%.

Phase change materials (PCMs) serve as an effective approach to enhance the thermal performance of buildings. Previous research has demonstrated that achieving an effective contribution from PCMs in enhancing building walls requires optimization of various parameters, such as PCM position, melting temperature, latent heat, and PCM thickness. The optimization of these parameters is influenced by the thermal inertia of the wall, which depends on the thermal properties of the wall materials. Additionally, climatic zone, indoor

conditioning or non-conditioning, wall orientation, and seasonal conditions also play vital roles in the optimization process [38].

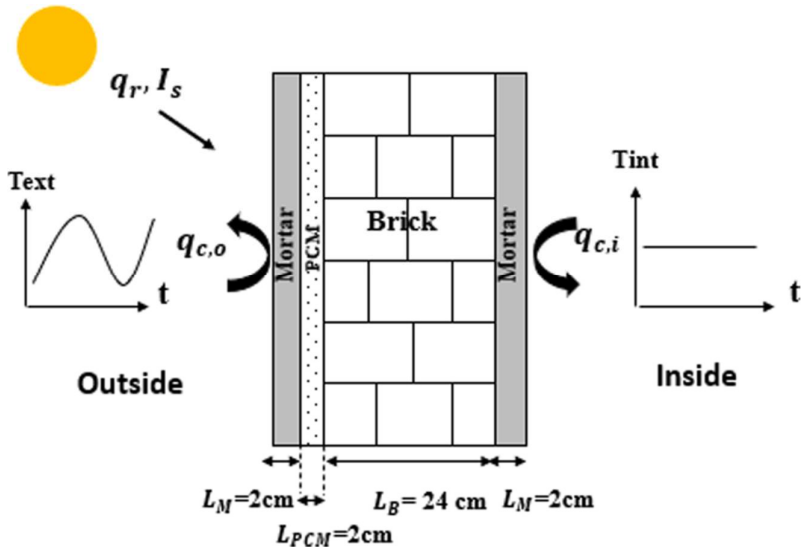

Figure 1.6 Wall with PCM [39].

1.4.2.1.1 Optimize the PCM position

To optimize the position of phase change materials (PCMs) within building walls, researchers have explored various PCM locations [38]. For instance, Fateh et al.[43] and Zwanzig et al. [44] found that the best position for PCMs is inside the wall section. Alternatively, Kong et al. [45] and Zhu et al. [46] suggested placing PCMs in the internal layer of the wall, while Lei et al. [47] and Gounni and El Alami [48] proposed positioning PCMs in the external layer of the wall. An example study by Shi et al. [49] conducted experiments on room models with concrete walls incorporating macro-encapsulated PCM under real conditions. The results demonstrated that the model with PCM integrated within the concrete walls exhibited superior temperature control compared to other models. Moreover, this configuration effectively reduced the maximum temperature by up to 4 °C.

The research conducted by Al-Absi et al. [38] highlighted that the optimal locations for phase change materials (PCMs) depend significantly on implementing a daily full melting/freezing cycle to prepare for the next day. In the study by Sun et al. [50], It was noticed that with an increase in thermal resistance of the wall insulation, the ideal placement of the PCM layer shifted slightly toward the outer side of the wall. Lagou et al. [51]

demonstrated that in non-conditioned indoor spaces, the PCM layer should be integrated into the inner surface of the wall. Furthermore, Liu et al. [52] investigated the incorporation of PCMs into lightweight building walls (LBW) to enhance thermal inertia and improve indoor thermal comfort. Through numerical simulations, they analyzed and evaluated the impact of different PCM parameters on the thermal performance of LBW. The findings revealed that installing PCM in the middle of the wall at an appropriate phase-transition temperature yielded superior performance compared to installation on the outer or inner surfaces.

1.4.2.1.2 Optimize the melting temperature

As mentioned earlier, optimizing the melting temperature is a crucial factor to ensure the efficient performance of the wall.

In a numerical study conducted by Sun et al. [50], the study examined and verified the thermal performance of a building wall incorporating a phase change material (PCM) for passive cooling using experimental data. The study examined the impact of six factors, including the optimal PCM phase transition temperature for achieving heat flux reductions. The results demonstrated that for improved space cooling performance, with the indoor air temperature set at 24 °C, the PCM phase transition temperature was found to be within the range of 27-31 °C.

The objective of Bozzhigitov et al. [53] was to optimize the melting temperature of phase change materials (PCM) to enhance energy-saving potential in office buildings located within the temperate oceanic climate region (Cfb climate zone). The study utilized the Fanger model and found that PCM temperatures ranging from 22 to 25 °C were optimal for the entire Cfb climate zone. Implementing these optimal PCM temperatures resulted in energy consumption reductions of up to 37.6%.

In their study, Lagou et al. [51] investigated the incorporation of phase change materials (PCMs) into building envelopes and provided valuable insights regarding the suitable melting temperatures for PCMs in non-conditioned buildings. The findings indicated that for the southern European zone, an optimal melting temperature of 35 °C during summer was identified. On the other hand, for the central European zone, the optimal melting temperature during summer was found to be 22 °C.

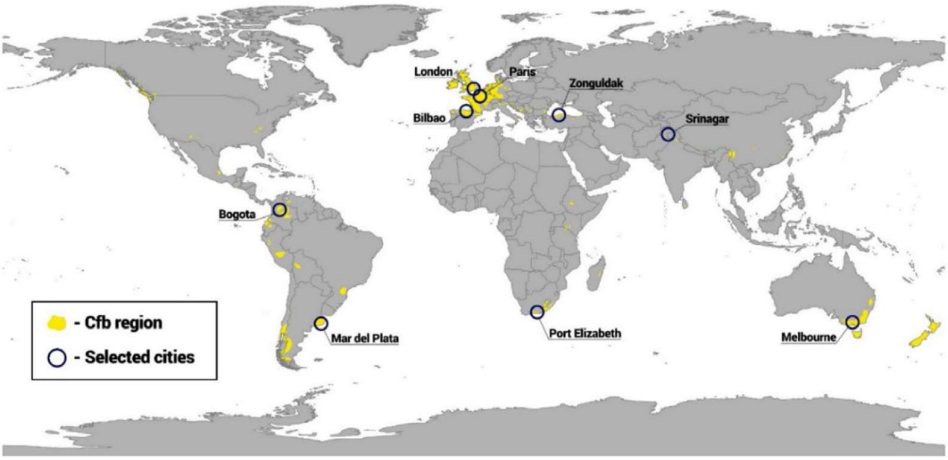

Figure 1.7 Area of Cfb region and location of selected cities [53].

Zhou and Eames [54] focused on the application of phase change materials with a solid-liquid phase change (PCMW) in partition walls of buildings. They considered several key factors that influence the selection of the optimal melting temperature, such as outdoor temperature, solar radiation, window size, air change rate, and the U-values of external walls and windows. To study this, a lightweight building case was examined using actual weather data from the summer months in the United Kingdom. The simulation was performed using EnergyPlus software, with the aim of reducing energy consumption while maintaining desired internal temperatures. Through their analysis, the optimal melting temperature during the summer in the United Kingdom was found to be 23.4 °C.

In their study, Tunçbilek et al. [55] examined the impact of nanoparticle-enhanced PCM on building energy savings. They used a PCM enriched with aluminium oxide nanoparticles (Al_2O_3) at varying content levels of 1, 2, and 3 vol%. The results indicated that using pure PCM in the wall led to a yearly energy saving of 20.7%. However, when 3 vol% of Al_2O_3 was added to the PCM, the heating energy saving reduced by 1.7%.

Li et al. [56] conducted a numerical investigation with the objective of exploring the effects of critical design parameters, For instance, the choice of the melting point for the PCM can be influenced by varying loading conditions associated with different climate zones and months. They employed COMSOL Multiphysics software to assess the thermal performance of multilayer walls containing PCM under various climate loading conditions. The findings demonstrate that selecting the appropriate PCM melting point based on these design

parameters can effectively reduce indoor peak temperatures and temperature oscillations. As a result, the energy consumption by the HVAC system for indoor temperature regulation is reduced.

1.4.2.1.3 Optimize the heat latent

Using phase change material (PCM) in buildings effectively enhances the thermal mass of walls, especially when considering the latent heat of the PCM. In their study, Liu et al. [52] chose seven sets of data with intervals of 50 kJ/kg, ranging from 25 kJ/kg to 325 kJ/kg, as research indicators, while keeping other non-research parameters at their base values. This study illustrates the changes in various evaluation indicators corresponding to different phase change latent heats. Where it is shown that, a higher latent heat leads to a longer phase change duration (φ) and a lower the attenuation rate of inner surface temperature (f). Specifically, when the latent heat increased from 25 kJ/kg to 175 kJ/kg, φ increased by 2.28 to 4.28 hours, and f decreased from 5.34% to 0.54% (89.89% reduction) compared to the reference wall without PCM. However, when the latent heat increased from 175 kJ/kg to 325 kJ/kg, φ only increased by 0.86 hours, and f decreased from 0.54% to 0.29%. This demonstrates that the greatest benefit is observed when the latent heat is set at 175 kJ/kg. Beyond that point, further increases in latent heat weaken the impact on φ and f. They also showed that, the peak heat flux (q_{peak}) at the inner surface gradually decreases as the latent heat increases. When the latent heat is raised from 25 kJ/kg to 325 kJ/kg, q_{peak} can be reduced by 37.37% to 66.52% compared to the case without PCM. However, it becomes apparent that the rate of q_{peak} reduction levels off when the latent heat exceeds 175 kJ/kg. This finding aligns with the conclusion drawn from increased PCM thickness, indicating that the heat storage capacity improves with higher latent heat, but beyond a certain threshold, the effect stabilizes due to the limited amount of outdoor heat available.

The findings in this study differ significantly from the previous research of Kishore et al. [57], where the effect of PCM tends to stabilize once the latent heat exceeds 50 kJ/kg. This discrepancy suggests that variations in outdoor thermal boundaries and the thermal resistance of the base layer (without PCM) can influence the efficiency of PCM's contribution. Furthermore, unlike the considerable changes observed in q_{peak}, the q_{ave} (average heat flux) remains relatively unchanged as the phase change latent heat strengthens. This further highlights that PCM primarily adjusts temperature fluctuations through its inherent thermal

mass without significantly diminishing the heat transfer effect. While walls with high thermal storage capacity and superior thermal regulation mechanisms can yield energy-saving benefits for q, these benefits become negligible when the latent heat surpasses a specific threshold (175 kJ/kg). Specifically, when the phase change latent heat is 175 kJ/kg, the q_{peak} is only 0.7 W/m^2 (13.33%) higher than the q_{ave}, while compared to the reference wall (without PCM), the q_{peak} and q_{ave} are reduced by 62.12% and 24.41%, respectively.

Within this work Arici et al. [58] carried out a study in order to uncover the role of latent heat in the wall's thermal efficiency and establish the optimal location, thickness, and melting temperature of PCM for exploiting latent heat to the fullest extent in diverse climatic situations. The computed outcomes indicate that the monthly optimal PCM melting temperature and PCM layer thickness differ from 6 to 34 °C and from 1 to 20 mm, respectively, based on the climate conditions. It was deduced that an optimization analysis must be performed to prevent PCM from acting like PSM.

1.4.2.2 Double PCM layer in Building

The incorporation of a single PCM layer in building walls often poses the challenge of being suitable for only one specific season, depending on the PCM's melting or solidification temperature. To overcome this limitation, several studies have been conducted. As an example, scientists have investigated employing natural nighttime ventilation to charge the PCM in preparation for the upcoming phase change cycle [59,60]. Another approach is to consider the incorporation of double PCM layers in building envelopes, where each layer is optimized to function optimally during its respective season. This enables better thermal management and ensures the PCM's effective performance throughout the different seasons.

Therefore, to combine the advantages of different PCMs with different melting properties, the concept of double PCM is carried out [61].

In their study, Kong et al. [62] introduce a novel double-layer PCM Trombe wall with multiple phase transitions. The results reveal significant benefits of the new double-layer PCM Trombe wall in regulating indoor temperature. During winter, the average temperature in the room can be increased by 0.3 to 6.6 °C, while in the summer, it can be decreased by 0.4 to 0.93 °C. Moreover, the peak temperature occurrence during the summer can be significantly delayed. Additionally, the heat flux can be reduced by 9.1 to 92% in the summer

and by 1.8 to 75.7% in the winter. These findings underscore the superior performance of the proposed double-layer PCM Trombe wall in effectively managing the indoor thermal environment.

In their study, Louanate et al. [61] conducted numerical simulations using EnergyPlus software to investigate the thermal behavior and energy efficiency of a residential home in a Mediterranean climate. They explored the integration of several phase change materials (PCMs) based on various ideas, including reducing average temperature fluctuation and achieving monthly energy savings. The evaluation included both single and double phase change material layers. The findings revealed that double-layer systems comprising two different phase change materials outperformed single-layer systems throughout the year. The yearly energy savings rates for single and double phase change material layers were 41.42% and 55.41%, respectively.

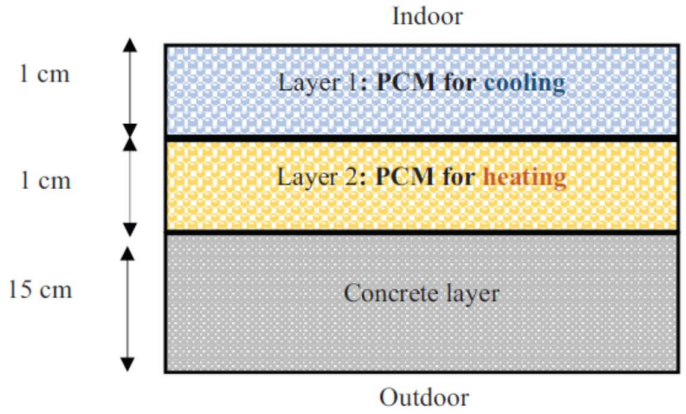

Figure 1.8 The schematic of the double-layer system [61].

Arıcı et al. [63] conducted research with the objective of enhancing the utilization of latent heat by dividing the phase change material (PCM) into two layers and optimizing their location and melting temperature. The study findings demonstrated that incorporating two PCM layers, with one situated on the outside of the wall and a melting temperature of 17°C, and the other on the inside with a melting temperature of 25°C, resulted in higher annual energy savings (17.2%) compared to using a single PCM layer (16.8%). Through the implementation of two PCM layers, the energy savings achieved through latent heat activation increased from 2.5% to 3.2%. Furthermore, this design contributed to a significant reduction in CO_2 emissions, reaching up to 18.4%.

In their research focused on the energy efficiency as well as the thermal behavior of a residential building, Reddy et al. [64] discovered that the strategic incorporation of multiple phase change material (PCM) layers with appropriate thickness can effectively maintain a comfortable interior temperature of 28 °C throughout the day in Chennai, India. This approach highlights the potential for significant energy savings and enhanced thermal comfort. Furthermore, the study highlights the benefits of utilizing PCM layers in roofs. A roof with a single PCM layer was found to reduce heat gain by 17 to 26%, providing substantial energy savings and improved indoor thermal conditions. For even higher heat gain reductions, a roof with a double PCM layer can achieve reductions of 25 to 36% during different months of the year, demonstrating the remarkable potential of PCM technology in mitigating temperature fluctuations and promoting energy efficiency in buildings.

In their investigation, Jin and Zhang [65] examined the thermal performance of a floor system that incorporated a double layer of phase change material (PCM) using a numerical model. The findings revealed notable improvements, including reduced heat fluxes and temperature fluctuations at the floor's surface. Additionally, the system demonstrated the ability to generate a certain amount of heat or cold energy even after the heat pump or chiller had been turned off for an extended period. The study observed that the floor system with PCM exhibited increased energy release during heating and cooling by 41.1% and 37.9%, respectively, compared to the floor without PCM. This significant enhancement can be attributed to the high heat of fusion of the PCM, which is 150 kJ/kg, allowing for efficient storage and release of thermal energy.

Zhu et al. [66] proposed and validated a novel and simplified dynamic construction model in their research. The new wall system consisted of a three-layer sandwich-type construction, where the center layer was made of traditional brick, and the outer layers were shape-stabilized phase change material (SSPCM) wallboards. The inner layer, which connects to the interior of the building, had a PCM melting temperature close to the indoor set point used in winter, while the outer layer, connected to the exterior, had a higher PCM melting temperature for use in summer. The brick layer in the middle acted as insulation. Notably, there were limited studies incorporating simplified dynamic models of building structures with double layers of SSPCMs. The simplified dynamic model represented each wall layer (brick or double layers of SSPCMs) by specific combinations of resistances and capacitances.

The validation outcomes indicated that the simplified dynamic model provided an accurate description of lightweight and medium-weight walls incorporating dual layers of SSPCMs.

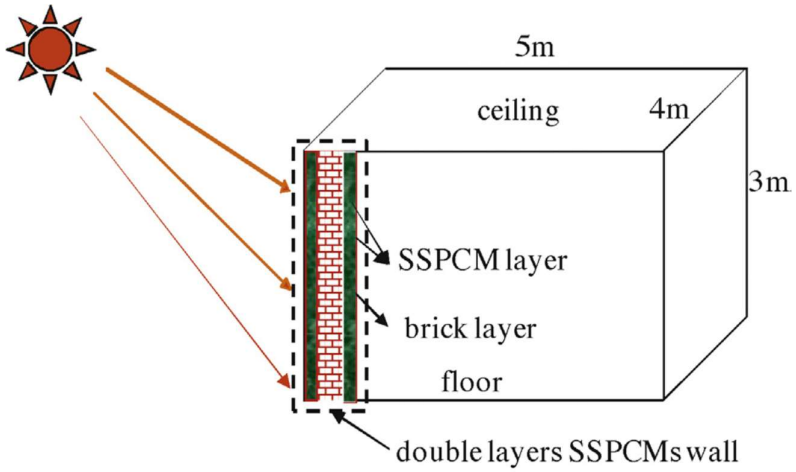

Figure 1.9 Schematic of double layers SSPCM wall [66].

Zhu et al. [67] conducted a study focusing on a wall system with a three-layer sandwich construction. The exterior and interior layers of the wall consisted of wallboards made of shape-stabilized phase change material (SSPCM), while the intermediate layer was made of traditional concrete. The research included a simulation study that considered the climatic conditions of Wuhan city, China, which experiences hot summers and cold winters. Based on the test results, it was determined that the SSPCM wallboard should have a thickness ranging from 30 to 60 mm on both the inside and outside of the wall. The study revealed annual energy savings for cooling between 3.4% and 3.9%, while for heating, the savings were in the range of 14.8% to 18.8%. The cooling peak load reductions exhibited variability from 3.1% to 3.8%, and for heating, the range was between 8.6% and 11.3%. The external and internal layers of the wall contributed to the reduction of annual energy demand and peak load, with the external layer primarily impacting cooling in hot seasons and the internal layer mainly influencing heating in cold seasons.

Rehman et al. [68] conducted a study proposing a dual-layer PCM configuration for brick walls to enhance human comfort in both hot and cold climatic conditions. The research employed Ansys Fluent to perform numerical simulations for the dual PCMs integrated within a brick wall, when evaluating scenarios in June and January, with respective melting temperatures set at 29°C and 13°C, it is observed that employing both of these PCM types

concurrently enhances human comfort and decreases energy consumption in Islamabad throughout the year, as opposed to using a single PCM at 29°C for summer or 13°C for winter. This innovative dual-layer PCM approach demonstrates its potential in effectively regulating indoor temperature to maintain comfortable living conditions in diverse weather conditions.

In their 2010 study, Almeida et al. [69]. utilized the ESP-r building simulator to contrast the impact of employing multiple PCM layers with that of a single layer. Their research demonstrated that the integration of PCM can have a substantial impact on a building's thermal performance. Remarkably, in specific scenarios, the implementation of multi-layered PCM was shown to provide more practical thermal advantages compared to a single PCM layer.

Jin and Zhang [65] present a novel double-layer phase change material (PCM) floor in their study. The researchers investigate the floor's thermal performance using a numerical model developed specifically for this research. The study highlights the significance of optimizing the melting temperatures of PCMs. Due to the high heat of fusion (150 kJ/kg) of the PCM, the floor with PCM exhibits remarkable energy release during peak times. More precisely, the energy discharged from the PCM-integrated floor increases by 41.1% during heating and by 37.9% during cooling, in comparison to a floor without PCM.

In a study carried out by Sun et al. [70], the focus was on improving thermal conductivity for both winter and summer climates by blending two hydrated salts with distinct melting points alongside expanded graphite. The floor systems were designed with a heat storage layer using a composite based on $Na_2(HPO)_4(H_2O)_{12}$ (melting point: 31.3 °C) and a cold storage layer using a composite based on $CaCl_2•6(H_2O)$ (melting point: 20.2 °C). The radiant floor system, comprising an upper heat storage layer and a lower cold storage layer, extended the duration of thermal comfort by 2.2 times compared to the reference room with pebbles in the floor in a winter climate. Additionally, enhancing the thermal conductivity of the composites contributed to energy savings by reducing the active system's working duration. This approach demonstrates potential for improving thermal performance and energy efficiency in buildings across different climatic conditions.

Pasupathy and Velraj [71] carried out a study investigating the impact of PCM panels on a building's roof. Their experiment comprised two identical test rooms, where the thermal behavior of the roof with PCMs was analyzed using a mathematical model based on the finite volume method. The research aimed to explore the effectiveness of a double layer PCM for year-round thermal management. The developed mathematical model allowed them to compare the thermal performance of the double layer PCM configuration with that of a single layer PCM. Through this study, insights were gained into the potential benefits and thermal regulation capabilities of incorporating PCM panels on the building's roof.

Reddy et al. [64] provided simulations to assess the impact of PCM-integrated roofs throughout the entire year. The results demonstrated that incorporating PCM in the roof structure leads to significant reductions in heat gain. Specifically, for a single PCM layer, the heat gain was reduced by 17% to 26%, while for a double PCM layer, the reduction ranged from 25% to 35%. These energy-saving measures were achieved while ensuring a comfortable temperature inside the building, making PCM integration an effective solution for enhancing thermal performance and energy efficiency in roofing systems.

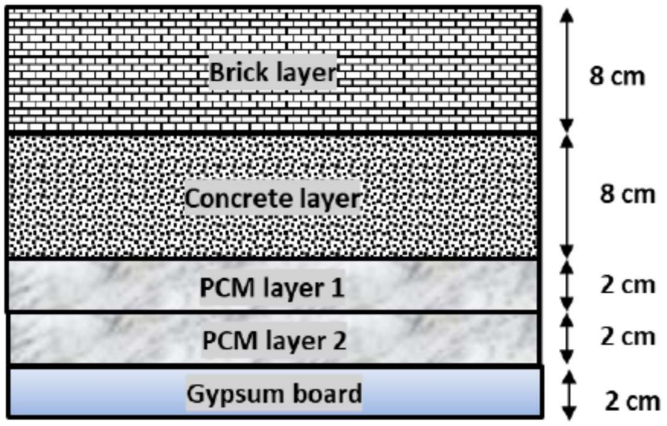

Figure 1.10 Constructional details of a double PCM-integrated roof [64].

In certain configurations or climate zones, the implementation of double PCM layers in buildings may not yield significant improvements. For example, Zhu et al. [72] conducted a study to examine the energy efficiency of an office building incorporating a double PCM wallboard across five diverse climate zones. The findings revealed that the double SSPCM wallboard was not suitable for Guangzhou city as it did not provide any positive effects

during the winter. Additionally, this novel wallboard might not be well-suited for cities with hot summers and warm winters.

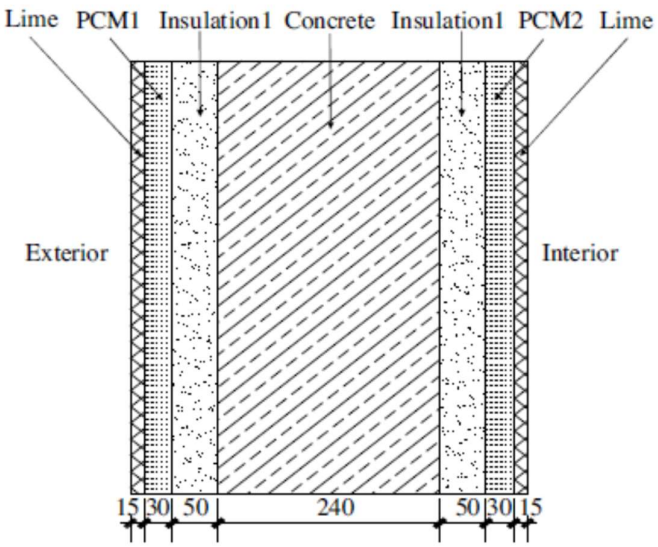

Figure 1.11 Double SSPCMs wallboard [72].

Similarly, Zastawna-Rumin et al. [73] showed that the second layer of the PCM system only became operational after an extended period of overheating. In cases of slight overheating in the premises, the system functioned in a manner akin to a single layer of a bio PCM mat. These studies highlight the importance of considering specific climate conditions and configurations when implementing double PCM layers to ensure optimal performance and energy efficiency in buildings.

1.4.2.3 Dynamic insulation

To improve the energy efficiency of buildings, the concept of dynamic insulation has arisen. This approach entails adjusting the thermal resistance of the building envelope to regulate the heat transfer rate. Dynamic insulation integrates traditional insulation with dynamic heat exchange mechanisms within the envelope [74].

Dynamic insulation encompasses the integration of a circulating fluid within the insulating layer, capturing heat loss across the entire building envelope. This fluid can consist of water, air, or refrigerant [75,76].

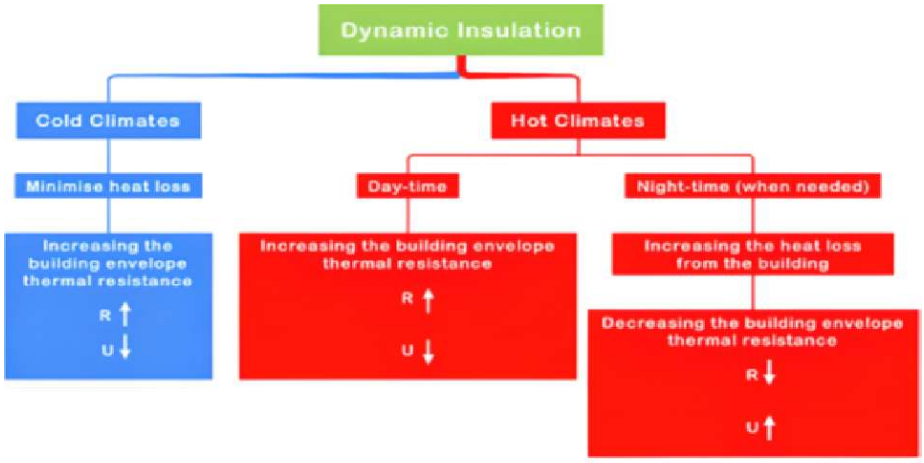

Figure 1.12 Strategies for Utilizing Dynamic Insulation as a Variable Thermal Insulator [75].

Dynamic insulation comprises a range of strategies that are tailored to different climates. In colder climates, its objective is to reduce heat loss to the surroundings by enhancing the building envelope thermal resistance [77]. Conversely, in hot climates, it focuses on increasing the envelope thermal resistance during the daytime to reduce heat gain [78]. During nighttime, the thermal resistance can be decreased to promote heat dissipation [79]. Dynamic thermal insulation has shown energy savings exceeding 40% when compared to static thermal insulation options [75].

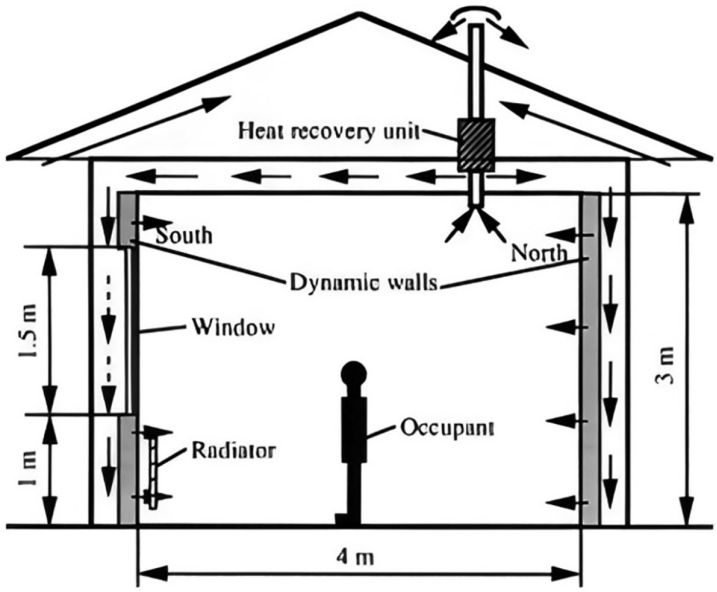

Figure 1.13 The dynamic insulation approach for evaluating the thermal environment [76].

1.4.2.4 Dynamic single PCM layer

In a study conducted by De Gracia [80], An investigation was carried out to explore a dynamic application of phase change materials (PCM) in building envelopes. The concept involved a PCM layer that could be positioned variably in relation to the insulating layer of the building envelope. During the night, the PCM could be placed on the outer part of the insulation to increase its chances of solidifying and charging for the next day. This configuration allowed the PCM to release the heat it absorbs during peak cooling hours to the outdoors instead of indoors. However, to handle peak cooling loads and potential internal heat gains, the PCM would be repositioned during the day to face the indoor space. The numerical results of the study indicated that this technology could serve as an effective cooling supplier system. Furthermore, it acted as a thermal barrier, as it had the ability to charge the PCM, which solidifies at temperatures lower than the interior set point. This dynamic use of PCM in building envelopes has the potential to optimize cooling efficiency and thermal comfort while contributing to energy savings.

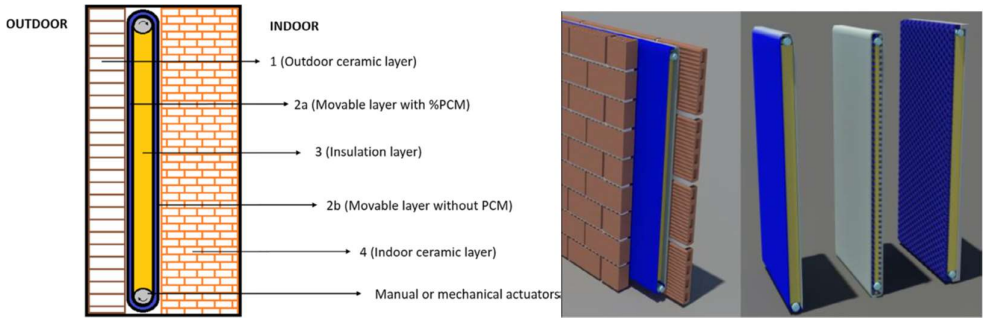

Figure 1.14 Sketch of possible implementation of the dynamic PCM system in a ceramic-based vertical building envelope [80].

1.5 Conclusion

This chapter has introduced the basics of phase change materials (PCMs) and their potential to revolutionize a variety of applications, notably in the fields of building techniques and energy management. Phase transition processes, material characteristics, and their impact in various situations have been studied in detail. Through the sections that have been provided, it has become clear how important PCMs are as adaptable instruments for energy storage, thermal regulation, and sustainable development, especially in building field.

However, in order to overcome the limitations identified in the prior study, it is imperative to conduct a thorough examination of the phase change phenomenon in a building envelope equipped with a dual PCM layer during the charging cycle. The present research is designed to assess the effectiveness of the phase change process within this double PCM layer building envelope, taking into account the storage of cold or heat through sensible or latent heat, and investigating the kinetics of phase change fronts. In particular, the study concentrates on evaluating the consequences of employing two PCM layers with distinct melting temperatures or latent heats. The difference between both melting temperatures ($|\theta_{m1}-\theta_{m2}|$) and latent heats (represented by Stefan numbers, $|Ste_1- Ste_2|$) is carefully analyzed, considering various combinations of $(\theta_{m1}, \theta_{m2})$ and (Ste_1, Ste_2). Moreover, the research investigates the time required to reach the limit point of solidification as a function of $|\theta_{m1}-\theta_{m2}|$ and $|Ste_1-Ste_2|$. Additionally, a detailed analysis of the heat dissipation during the charging cycle is conducted. The mathematical model governing this configuration is derived from the conduction heat transfer equation in an enthalpy-based formulation. To solve this model computationally, the finite volume method is employed and implemented through programming in the FORTRAN language. Through this detailed analysis, the study aims to shed light on the dynamic behavior and efficiency of the double PCM layers building envelope.

Moreover, this research requires an investigation into the impact of incorporating two movable PCM layers within a building envelope, with each layer tailored for a particular season (either summer or winter). Both layers possess the ability to adapt their placement in relation to each other, guided by the ideal position corresponding to the current season (whether summer or winter). Various combinations of melting temperatures $(\theta_{m1}, \theta_{m2})$ are proposed, where the study delves into how the wall behaves in both summer and winter. The research delves into the evolution of temperature and enthalpy, as well as the phase change fronts (solidification or fusion) of the PCM throughout the seasonal cycles. Moreover, the research investigates the operational PCM fraction for each season, the length of the PCM charging and discharging cycles, and the temporal changes in heat flux. Through this comprehensive analysis, the aim is to gain insights into the dynamic performance and effectiveness of the building wall with the two mobile PCM layers, providing valuable information for optimizing thermal management strategies in different seasons.

Chapter 2 : Single PCM layer building envelope Assessment during charging cycle

2.1 Introduction

The objective of this chapter was to demonstrate and assess the efficiency of the phase change process within a building envelope containing a single phase change material (PCM) layer. This was accomplished by illustrating the different methods of cold (or heat) storage through sensible or latent heat, and by tracking the progression of phase change boundaries. The investigation also involved a detailed examination of the impact of factors such as melting temperature and latent heat. Additionally, the time required to reach the solidification limit point was analyzed in relation to the melting temperature or latent heat. Moreover, the heat lost during the charging cycle was also investigated.

2.2 Physical problem

To model the behavior of the building envelope during the PCM charging cycle, a wall structure consisting of three layers is taken into account, as illustrated in Figure 2.1. This wall comprises two solid concrete layers on both the exterior and interior, with a single PCM layer positioned at the center of the wall, where it undergoes solidification as part of the phase change process. The interaction between these distinct regions occurs at the interfaces, namely PCM2-solid in ($S_{in,in}$) and PCM-solid out ($S_{out,in}$). The interior convective condition assumes varying values, including both hot and cold, represented as (h_{in}, $T_{\infty,in}$), while the exterior convective condition remains consistently cold, specified as (h_{out}, $T_{\infty,out}$). To facilitate the solidification process in all numerical simulations, it is imperative to maintain the condition ($T_{\infty,out} < T_m$), where T_m represents the phase change temperature.

2.3 Modeling and governing equations

The simplifying assumptions employed in this study include:

- The volume of the multi-layered wall remains constant.
- Both solid layers act as passive conductors.
- Natural convection within the liquid PCM is not considered.
- Heat transfer is assumed to be one-dimensional.
- The PCM layer's envelope is assumed to be thin and to possess high thermal conductivity to disregard its thermal resistance.

- The temperature and heat transfer coefficient of the surrounding convective fluids are held constant.
- For the PCM layer, properties of the solid and liquid phases are assumed to be identical.

With these assumptions in place, the physical model is described by the unsteady one-dimensional heat equation

Subsequently, we refer to the inside concrete layer as 'solid in,' which is exposed to internal convective conditions, and to the outside concrete layer as 'solid out,' subjected to external cold convective conditions.

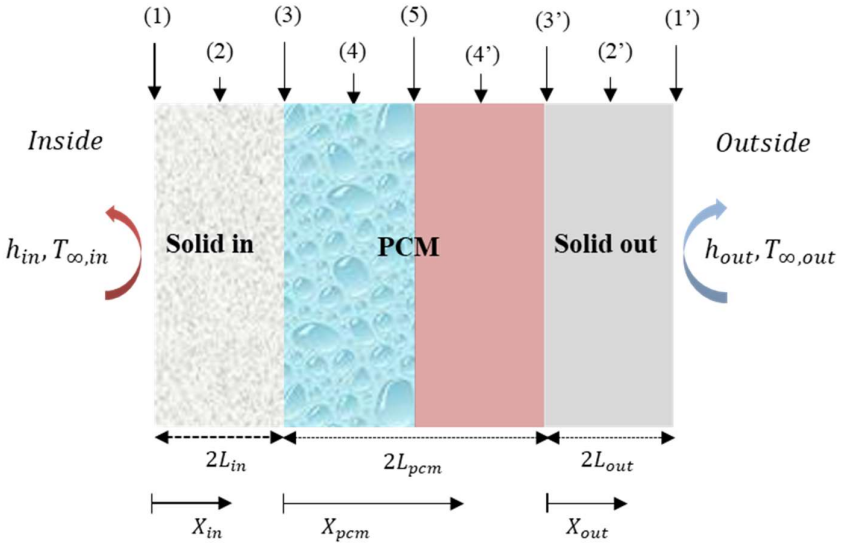

Figure 2.1 The wall's configuration, coordinate systems, and chosen surfaces

(1) $S_{in,out}$, (1') $S_{out,out}$, (2) $S_{in,1/2}$, (2') $S_{out,1/2}$, (3) $S_{in,in}$, (3') $S_{out,in}$, (4) $S_{pcm\ 1/4}$, (4') $S_{pcm\ 3/4}$, (5) $S_{pcm\ 1/2}$

Phase change material (PCM layer):

$$\begin{cases} Liquid\ region: T > T_m: \rho_l C_l \frac{\partial T_l}{\partial t} = \frac{\partial}{\partial x}\left(k_l \frac{\partial T_l}{\partial x}\right) \\ Solid\ region: T < T_m: \rho_s C_s \frac{\partial T_s}{\partial t} = \frac{\partial}{\partial x}\left(k_s \frac{\partial T_s}{\partial x}\right) \end{cases} \quad (2.1)$$

Solid in and out:

$$\rho_{in} C_{in} \frac{\partial T_{in}}{\partial t} = \frac{\partial}{\partial x}\left(k_{in} \frac{\partial T_{in}}{\partial x}\right) \tag{2.2}$$

$$\rho_{out} C_{out} \frac{\partial T_{out}}{\partial t} = \frac{\partial}{\partial x}\left(k_{out} \frac{\partial T_{out}}{\partial x}\right) \tag{2.3}$$

2.3.1 Initial and boundary conditions

At t = 0, all layers of the wall share the same initial temperature, signifying that the wall is in an initial state of thermal equilibrium. This initial condition is defined as follows:

$$T(x,0) = T_{in}(x_{in},0) = T_{out}(x_{out},0) = T_i \tag{2.4}$$

The boundary conditions on surfaces $(S_{out,out})$, $(S_{out,in})$, $(S_{in,in})$, $(S_{in,out})$ are presented below:

At the outer surface of the solid outer layer$(S_{out,out})$

$$-k_{out} \left.\frac{\partial T_{out}}{\partial x_{out}}\right|_{x_{out}=2L_{out}} = h_{out}\left(T_{out}|_{X_{out}=2L_{out}} - T_{\infty,out}\right) \tag{2.5}$$

At the inner surface of the solid outer layer $(S_{out,in})$

$$-k_s \left.\frac{\partial T}{\partial x}\right|_{x=2L_{pcm}} = -k_{out} \left.\frac{\partial T_{out}}{\partial x_{out}}\right|_{x_{out}=0} \tag{2.6}$$

At the inner surface of the solid inner layer $(S_{in,in})$

$$-k_s \left.\frac{\partial T}{\partial x}\right|_{x=0} = -k_{in} \left.\frac{\partial T_{in}}{\partial x_{in}}\right|_{x_{in}=2L_{in}} \tag{2.7}$$

At the outer surface of the solid inner layer $(S_{in,out})$

$$-k_{in}\frac{\partial T_{in}}{\partial x_{in}}\Big|_{x_{in}=0} = h_{in}\left(T_{\infty,in} - T_{in}|_{X_{in}=0}\right) \tag{2.8}$$

Where T is the temperature, K the thermal conductivity and x is axial position. The indexes (in) and (out) relate respectively to the inner or outer solid layer.

2.3.2 Dimensionless parameters

To facilitate the numerical analysis and identify the key physical factors that influence thermal heat transfer combined with phase change in the two PCM layers, dimensionless parameters are employed. The spatial coordinate and time are represented as per Arfi and Mezaache [81].

$$X_k = \frac{x_k}{L_k} \;\; ; \;\; \tau = \frac{\alpha_{1,s}}{L_{pcm}^2}t \tag{2.9}$$

The dimensionless time, denoted as τ, is established using the physical properties of the reference phase change material PCM. In this context, *x* represents the spatial coordinate, and the subscript '*k*' pertains to the solid mediums 'in' and 'out,' as well as PCM (where *k* can take values of *pcm, in*, or *out*). The dimensionless temperature and enthalpy are defined as follows [82]:

$$\theta = \frac{T - T_{\infty,out}}{T_i - T_{\infty,out}} \;\; ; \;\; H = \frac{\hbar}{\hbar_{ref}} \tag{2.10}$$

It's important to note that with this chosen dimensionless temperature, the melting temperature falls within the range $0 \leq \theta_{m,k} \leq 1$ (where $(T_{\infty,out} \leq T_{m,k} \leq T_i)$. The external cold convective temperature corresponds to $\theta_{\infty,out} = 0$ $(T = T_{\infty,out})$, while the internal convective temperature ranges from $\theta_{\infty,in} \geq 0$ $(T_{\infty,in} \geq T_{\infty,out})$. As a result, various physical scenarios can be examined:

$$\begin{cases} \theta_{\infty,in} = 0 \ (T_{\infty,in} = T_{\infty,out}) \\ \theta_{\infty,in} < 1 \ (T_{\infty,in} < T_i) \\ \theta_{\infty,in} = 1 \ (T_{\infty,in} = T_i) \\ \theta_{\infty,in} > 1 \ \ (T_{\infty,in} > T_i) \end{cases} \tag{2.11}$$

The primary dimensionless parameters that govern the system are the Biot number, Stefan number, and melting temperature, defined as follows:

$$Bi_{out} = \frac{h_{out} L_{out}}{k_{out}} \ ; \ Bi_{in} = \frac{h_{in} L_{in}}{k_{in}} \ ; \ Ste = \frac{\hbar_{ref}}{\rho_{ref} L_f} \tag{2.13}$$

$$\theta_m = \frac{T_m - T_{\infty,out}}{T_i - T_{\infty,out}} \ ; \tag{2.14}$$

These are the dimensionless heat capacity and thermal conductivity expressions

$$K_k = \frac{k_k}{k_{k,s}} \ ; \ C_k = \frac{c_k}{c_{k,s}} \tag{2.15}$$

2.3.3 Dimensionless heat equations

The model equations are written using the previously mentioned dimensionless parameters and assumptions. The issue of phase transition and moving fronts is solved for PCM layer using the enthalpy formulation variable. The generalized one-dimensional heat transfer equation describes how heat moves across the various wall layers [81,83]:

$$\frac{\partial H_k}{\partial \tau} = f_k \frac{\partial}{\partial X_k} \left(K_k \frac{\partial \theta}{\partial X_k} \right) \tag{2.16}$$

It is possible to conclude the following from the definition of the dimensionless time τ:

$$f_k = \frac{\alpha_{k,s}}{\alpha_{1,s}}\left(\frac{L_1}{L_k}\right)^2 \tag{2.17}$$

The correlations linking temperature and enthalpy for PCM materials are provided in accordance with the previous works [84, 85]:

$$H_k = \begin{cases} C_k(\theta_k - \theta_{m,k}) \\ C_k(\theta_k - \theta_{m,k}) + 1/Ste_k \end{cases} \text{ for } \begin{cases} \theta_k < \theta_{m,k} \\ \theta_k > \theta_{m,k} \end{cases} \tag{2.18}$$

$$\theta_k = \begin{cases} H_{k+}\theta_{m,k} \\ \theta_{m,k} \\ (H_k - 1/Ste_k)/C_k + \theta_{m,k} \end{cases} \text{ for } \begin{cases} H_k < 0 \\ 0 \le H_k \le 1/Ste_k \\ H_k > 1/Ste_k \end{cases} \tag{2.19}$$

The link between enthalpy and temperature is easily described for the two solid layers (outside) and (inside) by:

$$H_{out} = C_{out}\theta_{out}\ ; H_{in} = C_{in}\theta_{in} \tag{2.20}$$

2.3.4 Dimensionless thermal boundary conditions

At t = 0, all layers of the wall are initially at the same temperature, T_i, establishing thermal equilibrium within the wall. The initial dimensionless condition is expressed as $\theta(X_k, 0) = 1$. The boundary conditions are detailed below:

At the outer surface of the solid outer layer ($S_{out,out}$)

$$K_{out}\frac{\partial\theta}{\partial X_{out}}\bigg|_{X_{out}=2} = -Bi_{out}\theta_{out}|_{X_{out}=2} \tag{2.21}$$

At the inner surface of the solid outer layer ($S_{out,in}$)

$$K\frac{\partial\theta}{X}\Big|_{X=0} = \frac{L}{L_{out}}\frac{k_{out}}{k_{,s}}K_{out}\frac{\partial\theta}{X_{out}}\Big|_{X_{out}=2} \tag{2.22}$$

At the inner surface of the solid inner layer ($S_{in,in}$)

$$K\frac{\partial\theta}{X}\Big|_{X=2} = \frac{L}{L_{in}}\frac{k_{in}}{k_{,s}}K_{in}\frac{\partial\theta}{X_{in}}\Big|_{X_{in}=0} \tag{2.23}$$

At the outer surface of the solid inner layer ($S_{in,out}$)

$$K_{in}\frac{\partial\theta}{\partial X_{in}}\Big|_{X_{in}=0} = Bi_{in}\left(\theta|_{X_{in}=0} - \theta_{\infty,in}\right) \tag{2.24}$$

2.4 Numerical solution

The finite-volume method is employed to solve the physical model representing the phenomenon [86,87].

2.4.1 Mesh

The governing equations for the different layers of the wall are discretized using a uniform mesh for each layer. The spatial interval between two consecutive interior nodes is designated as ΔX, and it's important to note that each node serves as the central point within its respective control volume. The quantities specifying the total number of nodes and space steps for the solid inner layer, solid outer layer, and PCM layer are as follows: $(N_{in}, \Delta X_{in}), (N_{out}, \Delta X_{out}), (N, \Delta X)$, respectively. Half control volumes mark the starting and ending points of each layer. The gradient terms related to the time variable are discretized using an explicit scheme. Consequently, an examination of solution stability and mesh impact has led to the determination of an appropriate mesh configuration, where: $N_{in} = N = N_{out} = 81$.

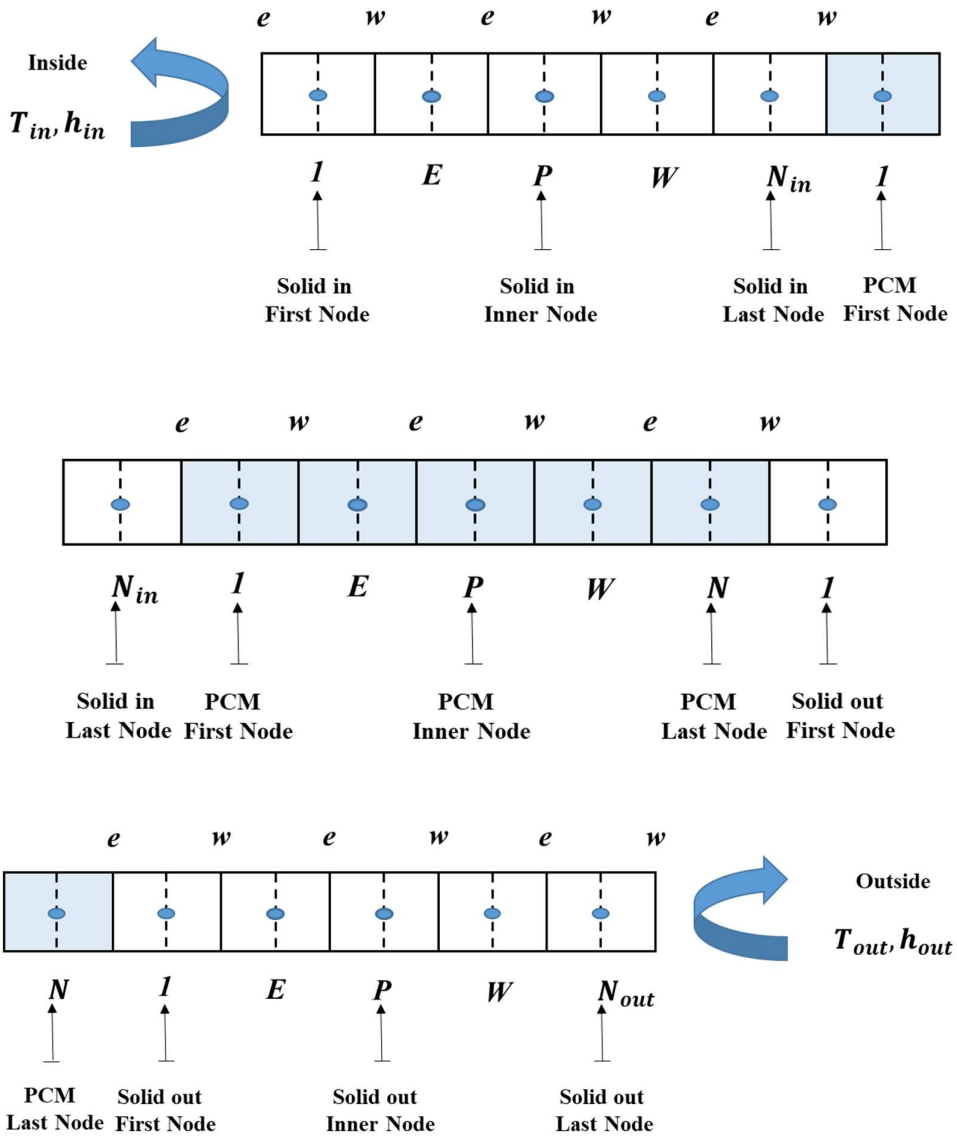

Figure 2.2 The multilayer wall mesh

2.4.2 Discretized equations of the inner solid layer

For an interior node

$$\theta_{in,j+1}^{P} = \theta_{in,j}^{P} + f_{in}\frac{\Delta\tau}{X_{in,w}-X_{in,e}}\left(K_{in,w}\frac{\theta_{in,j}^{W}-\theta_{in,j}^{P}}{\Delta X_{in}} - K_{in,e}\frac{\theta_{in,j}^{P}-\theta_{in,j}^{E}}{\Delta X_{in}}\right) \quad (2.25)$$

For the first node

$$\theta_{in,j+1}^{1} = \theta_{in,j}^{1} + f_{in}\frac{\Delta\tau}{X_{in,w}-X_{in,e}}\left(K_{in,w}\frac{\theta_{in,j}^{2}-\theta_{in,j}^{1}}{\Delta X_{in}} - Bi_{in}\left(\theta|_{X_{in}=0,j} - \theta_{\infty,in}\right)\right) \quad (2.26)$$

For the last node

$$\theta_{in,j+1}^{N_{in}} = \theta_{in,j}^{N_{in}} + f_{in}\frac{\Delta\tau}{X_{in,w}-X_{in,e}}\left(\frac{L_{in}}{L_{pcm}}\frac{k_s}{k_{in}}K_w\frac{\theta_j^1-\theta|_{X_{in}=2,j}}{\Delta X/_2} - K_{in,e}\frac{\theta_{in,j}^{N_{in}}-\theta_{in,j}^{N_{in}-1}}{\Delta X_{in}}\right) \quad (2.27)$$

2.4.3 Discretized equations of the PCM:

For an interior node

$$H_{j+1}^{P} = H_j^P + f\frac{\Delta\tau}{X_w-X_e}\left(K_w\frac{\theta_j^W-\theta_j^P}{\Delta X} - K_e\frac{\theta_j^P-\theta_j^E}{\Delta X}\right) \quad (2.28)$$

For the first node

$$H_{j+1}^{1} = H_j^1 + f\frac{\Delta\tau}{X_w-X_e}\left(K_w\frac{\theta_j^2-\theta_j^1}{\Delta X} - \frac{L_{pcm}}{L_{in}}\frac{k_{in}}{k_s}K_{in,w}\frac{\theta|_{X=0,j}-\theta_{in,j}^{N_{in}}}{\Delta X_{in}/_2}\right) \quad (2.29)$$

For the last node

$$H_{j+1}^{N} = H_j^N + f\frac{\Delta\tau}{X_w-X_e}\left(\frac{L_{pcm}}{L_{out}}\frac{k_{out}}{k_s}K_{out,w}\frac{\theta_{out,j}^1-\theta|_{X_{out}=0,j}}{\Delta X_{out}/_2} - K_e\frac{\theta_j^N-\theta_j^{N-1}}{\Delta X}\right) \quad (2.30)$$

2.4.4 Discretized equations of the outer solid layer:

For an interior node

$$\theta_{out,j+1}^{P} = \theta_{out,j}^{P} + f_{out}\frac{\Delta\tau}{X_{out,w}-X_{out,e}}\left(K_{out,w}\frac{\theta_{out,j}^W-\theta_{out,j}^P}{\Delta X_{out}} - K_{out,e}\frac{\theta_{out,j}^P-\theta_{out,j}^E}{\Delta X_{out}}\right) \quad (2.31)$$

For the first node

$$\theta_{out,j+1}^{1} = \theta_{out,j}^{1} + f_{out}\frac{\Delta\tau}{X_{out,w}-X_{out,e}}\left(K_{out,w}\frac{\theta_{out,j}^2-\theta_{out,j}^1}{\Delta X_{out}} - \frac{L_{out}}{L_{pcm}}\frac{k_s}{k_{out}}K_w\frac{\theta|_{X_{out}=0,j}-\theta_j^N}{\Delta X/_2}\right) \quad (2.32)$$

For the last node

$$\theta_{out,j+1}^{N_{out}} = \theta_{out,j}^{N_{out}} + f_{out}\frac{\Delta\tau}{X_{out,w}-X_{out,e}}\left(-Bi_{out}\theta_{out}|_{X_{out}=2} - K_{out}\frac{\theta_{out,j}^{N_{out}}-\theta_{out,j}^{N_{out}-1}}{\Delta X_{out}}\right) \quad (2.33)$$

2.4.5 Determination of the solid-liquid front position

For figuring out where the solid-liquid front located in the PCM layer, the following equation represents the total energy present in a control volume with center node i [83]:

$$H^i V_e^i = \left[(\theta^i - \theta_m)V_s^i + \left(C(\theta^i - \theta_m) + \frac{1}{Ste}\right)V_l^i\right] \quad (2.34)$$

In this context, V_e^i, V_s^i, V_l^i represent, the volume of the control volume, expressed in dimensionless units, the fraction of the PCM phase that is in a solid state and the fraction of the PCM phase that is in a liquid state, respectively. When a control volume experiences a phase change with $\theta^i = \theta_m$, the equation transforms to:

$$H^i V_e^i = (1/Ste)V_l^i \quad \text{or} \quad H^i = (1/Ste)V_l^i/V_e^i \quad (2.35)$$

The value of the enthalpy when the solidification front reaches the node i, is as follows:

$$H_c^i = 1/(2Ste) \quad (2.36)$$

This equation serves as a criterion for managing the front's position. To determine the solidification time at a specific node i, we examine two consecutive time instants, $\tau(j)$ and $\tau(j+1)$.

If $H^i(j+1) \le H_c \le H^i(j)$, then the solidification process takes place at a specific moment τ_{sol} within the time range of $\tau(j)$ to $\tau(j+1)$, and this moment can be determined using interpolation, $\tau(j) \le \tau_{\text{sol}} \le \tau(j+1)$.

The enthalpy is supposed to vary linearly across the whole time range. The equation for the solidification time of node i is: $\tau^i = (j+X)\Delta\tau$, Where X is determined through linear interpolation in the time domain, thus [83]:

$$X = \frac{H_c - H^i(j+1)}{H^i(j) - H^i(j+1)} \quad ; \quad \tau^i = \left(j + \frac{H_c - H^i(j+1)}{H^i(j) - H^i(j+1)}\right)\Delta\tau \quad (2.35)$$

2.5 Validation

By comparing it to the analytical benchmark provided by Neumann, the numerical solution is validated. (**Fig. 3**) [88], which addresses the solidification or melting process of a pure PCM semi-infinite media under conditions of insulation on all other sides, constant temperature on one surface, and assuming constant thermophysical characteristics (Stefan problem).

The following solution dictates the location of the phase change interface:

$$s(t) = 2\lambda\sqrt{\alpha_l t}$$

With λ is the root of the subsequent transcendental equation [89]:

$$\lambda \exp(\lambda^2)\, erf(\lambda) = Ste/\sqrt{\pi}$$

In order to adapt our design to the Stefan problem, it is assumed that both PCM layers are made of the same material and have constant physical characteristics $(\rho_l\,, c_l\,, k_l\,, \alpha_l)$. In order to address the Stefan problem, we select solid layers whose thicknesses and thermophysical properties enable only the PCM layer to be considered for heat transfer.[90]. Therefore, solid layers must have extremely low thicknesses, and thermal diffusivity must be sufficient high compared to PCM: $(L_{solid} \ll L_{pcm})$, $(\alpha_{solid} \gg \alpha_{pcm})$.

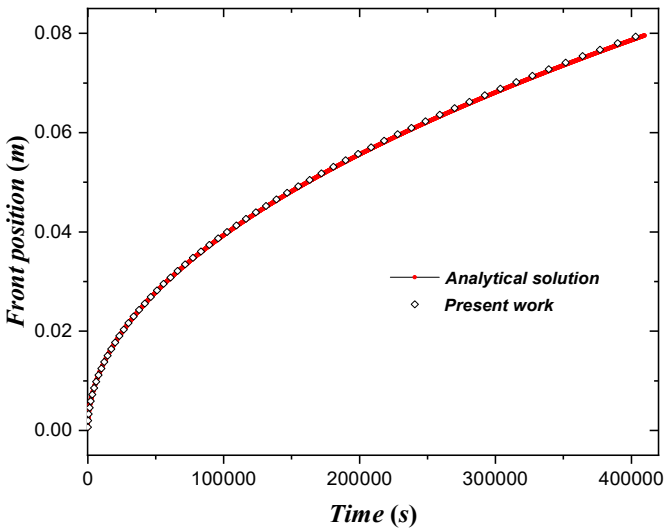

Figure 2.3 Phase change front position as function of time

2.6 Results and discussion

2.6.1 Studied cases

As a part of the PCMs charging cycle for the summer, three different scenarios represent a variety of building types and climate zones. For example, during the night and in certain climate zones, residential buildings' interior temperatures may be equivalent to the ambient temperature outside. ($T_{\infty,in} = T_{\infty,out}$), this situation is depicted by ($\theta_{\infty,in} = 0$). However, in certain buildings with significant thermal loads, such as in kitchens, baths, and other rooms, the ambient temperature inside the building is greater than the ambient temperature outdoors the building during the charging period (at night) ($T_{\infty,in} > T_{\infty,out}$), this situation is depicted by ($\theta_{\infty,in} = 1.2$). Additionally, after the running cycle and just before the charging cycle starts, the temperature throughout the wall might be close to the interior ambient temperature($T_{\infty,in} = T_{inital}$), in some climate zones, this case is represented by ($\theta_{\infty,in} = 1$).

2.6.2 Enthalpy and temperature evolution

The temperature and enthalpy evolution findings that are shown were achieved under the following conditions: The PCM layer's melting temperatures ranges between several values (θ_m), as well as the latent heat (Ste), ($Bi_h = Bi_c = 4.5$) . The two solid layers have the same thickness ($f_h = f_c = 4.43$).

2.6.2.1 Case 1 ($\boldsymbol{\theta_{\infty,in} = 0}$)

Figure 2.4 illustrates the evolution of enthalpy and temperature over dimensionless time for the three layers. The figure also highlights the phase change instances and positions throughout the wall, characterized by a rapid decline in enthalpy and a steady temperature which is the solidification point. This abrupt change signifies the solidification process, where the enthalpy becomes negative, indicating heat removal from the system. Conversely, during melting, the enthalpy becomes positive, signifying heat addition to the PCM. The sudden transition from positive to negative of the enthalpy indicates the phase change point reaching (and from negative to positive for melting), resulting in the transformation of the matter from liquid to solid state.

The PCM generates heat (stores cold) through latent heat during these phase change times. A considerable drop in the material's temperature outside of these times indicates that there is

stored cold by sensible heat. It is crucial to keep in mind that sensible heat corresponds to the thermal energy needed to modify the temperature of a material without altering its phase. Conversely, latent heat represents the amount of thermal energy needed to trigger a phase transition without the temperature of the material. Furthermore, the figure demonstrates that the entire PCM layer achieves full solidification, indicating that the entire layer undergoes times of storing cold through latent heat. Additionally, the temperature and enthalpy evolution shows a similar behavior in the symmetrical PCM points relative to the middle of the wall. Due to the symmetry of boundary conditions, geometry, and other thermophysical characteristics like ($\theta_{\infty,in} = \theta_{\infty,out} = 0$, $Bi_{in} = Bi_{out} = 4.5$), this resemblance is shown.

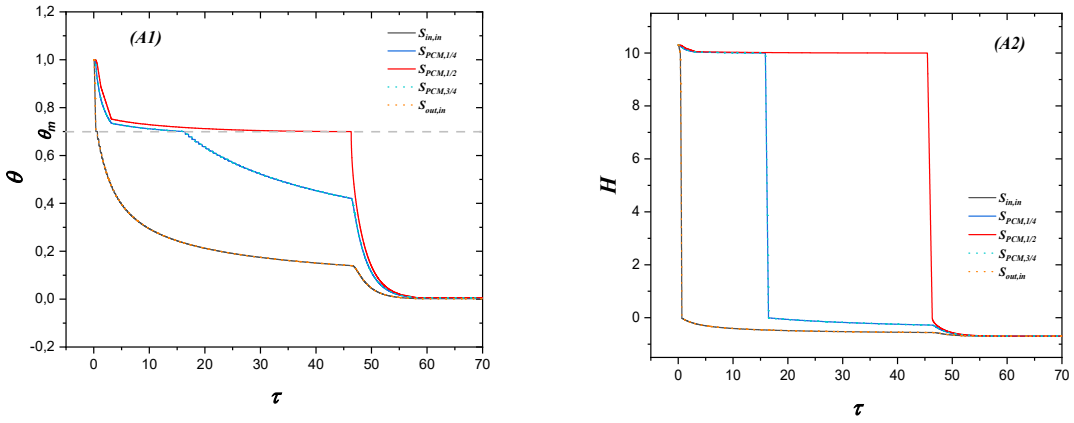

Figure 2.4 Enthalpy and temperature evolution for $(\boldsymbol{\theta_{\infty,in} = 0})$

2.6.2.2 Case 2 ($\boldsymbol{\theta_{\infty,in} = 1}$)

Based on Figure 2.5, it is evident that the combination of outside cold excitation and initial temperature (which is higher than the solidification temperature $\theta_m = 0.7$) drives to the temperature gradient shrinking down along the PCM layer. As a result, the PCM regions close to the outside reach the phase change point more quickly than other regions. However, the solidification point is not reached within the region near the inside ambient.

As the PCM undergoes partial solidification, the utilization of latent heat for cold storage is only partially effective. The portion that doesn't undergo a phase transition retains its liquid

phase and preserves cold by sensibly lowering its temperature. Then, As a result of these dual excitations, specific areas can attain the phase change temperature, allowing them to store cold through a combination of latent and sensible ways. In contrast, some areas fail to achieve the solidification temperature, thus relying solely on sensible temperature decrease for cold storage.

Additionally, it is evident that regions with the ability to reach the phase change threshold undergo a phase transition process during which the temperature takes a constant value for certain duration. This phase change also influences the temperature behavior of nearby regions, causing them to maintain a constant temperature for a brief duration, despite the fact that they do not attain the phase transition temperature, as indicated by the enthalpy evolution, which affirms the absence of any phase transition in those areas. The similarity in this impact can be likened to the temperature behavior observed at the location $S_{pcm,1/4}$ when τ = 150. However, the impact of phase change diminishes gradually as one moves away from these regions, as shown in points $S_{in,\,in}$ Figure 4 (A1).

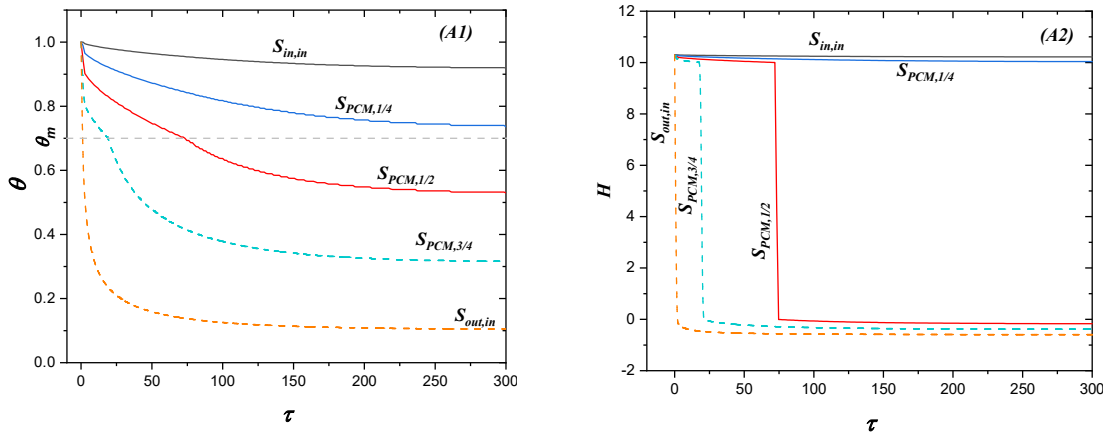

Figure 2.5 Enthalpy and temperature evolution for $(\boldsymbol{\theta_{\infty,in} = 1})$

2.6.2.3 Case 3 $(\boldsymbol{\theta_{\infty,in} = 1.2})$

Based on Figure 2.6, Comparable findings can be deduced, as previously discussed, in the context of stimulation $(\theta_{\infty,in} = 1)$. It is worth noting that while the PCM layer near the outside excitation $(\theta_{\infty,out} = 0)$ is capable of reaching the solidification point, the other part

of the layer remains unable to reach it, thus maintaining its liquid state. In the zone closer to the inside ambient, The impact of the external cold ambient is offset by the effect of the internal hot environment($\theta_{\infty,in} = 1.2$). Moreover, the temperature and enthalpy plots within that area demonstrate heat storage through a sensible increase in temperature. Conversely, the section situated between these two areas preserve cold by sensibly reducing the temperature.

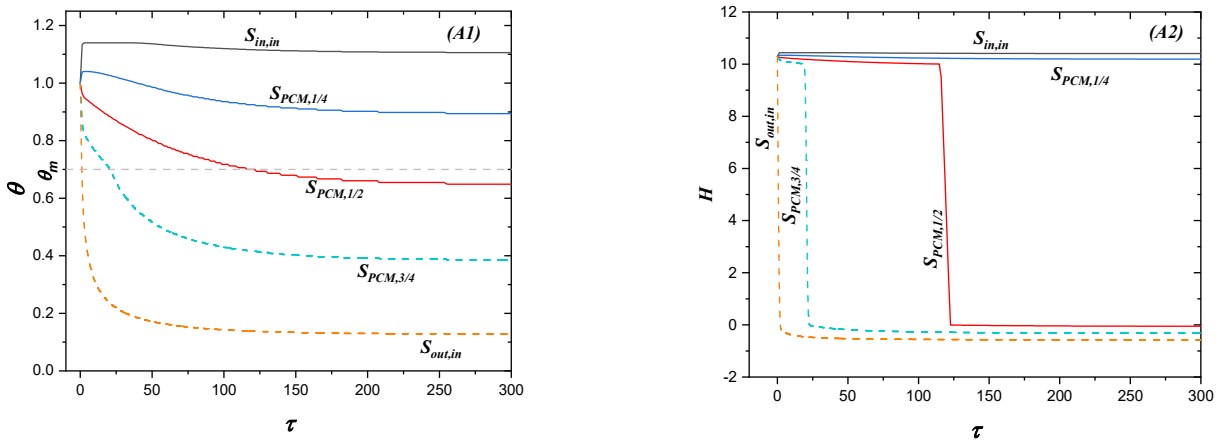

Figure 2.6 Enthalpy and temperature evolution for $(\boldsymbol{\theta_{\infty,in} = 1.2})$

Additionally, in this case, the PCM layer experiences partial solidification, enabling it to store cold through both sensible and latent ways. Furthermore, it is noted that the phase change process affected the temperature behavior within the neighboring zone, while the propagation of this effect diminishes as we depart from these locations. This decrease is ascribed to the impact of external ambient.

2.6.3 Front kinetic

2.6.3.1 Melting temperature effect

The number of phase transition interfaces is shown in Fig. 6 to be dependent on the external ambient temperature. Similar to Figure 2.7(A1), in the case of symmetry where ($\theta_{\infty,in} = \theta_{\infty,out} = 0$), two phase change fronts are observed at the interfaces of the PCM with the solid outside and solid inside. Both fronts initiate their movement simultaneously towards the interface of the PCM medium (S_m), which acts as the meeting point. As a result, complete solidification is attained. It is noteworthy that an increase of the solidification temperature θ_m

reduces the needed time for both fronts in order to achieve the meeting point at the center of the PCM. This phenomenon can be explained by considering the influence of the diffusion of external and internal cold excitations within the PCM layer, leading to a temperature gradient. This temperature gradient facilitates the faster achievement of the solidification process for higher solidification temperatures.

Based on Figure 2.7(B1), the plotted curves representing the kinetics of the phase transition interfaces indicate that the process of solidification is only partially finished. This is because the building envelope is exposed to a single cold excitation, specifically applied to the outer surface, resulting in the presence of only one phase change front. The solidification process occurs within the PCM layer, starting from the PCM-solid interface on the outer side and progressing towards the PCM-solid interface on the inner side, driven by the impact of the cold excitation originating from the outside. In which($\theta_{\infty,in} = 1$) indicating that the wall initial temperature and the internal temperature are the same, where both are above the solidification point, the solidification process takes place. This is different from the scenario where ($\theta_{\infty,in} = 0$). Additionally, it is worth noting that increasing the solidification temperature enables the phase change front to penetrate deeper into the PCM layer.

Referring to Figure 2.7(C1), it presents similar observations as mentioned earlier for the case of $\theta_{\infty,in} = 1$. Additionally, in this instance, the process of solidification in the Phase change material (PCM) layer is less evident. The phase change front fails to reach the inner half of the PCM layer, except in the cases where $\theta_m = 0.7$, and $\theta_m = 0.8$, which is attributed to the presence of a hot excitation $\theta_{\infty,h} = 1.2$ that halts the advancement of the phase change front.

2.6.3.2 Stefan number effect

For situations when boundary conditions exhibit symmetry, specifically when ($\theta_{\infty,in} = \theta_{\infty,out} = 0$), Figure 2.7(A2) demonstrates a corresponding symmetry in the kinetics of the phase change fronts. At the PCM-Solid in and PCM-Solid out interfaces, two fronts are noticeable, influenced by the outside cold excitations. These fronts initiate their movement towards the middle of the PCM layer (Sm), which serves as the meeting point, ensuring the whole PCM layer solidification. It is worth noting that higher Stefan numbers ensures a more rapidly full solidification.

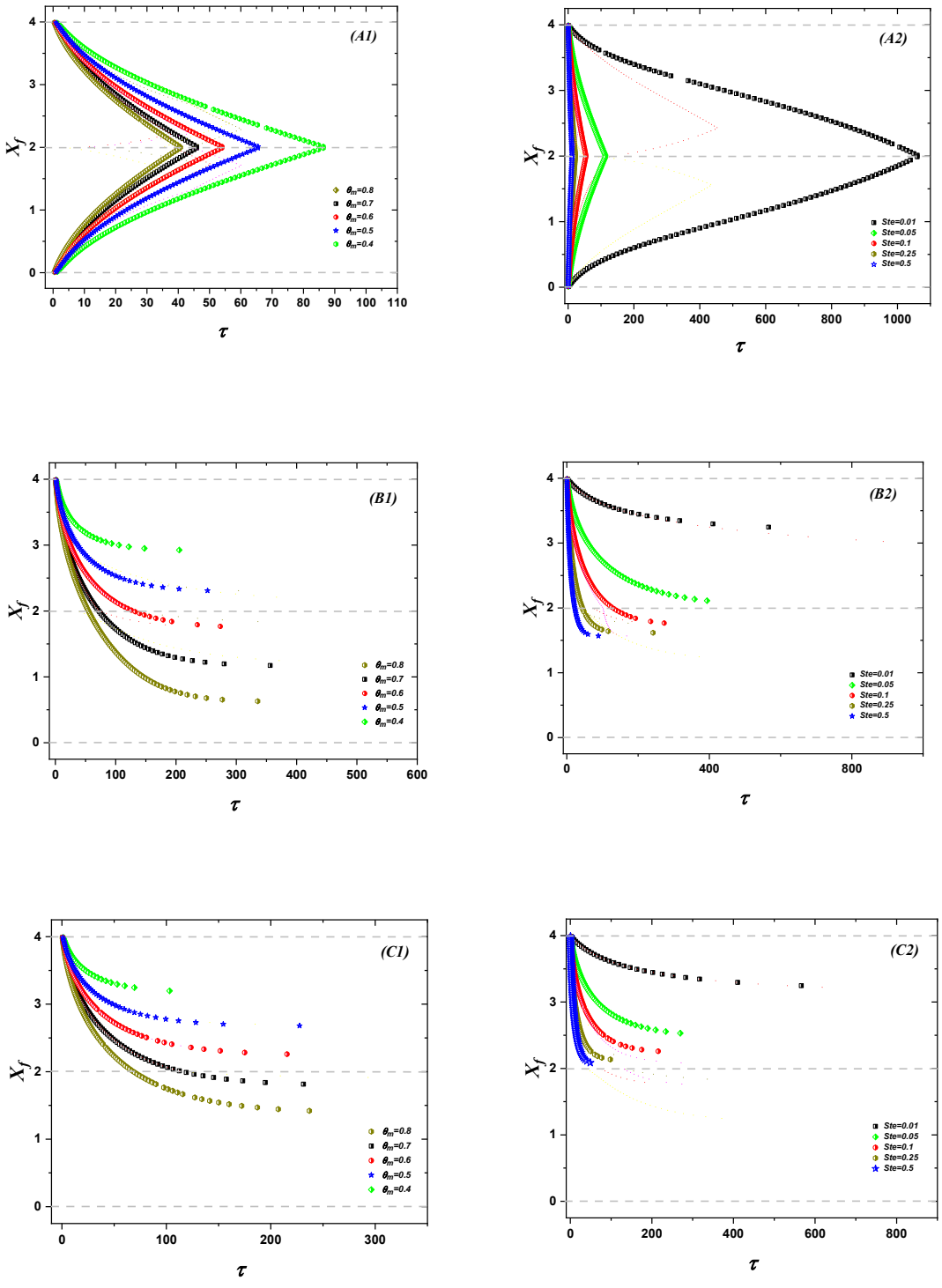

Figure 2.7 Evolution of front positions for various melting temperatures and Stefan numbers (A1, A2) $\boldsymbol{\theta_{\infty,in} = 0}$, (B1, B2) $\boldsymbol{\theta_{\infty,in} = 1}$, (C1, C2) $\boldsymbol{\theta_{\infty,in} = 1.2}$

This finding can be linked to how the Stefan number is defined, expressing the proportion of sensible heat to latent heat. An inferior Stefan number implies a higher proportion of latent energy storage relative to sensible energy storage, while a higher Stefan number implies the opposite. Thus, in situations where the Stefan number is small, a substantial quantity of heat must either be accumulated or dissipated to facilitate the phase change process, necessitating more time.

Figure 2.7(B2) illustrates the presence of a single solidification front, originating from the PCM-Solid out interface near to the outside excitation (cold), and moving towards the PCM-Solid in interface. It's crucial to emphasize that the solidification operation within the PCM layer remains incomplete, as the phase transition point within the Phase change material (PCM) region close to the inside is not reached. As mentioned earlier, a low Stefan number indicates the need to dissipate a significant quantity of energy to achieve the solidification temperature. Conversely, a higher Stefan number enables the phase change front to penetrate deeper into the PCM layer, resulting in faster solidification. The lower latent energy storage relative to sensible energy storage is expressed by the higher Stefan numbers. As a result, a quick solidification process takes place, allowing a larger segment of the PCM to reach the solidification threshold.

In Figure 2.7(C2), it can be observed that the PCM region adjacent to the inside, in close proximity to the PCM-Solid in interface, and due to the influence of the hot stimulus($\theta_{\infty,in} = 1.2$) , it remains unaffected by the solidification process. Within this region, the impact of the cold stimulus coming from the opposing direction is attenuated, resulting in incomplete solidification process of the phase change material (PCM) layer. As stated earlier, a higher Stefan number enables faster solidification of the PCM, leading to a larger portion of solidified PCM. Conversely, the higher latent energy storage is indicated by a lower Stefan number. The Stefan number reflects the proportion between sensible energy storage and latent energy storage, with an inverse relationship to the latent heat. Consequently, a higher Stefan number implies a lower latent heat content. When the Stefan number is high, indicating low latent heat, the material demands less heat release to attain the solidification point in contrast to a low Stefan number, indicating high latent heat. This results in a faster solidification process with a larger amount of solidified material.

2.6.4 Solid fraction

When $\theta_{\infty,in} = 0$, It was noted that the solid portion of the phase change material (PCM) layer undergoes complete solidification, regardless of the melting temperature θ_m and Stefan number Ste. This finding pertains to the presence of symmetric boundary conditions where two external cold excitations exist.

2.6.4.1 Melting temperature effect

In the scenario where $\theta_{\infty,in} = 1$ (refer to Figure 2.8), it is anticipated that the solid fraction is highest when the melting temperature is also highest. This correlation can be attributed to the gradient of the temperature. In the region close to internal ambient $\theta_{\infty,in} = 1$, in order to attain the solidification threshold, a higher phase change temperature is required. Conversely, in the region adjacent to the external cold ambient, a lower phase change temperature is enough to guarantee solidification.

In the scenario where $\theta_{\infty,in} = 1.2$ (refer to Figure 2.8), due to the presence of a hot excitation, the solidification process does not occur in the PCM region adjacent to the inside ambient. However, in the other PCM region, it is seen that the solid proportion increases as the melting temperature is raised.

2.6.4.2 Stefan number effect

For $\theta_{\infty,in} = 1$, As illustrated in Figure 2.8, the solid fraction increases with increasing Stefan number, which means decreasing the latent heat, where the zone close to inside ambient couldn't reach the solidification process. As mentioned earlier, a low Stefan number indicates the need to dissipate a significant quantity of energy to achieve the solidification temperature. Conversely, a higher Stefan number enables the phase change front to penetrate deeper into the PCM layer.

In the scenario where $\theta_{\infty,in} = 1$, as shown in Figure 2.8, the solid fraction exhibits an upward trend as the Stefan number increases (which means a decrease in latent heat). This implies that the solidification process fails to reach the region near the inside ambient. As mentioned earlier, a low Stefan number signifies the requirement of releasing a substantial amount of energy to attain the solidification point. Conversely, a higher Stefan number allows the phase change front to penetrate further into the PCM layer.

In the case where $\theta_{\infty,in} = 1.2$, as depicted in Figure 2.8, the solid fraction increases as the Stefan number rises. This is attributed to the presence of a hot excitation ($\theta_{\infty,in} = 1.2$). However, the PCM region neighboring the inside ambient, particularly near the interface between PCM and solid, does not undergo solidification. It is worth noting that the cold excitation dissipates earlier compared to the previous scenarios of $\theta_{\infty,in} = 0$ and $\theta_{\infty,in} = 1$, providing less solid fraction.

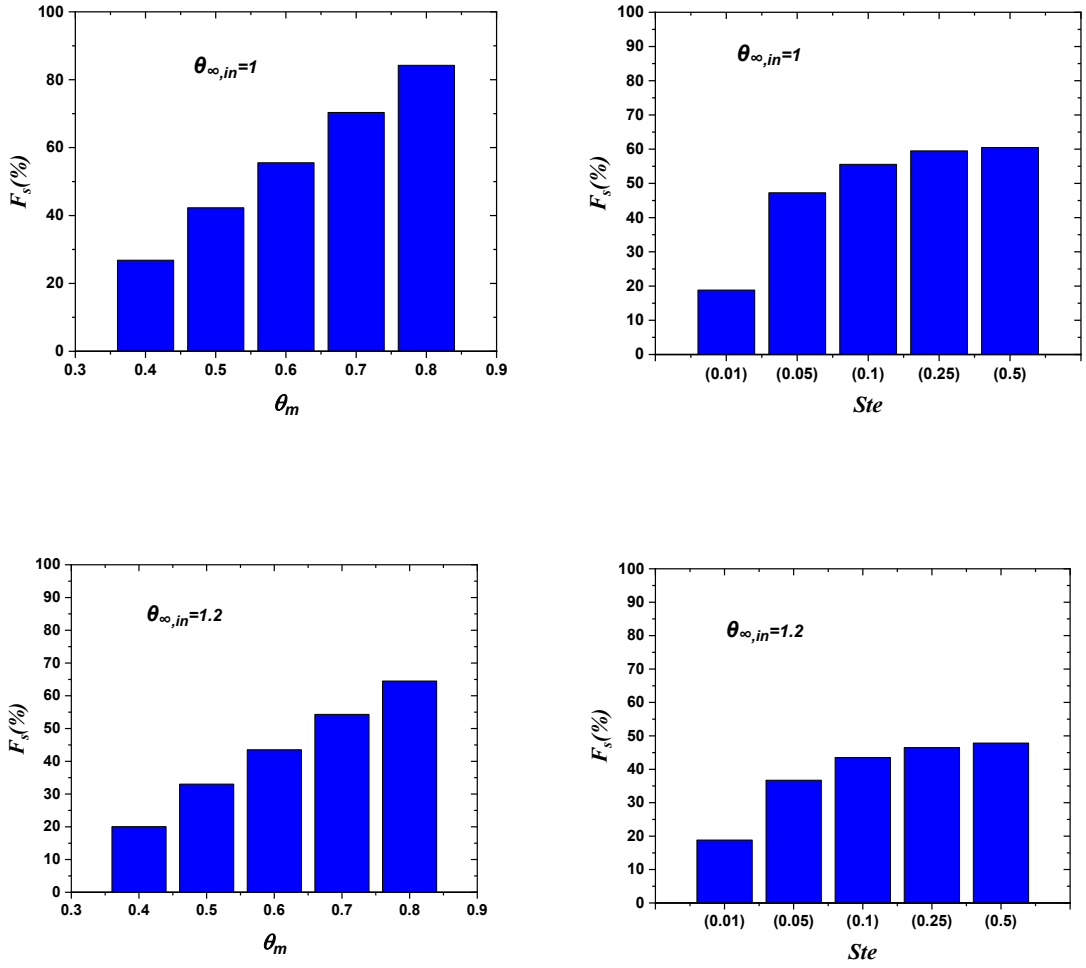

Figure 2.8 Variation in solid fraction based on melting temperatures and Stefan numbers for various combinations ($\boldsymbol{\theta_{m1}, \theta_{m2}}$) and ($Ste_1$, Ste_2)

2.6.5 Time needed in order to reach the limit of solidification

2.6.5.1 Melting temperature effect

In the scenario where $\theta_{\infty,in} = 0$, as Table 2.1 indicates , the required time for reaching the limit point of the solidification for the PCM layer decreases as the melting temperature θ_m increases. The presence of symmetry between the external and internal excitations ($\theta_{\infty,in} = \theta_{\infty,out} = 0$) enables complete solidification to be achieved, resulting in a consistent solid fraction of 100% regardless of the melting temperature. Consequently, reducing the melting temperature causes a delay in the attainment of the solidification process.

For the cases where $\theta_{\infty,in} = 1$ and $\theta_{\infty,in} = 1.2$, as indicated in Table 2.1, it is observed that the required time to reach the solidification limit for the PCM layer does not exhibit a clear correlation with the variation in PCM melting temperature. This lack of correlation can be explained by the different solid fractions achieved for each melting temperature. Consequently, raising the PCM melting temperature may result in either an increase or a shrinking down in the required time for reaching the limit point of the solidification. In contrast, within the previous case of $\theta_{\infty,in} = 0$ where solidification was completed (with the same limit point regardless of the melting temperature), this variability was not observed.

2.6.5.2 Stefan number effect

In the situation when $\theta_{\infty,in} = 0$, Table 2.2 illustrates the raising up of Stefan number effect on the time required to reach the solidification limit point within the phase change material (PCM) layer. The data indicates a diminishing of the required time as the Stefan number (Ste) increases. As far as the Stefan number depicts the proportion of sensible heat (cold) storage to latent heat (cold) storage. Therefore, an increase in the Stefan number signifies a higher proportion of sensible heat (cold) storage relative to latent heat (cold) storage. This, in turn, implies a reduction in the energy needed to achieve the solidification temperature. As a result, a decrease in the time required to achieve full solidification can be observed.

For $\theta_{\infty,in} = 1$ and $\theta_{\infty,in} = 1.2$, according to Table 2.2, and as far as the solidification of the PCM layer is not completed whatever Stefan number, where each Stefan number provide a different solid fraction, the needed time for reaching the solidification limit point also this time does not exhibit a clear correlation with the variation of Ste,

Table 2-1 Duration required to reach the solidification limit as a function of melting temperatures

θ_m	$\theta_{\infty,in} = 0$	$\theta_{\infty,in} = 1$	$\theta_{\infty,in} = 1.2$
	$\Delta\tau$	$\Delta\tau$	$\Delta\tau$
0.8	40.59	335.50	236.96
0.7	45.36	282.96	112.22
0.6	53.26	141.14	214.82
0.5	64.52	251.24	226.58
0.4	86.35	141.14	103.09

Table 2-2 Duration required to reach the solidification limit as a function of Stephan numbers

Ste	$\theta_{\infty,in} = 0$	$\theta_{\infty,in} = 1$	$\theta_{\infty,in} = 1.2$
	$\Delta\tau$	$\Delta\tau$	$\Delta\tau$
0.01	1058.02	564.24	564.24
0.05	112.96	393.60	269.65
0.1	53.26	141.14	214.82
0.25	22.37	242.15	98.15
0.5	11.71	66.05	48.40

2.6.6 Starting Time of solidification

2.6.6.1 Melting temperature effect

Table 2.3 clearly demonstrates that in the three cases of $\theta_{\infty,in} = 0$, $\theta_{\infty,in} = 1$, and $\theta_{\infty,in} = 1.2$, when the melting temperature θ_m decreases, the starting time of the solidification process within the PCM layer increases. This can be explained by the fact that lowering θ_m causes the gradient of the temperature, that carried out by the outside and inside excitations, to require more time in order for achieving the temperature of solidification.

Table 2-3 Starting time of solidification as function of melting temperatures

θ_m	$\theta_{\infty,in} = 0$	$\theta_{\infty,in} = 1$	$\theta_{\infty,in} = 1.2$
	τ_i	τ_i	τ_i
0.8	0.41	0.41	0.41
0.7	0.54	0.54	0.54
0.6	0.72	0.72	0.72
0.5	0.96	0.96	0.96
0.4	1.33	1.34	1.35

2.6.6.2 Stefan number effect

In the cases of $\theta_{\infty,in} = 0$, $\theta_{\infty,in} = 1$, and $\theta_{\infty,in} = 1.2$, as indicated by Table 2.4, it is evident that an increase in the Stefan number (Ste) leads to a reduction in the starting time of the solidification process. The higher Stefan number (Ste) corresponds to a lower proportion of latent heat (cold) storage in comparison to sensible heat (cold) storage, resulting in an earlier initiation of the solidification process.

Table 2-4 Starting time of solidification as function of Stefan numbers

Ste	$\theta_{\infty,in} = 0$	$\theta_{\infty,in} = 1$	$\theta_{\infty,in} = 1.2$
	τ_i	τ_i	τ_i
0.01	2.2	2.20	2.20
0.05	0.86	0.86	0.86
0.10	0.72	0.72	0.72
0.25	0.62	0.62	0.62
0.50	0.57	0.57	0.57

2.6.7 Heat lost during charging cycle

The total heat lost during charging cycle period is defined as the instantaneous dimensionless heat flux integrated over the time period [91] :

$$Q = \int_0^{\Delta\tau} \dot{Q}\ d\tau \tag{2.36}$$

The definition of the dimensionless heat flux at the external surface of the wall in an instantaneous context is provided by:

$$\dot{Q} = -Bi_{out}\ \ \theta_{out}|_{X_{out}=2} \tag{2.37}$$

In this section, it is presupposed that both PCM layers have completely melted during a prior operational cycle; All points of the wall have an identical initial temperature $\theta_i = 1$, which is equivalent to the ambient temperature on the inside $\theta_{\infty,in} = 1$. The estimated duration of the charging cycle is calculated using a 24-hour real daily period, assuming that the charging cycle takes approximately half a day to complete.

2.6.7.1 Melting temperature effect

Based on Figure 2.9, it is observed that using a charging period of half-day, equivalent to Δτ=57, the case of *PSM* where Phase Change Material is absent in the wall demonstrates the lowest amount of heat released throughout the charging cycle. This can be attributed to the limited amount of heat stored in a sensible manner during the operating cycle, as opposed to the other cases where phase change occurs, resulting in heat being stored (or released) in a latent manner within the operating cycle. Furthermore, it is noteworthy that the reduction in the melting temperature (θ_m) of the phase change material (PCM) layer leads to a decrease in heat loss. For instance, the case with $\theta_m = 0.8$ releases an additional 20% of heat compared to the reference case of PSM. Similarly, the case with $\theta_m = 0.4$ achieves an 11% increase. This can be attributed to the significant decrease in solidification process attainment with a decrease in the solidification temperature of the phase change material (PCM) layer, leading to a decrease in the cold storage by latent heat quantity. In comparison to the cold storage by

sensible heat, the cold storage by latent heat offers the benefit of higher energy density. Therefore, by reducing the phase change temperature of the phase change material (PCM), the quantity of emitted heat diminishes.

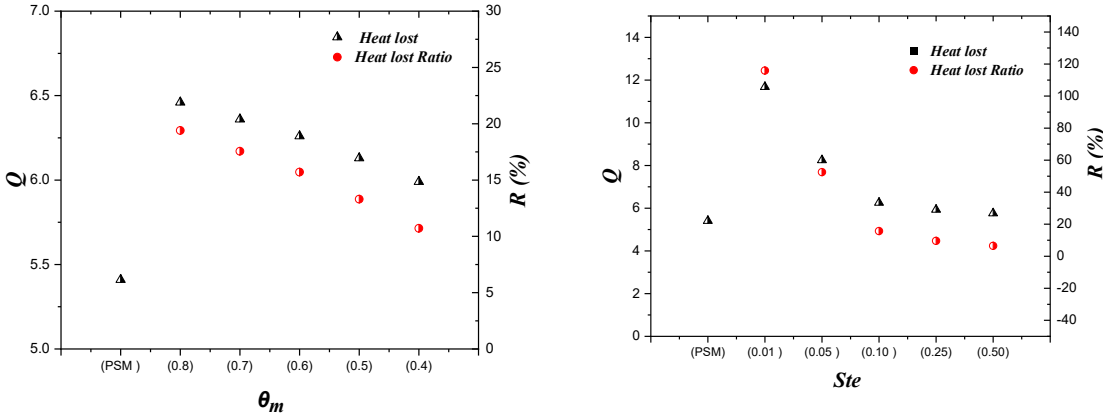

Figure 2.9 Heat Loss in the Charging Cycle and the Heat Release Ratio in relation to Melting Temperature and Stefan Number $(\boldsymbol{\theta_m})$ and (*Ste*)

2.6.7.2 Ste number effect

Figure 2.9 depicts that the case with a PCM layer exhibiting high latent heat (Ste=0.01) exhibit a higher amount of released heat over the charging cycle in comparison to the baseline scenario, PSM. Despite having a lower solid fraction than other cases, this high latent heat (Ste=0.01) demonstrates a supplementary heat release ratio of 120% in comparison to the baseline scenario, PSM. Conversely, cases with low latent heat of the phase change layer (Ste=0.25, 0.5) generally show a lower amount of released heat throughout a charging period lasting half a day compared to the first case (Ste=0.01), with a supplementary heat release ratio of 10% and 5% respectively, in comparison to the baseline scenario, PSM. This can be attributed to the restricted quantity of heat stored throughout the operational period when the PCM layer has low latent heat (Ste=0.25, 0.5) compared to the case with high latent heat (Ste=0.01) and the reference case PSM. Although heat storage in the reference case PSM occurs in a sensible manner, cases involving phase change store heat in a latent manner (either low or high depending on the PCM's latent heat). Additionally, reducing the latent heat of the PCM layer results in a reduction in both the solid fraction and the quantity of discharged heat.

2.7 Conclusion

This section seeks to demonstrate the influence of the PCM layer on the overall behavior of the building envelope under various conditions (varying in building type and climate zone) during the charging cycle. The following observations were made:

The evaluation of solid fraction reveals the following trends:

- The solid fraction increases when the melting temperature is increased. For instance:
  - When the indoor temperature exceeds the outdoor ambient temperature ($T_{\infty,in} > T_{\infty,out}$), the solid fraction was 80% for $\theta_m = 0.8$, but it decreased to 37% for $\theta_m = 0.4$.
  - Similarly, when the indoor temperature is equal to the initial wall temperature ($T_{\infty,in} = T_{inital} > T_{\infty,out}$), the solid fraction was 64% for $\theta_m = 0.8$, but it decreased to 20% for $\theta_m = 0.4$.
- It is noted that the solid fraction increases with increasing Stefan number, which means increases with decreasing the latent heat, for example:
  - When the indoor temperature exceeds the outdoor ambient temperature ($T_{\infty,in} > T_{\infty,out}$), the solid fraction reaches 58% for $= 0.5$, while when $Ste = 0.01$ the solid fraction was 18% .
  - When the indoor temperature is equal to the wall initial temperature ($T_{\infty,in} = T_{inital} > T_{\infty,out}$), for $Ste = 0.5$ the solid fraction was 47% , however for $Ste = 0.01$, the solid fraction was 18% .

When examining the time required to reach the solidification limit point, it is observed that:

- For ($T_{\infty,in} = T_{\infty,out}$), raising the melting temperature leads to diminishing the required time to reach the limit point of solidification, however, when ($T_{\infty,in} > T_{\infty,out}$) or ($T_{\infty,in} = T_{inital} > T_{\infty,out}$) it is observed that the required time to reach the solidification limit for the PCM layer does not exhibit a clear correlation with the variation in PCM melting temperature.
- While the time needed to reach the solidification limit point increases with increasing the latent heat when ($T_{\infty,in} = T_{\infty,out}$), it does not exhibit a clear

correlation with the variation of Ste when ($T_{\infty,in} > T_{\infty,out}$) or ($T_{\infty,in} = T_{inital} > T_{\infty,out}$).

The investigation of the heat released ratio reveals that:

- An increase in θ_m results in higher heat loss, as seen in the case of $\theta_m = 0.8$, the wall released a supplementary heat ratio of 20% in comparison to the baseline scenario, PSM. While, for $\theta_m = 0.4$ it achieves 11%.

- Additionally, decreasing the latent heat of the phase change (PCM) layer results in a decrease in both the solid fraction and the released heat quantity.

The latent heat of the PCM layer leads to a decrease in the amount of released heat as well as the solid fraction. For instance, the high latent heat (Ste=0.01) shows a supplementary heat ratio of 120% in comparison to the baseline scenario, PSM. Conversely, cases with low latent heat of the phase change material (PCM) layer (Ste=0.25, 0.5) generally show a lower amount of released heat throughout a charging period lasting half a day compared to the first case (Ste=0.01), with supplementary heat release ratios of 10% and 5%, respectively.

Chapter 3 : Examining the Performance of Building Envelope Containing PCM Layer during Charging/Discharging Cycles

3.1 Introduction

This section delves into an in-depth analysis aimed at addressing situations where a single PCM building envelope is not functioning optimally, through studying the processes of solidification/fusion, by exhibiting the kinetics of phase change fronts, the time taken for charging and discharging periods, along with the active fraction of the phase change material (PCM) in operation and the average heat transfer experienced during one complete cycle, considering a variety of melting temperatures.

3.2 Problems and methods

To simulate the building envelope's behavior with phase change material (PCM), we examined a wall comprising three layers (as depicted in Fig. 1). There are two concrete layers on the exterior and interior, while the PCM layer is positioned in the middle of the building envelope, experiencing a phase change. The interaction between these different sections occurs at the interfaces known as PCM-solid in ($S_{in,in}$) and PCM-solid out ($S_{out,in}$). The outer surface of the wall experiences a convective heat exchange with a temperature that varies sinusoidally in accordance with the season (summer or winter) (T_{out}, h_{out}), while the inner surface interacts with the indoor environment at a consistent temperature (T_{in}, h_{in}). The HVAC system is employed to regulate and maintain the indoor ambient temperature at the designated thermostat set point.

3.3 Modeling and governing equations

The simplifying assumptions employed in this study include:

- The volume of the multi-layered wall remains constant.
- Both solid layers act as passive conductors.
- Natural convection within the liquid PCM is not considered.
- Heat transfer is assumed to be one-dimensional.
- The PCM layer's envelope is assumed to be thin and to possess high thermal conductivity to disregard its thermal resistance.
- The temperature and heat transfer coefficient of the surrounding convective fluids are held constant.

- For the PCM layer, properties of the solid and liquid phases are assumed to be identical.

With these assumptions in place, the physical model is described by the unsteady one-dimensional heat equation

Subsequently, we refer to the inside concrete layer as 'solid in,' which is exposed to internal convective conditions, and to the outside concrete layer as 'solid out,' subjected to external cold convective conditions.

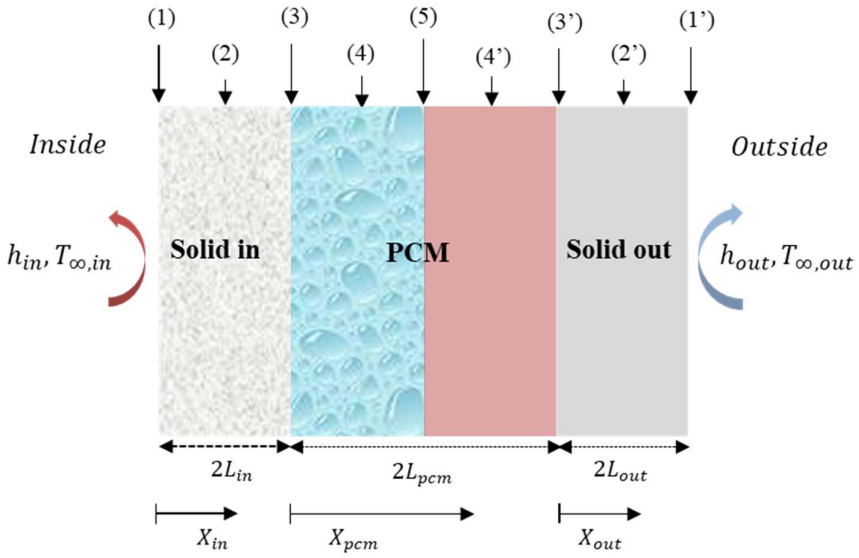

Figure 3.1 The wall geometry

(2) $S_{in,out}$, (1') $S_{out,out}$, (2) $S_{in,1/2}$, (2') $S_{out,1/2}$, (3) $S_{in,in}$, (3') $S_{out,in}$, (4) $S_{pcm\ 1/4}$, (4') $S_{pcm\ 3/4}$, (5) $S_{pcm\ 1/2}$

Phase change material (PCM) layer:

$$\begin{cases} Liquid\ region: T > T_m: \rho_l C_l \frac{\partial T_l}{\partial t} = \frac{\partial}{\partial x}\left(k_l \frac{\partial T_l}{\partial x}\right) \\ Solid\ region: T < T_m: \rho_s C_s \frac{\partial T_s}{\partial t} = \frac{\partial}{\partial x}\left(k_s \frac{\partial T_s}{\partial x}\right) \end{cases} \quad (3.1)$$

Solid in and solid out:

$$\rho_{in} C_{in} \frac{\partial T_{in}}{\partial t} = \frac{\partial}{\partial x}\left(k_{in} \frac{\partial T_{in}}{\partial x}\right) \quad (3.2)$$

$$\rho_{out} C_{out} \frac{\partial T_{out}}{\partial t} = \frac{\partial}{\partial x}\left(k_{out} \frac{\partial T_{out}}{\partial x}\right) \quad (3.3)$$

3.3.1 Initial and boundary conditions

At t = 0, all layers of the wall share the same initial temperature, signifying that the wall is in an initial state of thermal equilibrium. This initial condition is defined as follows:

$$T(x_1, 0) = T_{in}(x_{in}, 0) = T_{out}(x_{out}, 0) = T_i \quad (3.4)$$

The boundary conditions on surfaces $(S_{out,out})$, $(S_{out,in})$, $(S_{in,in})$, $(S_{in,out})$ are depicted below:

At the outer surface of the solid outer layer $(S_{out,out})$

$$-k_{out} \frac{\partial T_{out}}{\partial x_{out}}\Big|_{x_{out}=2L_{out}} = h_{out}\left(T_{out}|_{X_{out}=2L_{out}} - T_{\infty,out}\right) \quad (3.5)$$

At the inner surface of the solid outer layer $(S_{out,in})$

$$-k_s \frac{\partial T}{\partial x}\Big|_{x=2L_{pcm}} = -k_{out} \frac{\partial T_{out}}{\partial x_{out}}\Big|_{x_{out}=0} \quad (3.6)$$

At the inner surface of the solid inner layer $(S_{in,in})$

$$-k_s \frac{\partial T}{\partial x}\Big|_{x=0} = -k_{in} \frac{\partial T_{in}}{\partial x_{in}}\Big|_{x_{in}=2L_{in}} \quad (3.7)$$

At the outer surface of the solid inner layer $(S_{in,out})$

$$-k_{in} \frac{\partial T_{in}}{\partial x_{in}}\Big|_{x_{in}=0} = h_{in}\left(T_{\infty,in} - T_{in}|_{X_{in}=0}\right) \quad (3.8)$$

Where T is the temperature, K the thermal conductivity and the x axial position. The indexes in and out relate respectively to the inner or outer solid layer.

3.3.2 Dimensionless parameters

The time and spatial coordinate are represented as per Arfi and Mezaache [81] ,:

$$X_k = \frac{x_k}{L_k} \qquad \tau = \frac{\alpha_{pcm,s}}{L_{pcm}^2} t \tag{3.9}$$

The dimensionless temperature and enthalpy are determined as follows [82]:

$$\theta = \frac{T - T_{\infty,out}}{T_i - T_{\infty,out}} \qquad H = \frac{\hbar}{\hbar_{ref}} \tag{3.10}$$

The primary dimensionless parameters that govern the system are the Biot number, Stefan number, and melting temperature, defined as follows:

$$Bi_{out} = \frac{h_{out} L_{out}}{k_{out}}, \quad Bi_{in} = \frac{h_{in} L_{in}}{k_{in}}, \theta_m = \frac{T_m - T_{\infty,out}}{T_i - T_{\infty,out}}, \; Ste = \frac{\hbar_{ref}}{\rho_{ref} L_f} \tag{3.11}$$

These are the dimensionless heat capacity and thermal conductivity expressions

$$K_k = \frac{k_k}{k_{k,s}} \qquad C_k = \frac{c_k}{c_{k,s}} \tag{3.12}$$

3.3.3 Dimensionless heat equations

The model equations are written using the previously mentioned dimensionless parameters and assumptions. The issue of phase transition and moving fronts is solved for PCM layer using the enthalpy formulation variable. The generalized one-dimensional heat transfer equation describes how heat moves across the various wall layers [81,83]:

$$\frac{\partial H}{\partial \tau} = f_k \frac{\partial}{\partial X}\left(K \frac{\partial \theta}{\partial X}\right) \tag{3.13}$$

It is possible to conclude the following from the definition of the dimensionless time τ:

$$f_k = \frac{\alpha_{k,s}}{\alpha_{1,s}} \left(\frac{L_1}{L_k}\right)^2 \tag{3.14}$$

The correlations linking temperature and enthalpy for PCM materials are provided in accordance with the work of [84,85]:

$$H = \begin{cases} C(\theta - \theta_m) \\ C(\theta - \theta_m) + 1/Ste \end{cases} \text{ for } \begin{cases} \theta < \theta_m \\ \theta > \theta_m \end{cases} \quad (3.15)$$

$$\theta = \begin{cases} H + \theta_m \\ \theta_m \\ (H - 1/Ste)/C + \theta_m \end{cases} \text{ for } \begin{cases} H < 0 \\ 0 \le H \le 1/Ste \\ H > 1/Ste \end{cases} \quad (3.16)$$

3.3.4 Dimensionless thermal boundary conditions

At the outer surface of the solid outer layer ($S_{out,out}$):

$$K_{out} \frac{\partial \theta}{X_{out}}\Big|_{X_{out}=2} = -Bi_{out}\theta_{out}|_{X_{out}=2} \quad (3.17)$$

At the inner surface of the solid outer layer ($S_{out,in}$):

$$K \frac{\partial \theta}{X}\Big|_{X=0} = \frac{L}{L_{out}} \frac{k_{out}}{k_{,s}} K_{out} \frac{\partial \theta}{X_{out}}\Big|_{X_{out}=2} \quad (3.18)$$

At the inner surface of the solid inner layer ($S_{in,in}$):

$$K \frac{\partial \theta}{X}\Big|_{X=2} = \frac{L}{L_{in}} \frac{k_{in}}{k_{,s}} K_{in} \frac{\partial \theta}{X_{in}}\Big|_{X_{in}=0} \quad (3.19)$$

At the outer surface of the solid inner layer ($S_{in,out}$):

$$K_{in} \frac{\partial \theta}{X_{in}}\Big|_{X_{in}=0} = Bi_{in}\left(\theta|_{X_{in}=0} - \theta_{\infty,in}\right) \quad (3.20)$$

3.4 Numerical solution

The finite-volume method is employed to solve the physical model representing the phenomenon [86,87].

3.4.1 Mesh

The governing equations for the different layers of the wall are discretized using a uniform mesh for each layer. The spatial interval between two consecutive interior nodes is designated as ΔX, and it's important to note that each node serves as the central point within its respective control volume. The quantities specifying the total number of nodes and space steps for the

solid inner layer, solid outer layer, and PCM layer are as follows: $(N_{in}, \Delta X_{in}), (N_{out}, \Delta X_{out}), (N, \Delta X)$, respectively. Half control volumes mark the starting and ending points of each layer. The gradient terms related to the time variable are discretized using an explicit scheme. Consequently, an examination of solution stability and mesh impact has led to the determination of an appropriate mesh configuration, where: $N_{in} = N = N_{out} = 81$.

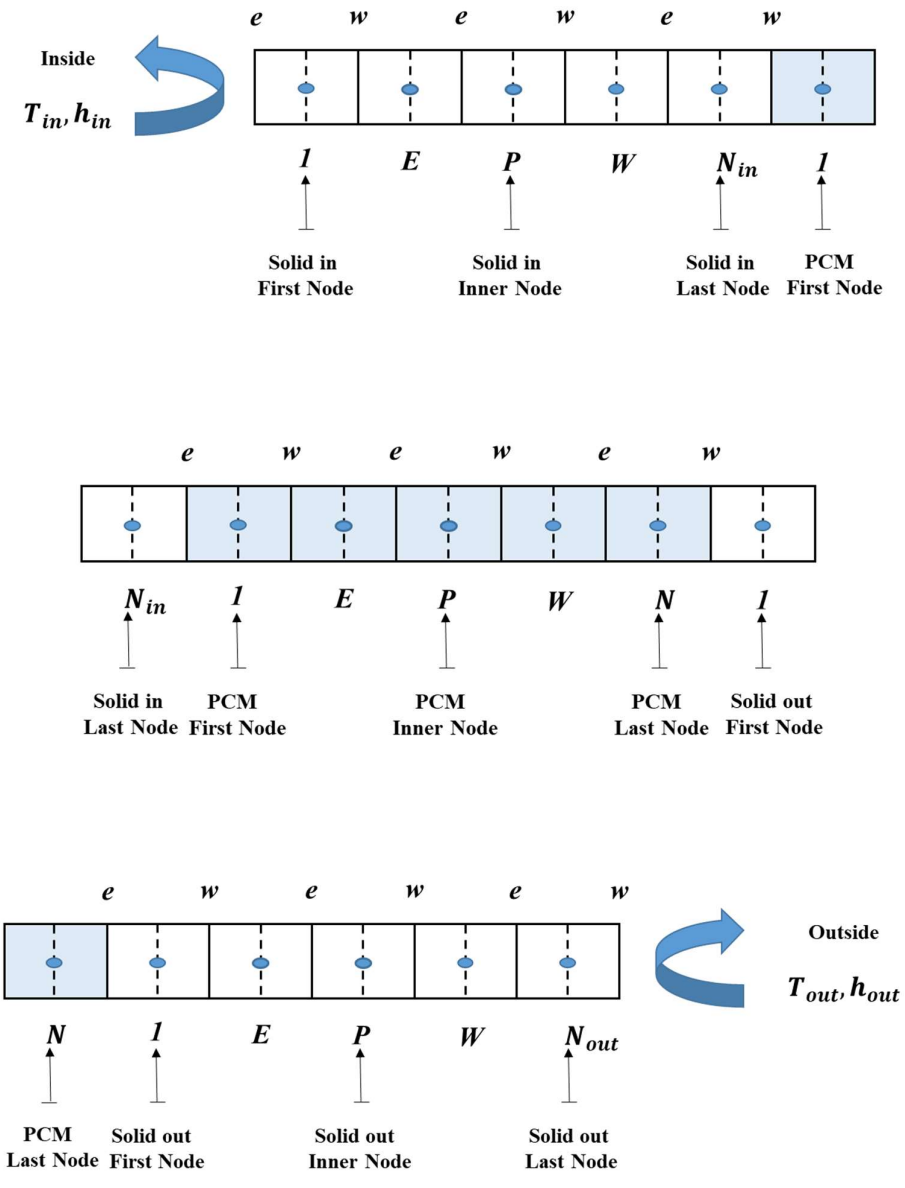

Figure 3.2 The multilayer wall mesh

3.4.2 Discretized equations of the inner solid layer

For an interior node

$$\theta_{in,j+1}^{P} = \theta_{in,j}^{P} + f_{in}\frac{\Delta\tau}{X_{in,w}-X_{in,e}}\left(K_{in,w}\frac{\theta_{in,j}^{W}-\theta_{in,j}^{P}}{\Delta X_{in}} - K_{in,e}\frac{\theta_{in,j}^{P}-\theta_{in,j}^{E}}{\Delta X_{in}}\right) \quad (3.21)$$

For the first node

$$\theta_{in,j+1}^{1} = \theta_{in,j}^{1} + f_{in}\frac{\Delta\tau}{X_{in,w}-X_{in,e}}\left(K_{in,w}\frac{\theta_{in,j}^{2}-\theta_{in,j}^{1}}{\Delta X_{in}} - Bi_{in}\left(\theta|_{X_{in}=0,j} - \theta_{\infty,in}\right)\right) \quad (3.22)$$

For the last node

$$\theta_{in,j+1}^{N_{in}} = \theta_{in,j}^{N_{in}} + f_{in}\frac{\Delta\tau}{X_{in,w}-X_{in,e}}\left(\frac{L_{in}}{L_{pcm}}\frac{k_s}{k_{in}}K_w\frac{\theta_j^1-\theta|_{X_{in}=2,j}}{\Delta X/_2} - K_{in,e}\frac{\theta_{in,j}^{N_{in}}-\theta_{in,j}^{N_{in}-1}}{\Delta X_{in}}\right) \quad (3.23)$$

3.4.3 Discretized equations of the PCM:

For an interior node

$$\mathrm{H}_{j+1}^{P} = \mathrm{H}_{j}^{P} + f\frac{\Delta\tau}{X_w-X_e}\left(K_w\frac{\theta_j^W-\theta_j^P}{\Delta X} - K_e\frac{\theta_j^P-\theta_j^E}{\Delta X}\right) \quad (3.24)$$

For the first node

$$\mathrm{H}_{j+1}^{1} = \mathrm{H}_{j}^{1} + f\frac{\Delta\tau}{X_w-X_e}\left(K_w\frac{\theta_j^2-\theta_j^1}{\Delta X} - \frac{L_{pcm}}{L_{in}}\frac{k_{in}}{k_s}K_{in,w}\frac{\theta|_{X=0,j}-\theta_{in,j}^{N_{in}}}{\Delta X_{in}/_2}\right) \quad (3.25)$$

For the last node

$$\mathrm{H}_{j+1}^{N} = \mathrm{H}_{j}^{N} + f\frac{\Delta\tau}{X_w-X_e}\left(\frac{L_{pcm}}{L_{out}}\frac{k_{out}}{k_s}K_{out,w}\frac{\theta_{out,j}^1-\theta|_{X_{out}=0,j}}{\Delta X_{out}/_2} - K_e\frac{\theta_j^N-\theta_j^{N-1}}{\Delta X}\right) \quad (3.26)$$

3.4.4 Discretized equations of the outer solid layer

For an interior node

$$\theta_{out,j+1}^{P} = \theta_{out,j}^{P} + f_{out}\frac{\Delta\tau}{X_{out,w}-X_{out,e}}\left(K_{out,w}\frac{\theta_{out,j}^{W}-\theta_{out,j}^{P}}{\Delta X_{out}} - K_{out,e}\frac{\theta_{out,j}^{P}-\theta_{out,j}^{E}}{\Delta X_{out}}\right) \quad (3.27)$$

For the first node

$$\theta^{1}_{out,j+1} = \theta^{1}_{out,j} + f_{out}\frac{\Delta\tau}{X_{out,w}-X_{out,e}}\left(K_{out,w}\frac{\theta^{2}_{out,j}-\theta^{1}_{out,j}}{\Delta X_{out}} - \frac{L_{out}}{L_{pcm}}\frac{k_s}{k_{out}}K_w\frac{\theta|_{X_{out}=0,j}-\theta^{N}_{j}}{\Delta X/_2}\right) \quad (3.28)$$

For the last node

$$\theta^{N_{out}}_{out,j+1} = \theta^{N_{out}}_{out,j} + f_{out}\frac{\Delta\tau}{X_{out,w}-X_{out,e}}\left(\mathrm{Bi}_{\mathrm{out}}\left(\theta_{\infty,\mathrm{out}} - \theta|_{\mathrm{X_{out}=2}}\right) - K_{out}\frac{\theta^{N_{out}}_{out,j}-\theta^{N_{out}-1}_{out,j}}{\Delta X_{out}}\right) \quad (3.29)$$

3.4.5 Determination of the solid-liquid front position

For figuring out where the solid-liquid front located in the PCM layer, the following equation represents the total energy present in a control volume with center node i [83]:

$$H^i V_e^i = \left[(\theta^i - \theta_m)V_s^i + \left(C(\theta^i - \theta_m) + \frac{1}{Ste}\right)V_l^i\right] \quad (3.30)$$

In this context, V_e^i, V_s^i, V_l^i represent, the volume of the control volume, expressed in dimensionless units, the fraction of the PCM phase that is in a solid state and the fraction of the PCM phase that is in a liquid state, respectively. When a control volume experiences a phase change with $\theta^i = \theta_m$, the equation transforms to:

$$H^i V_e^i = (1/Ste)V_l^i \quad \text{or} \quad H^i = (1/Ste)V_l^i/V_e^i \quad (3.31)$$

The value of the enthalpy when the solidification front reaches the node i, is as follows:

$$H_c^i = 1/(2Ste) \quad (3.32)$$

This equation serves as a criterion for managing the front's position. To determine the solidification time at a specific node i, we examine two consecutive time instants, $\tau(j)$ and $\tau(j+1)$.

If $H^i(j+1) \le H_c \le H^i(j)$, then the solidification process takes place at a specific moment τ_{sol} within the time range of $\tau(j)$ to $\tau(j+1)$, and this moment can be determined using interpolation, $\tau(j) \le \tau_{\mathrm{sol}} \le \tau(j+1)$.

The enthalpy is supposed to vary linearly across the whole time range. The equation for the solidification time of node i is: $\tau^i = (j + X)\Delta\tau$, Where X is determined through linear interpolation in the time domain, thus [83]:

$$X = \frac{H_c - H^i(j+1)}{H^i(j) - H^i(j+1)} \quad ; \quad \tau^i = \left(j + \frac{H_c - H^i(j+1)}{H^i(j) - H^i(j+1)}\right)\Delta\tau \tag{3.33}$$

3.5 Results and discussion

The selected melting temperatures are incorporated to align with the range of outside temperature variations while remaining near the desired indoor comfort temperature.

3.5.1 Temperature and enthalpy evolution

Based on Figure 3.3, the dimensionless enthalpy and temperature evolution within the situations when the envelope involves a phase change material layer ($\theta_m = 2.4$) demonstrates a reduction in temperature fluctuations, which caused by the external excitation throughout the wall, as compared to the case without PCM layers (PSM). Moreover, there are occurrences of phase transitions in which the temperature remains steady for a specific period throughout the temporal progression, while the enthalpy decreases/increases suddenly. These instances occur while the phase change material is solidifying, signifying the PCM's charging phase or fusion when it is in its active operational phase. In these instances, the phase change material (PCM) utilizes latent heat to release or store energy. Conversely, when not undergoing a phase change, the PCM exhibits a noticeable change in temperature as a result of either releasing or storing sensible heat. Sensible heat pertains to the thermal energy needed to increase or decrease the temperature of a material without causing a change in its physical state, whereas latent heat represents the thermal energy quantity necessary to induce a phase transition of a substance without affecting its temperature. The presence of these phases is contingent upon the melting temperature and the momentary external stimulus.

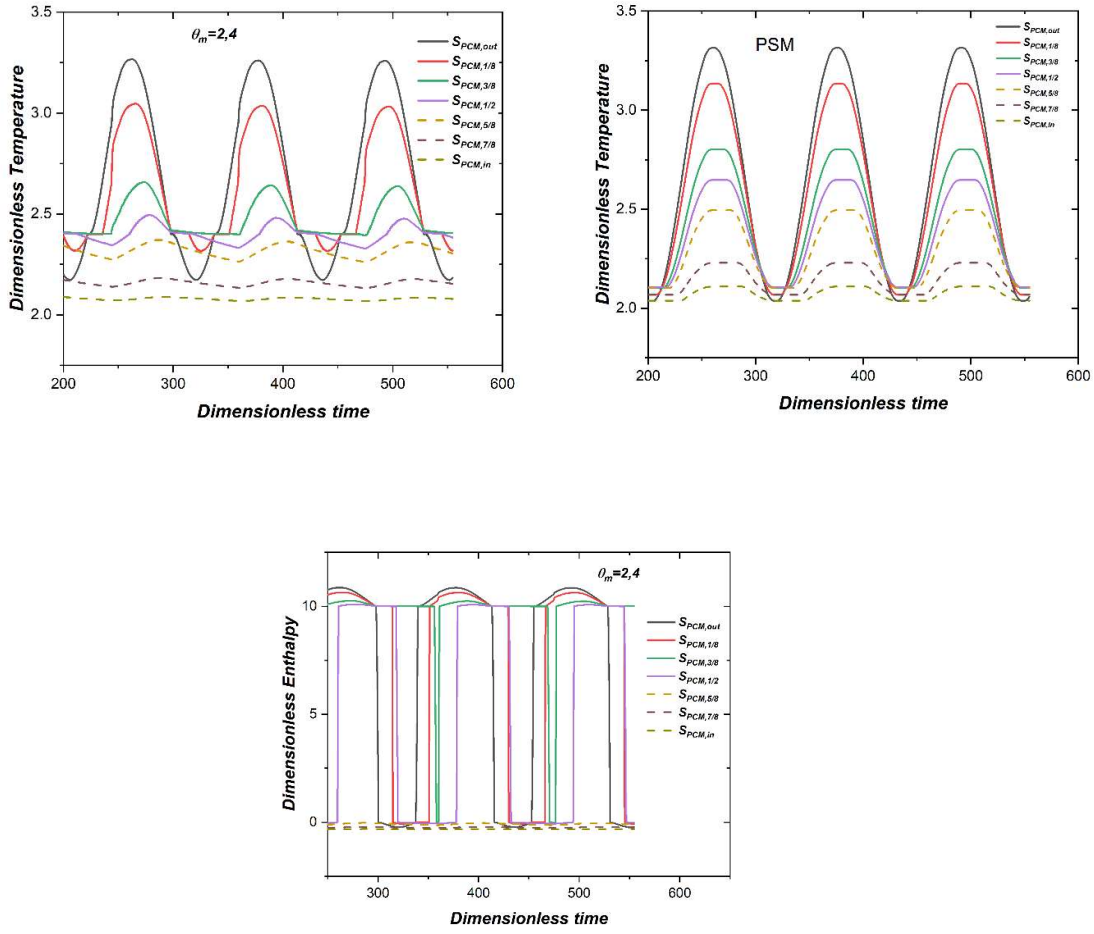

Figure 3.3 Dimensionless enthalpy and temperature evolution in summer for cases: $\boldsymbol{\theta_m = 2.4}$ and PSM

As it is mentioned previously within (summer part), According to figure 3.4 a minimizing of the temperature fluctuation amplitude (that is carried out by the outside excitation) throughout the wall is noted with incorporating the PCM layer compared to the situation (*PSM*) in which there is an absence of a PCM layer. Moreover, instances of phase transition are illustrated, during which the temperature remains constant for a certain duration as time progresses, whether through fusion, which corresponds to the PCM charging phase, or solidification, during which the PCM is in its operational state, depending to the instantaneous outside excitation. Also, the enthalpy decreases/increases suddenly via the time showing the instants of phase change.

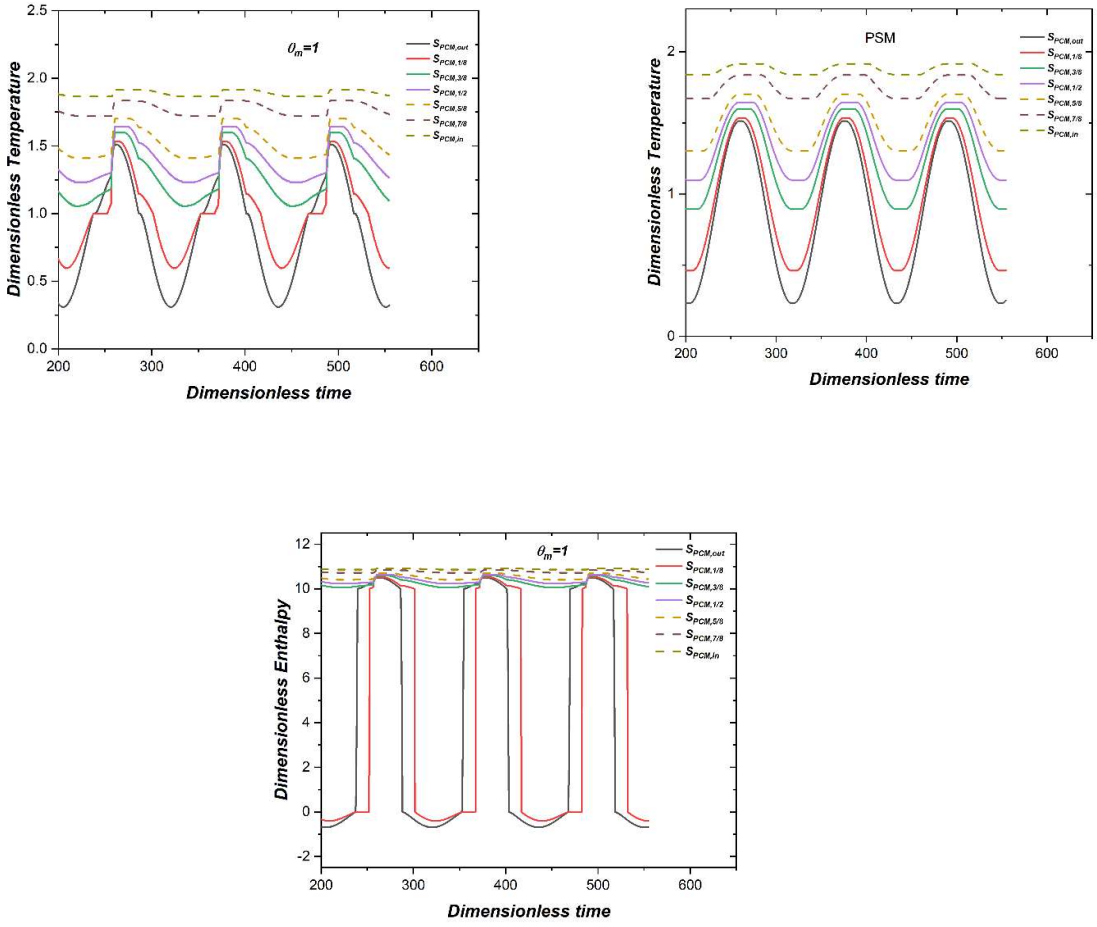

Figure 3.4 Dimensionless enthalpy and temperature evolution in winter for cases: $\boldsymbol{\theta_m = 1}$ and PSM

3.5.2 Heat flux evolution

Figure 3.5 depicts the progression of dimensionless heat flux across dimensionless time. Within the situation of (PSM), the impact of external summer excitation can reach the inner surface ($S_{in,out}$), leading to fluctuating heat flux. However, when ($\theta_m = 2.4$) the phase change process is achieved, a decrease in the amplitude of heat flux fluctuations is observed. Consequently, the influence of the external stimulus on the inner surface ($S_{in,out}$) diminishes. Conversely, in the case of ($\theta_m = 3$), the PCM layer performs poorly due to a weak phase change process. Correspondingly, as the operating fraction of PCM increases, the amplitude of heat flux reduction becomes more pronounced, and vice versa.

It is worth noting that while the case of ($\theta_m = 3$) demonstrates a restrained smoothing of heat flux, it showcases a significant shift in peak load compared to the baseline scenario (PSM). On the other hand, combinations involving ($\theta_m = 2.4$) not only result in smoothing of heat flux but also show a considerable shift of peak load when compared to the reference case (PSM).

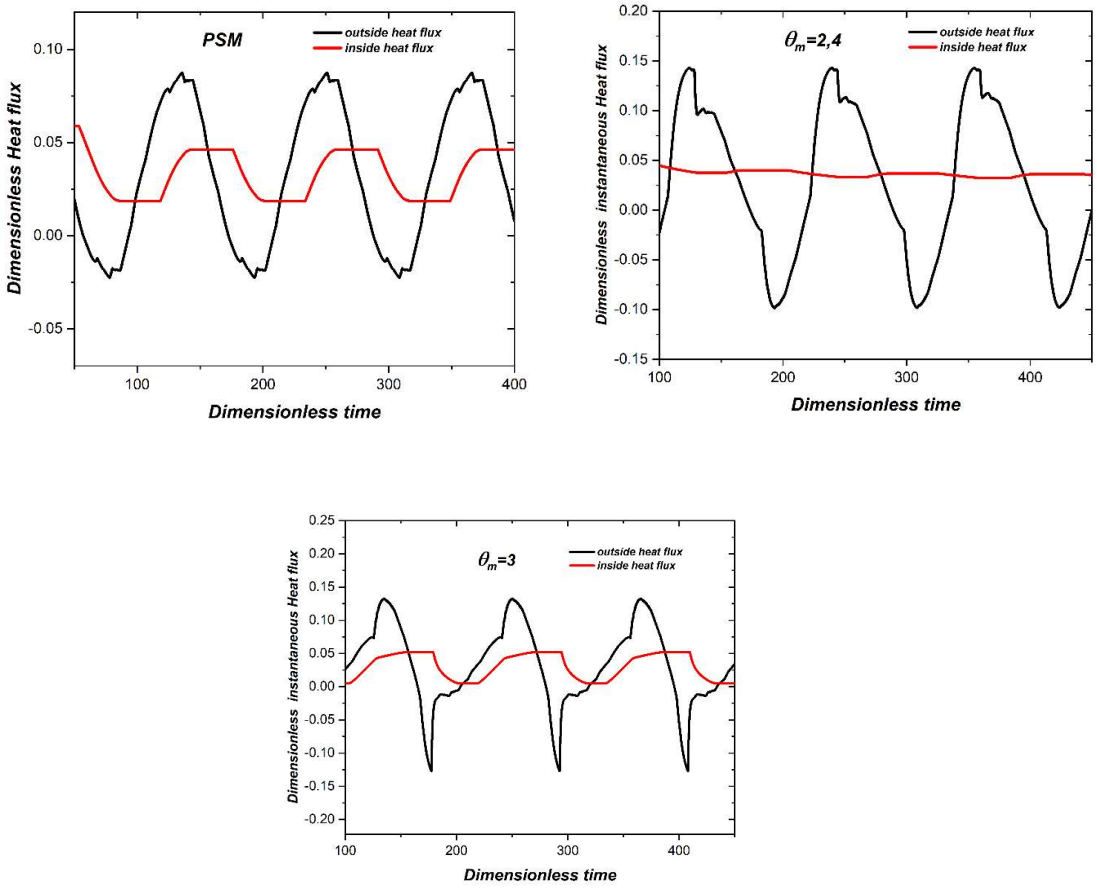

Figure 3.5 Heat flux evolution in summer for cases: $\boldsymbol{\theta_m = 2.4}$, $\boldsymbol{\theta_m = 3}$, and PSM.

Figure 3.6 demonstrates the dimensionless time-dependent heat flux during the winter period, alongside the summer scenario. In the case of (PSM) and another scenario in situations with limited phase change ($\theta_m = 0.4$), the outer stimulus's influence can extend to the inner surface ($S_{in,out}$), and the amplitude of heat flux fluctuations remains unchanged. Conversely, when the phase change process is well achieved ($\theta_m = 1$), a significant reduction in the fluctuation amplitude is observed. Additionally, similar to the previous case,

the fluctuation amplitude of heat flux reduction is greater as the proportion of PCM in operation is raised, and conversely, it decreases as the PCM fraction decreases.

Unlike the previous season, during winter, there is a noticeable lack of heat flux fluctuation smoothing. Moreover, the displacement of peak loads, in contrast to the baseline scenario (PSM), is only evident in the scenario where ($\theta_m = 1$).

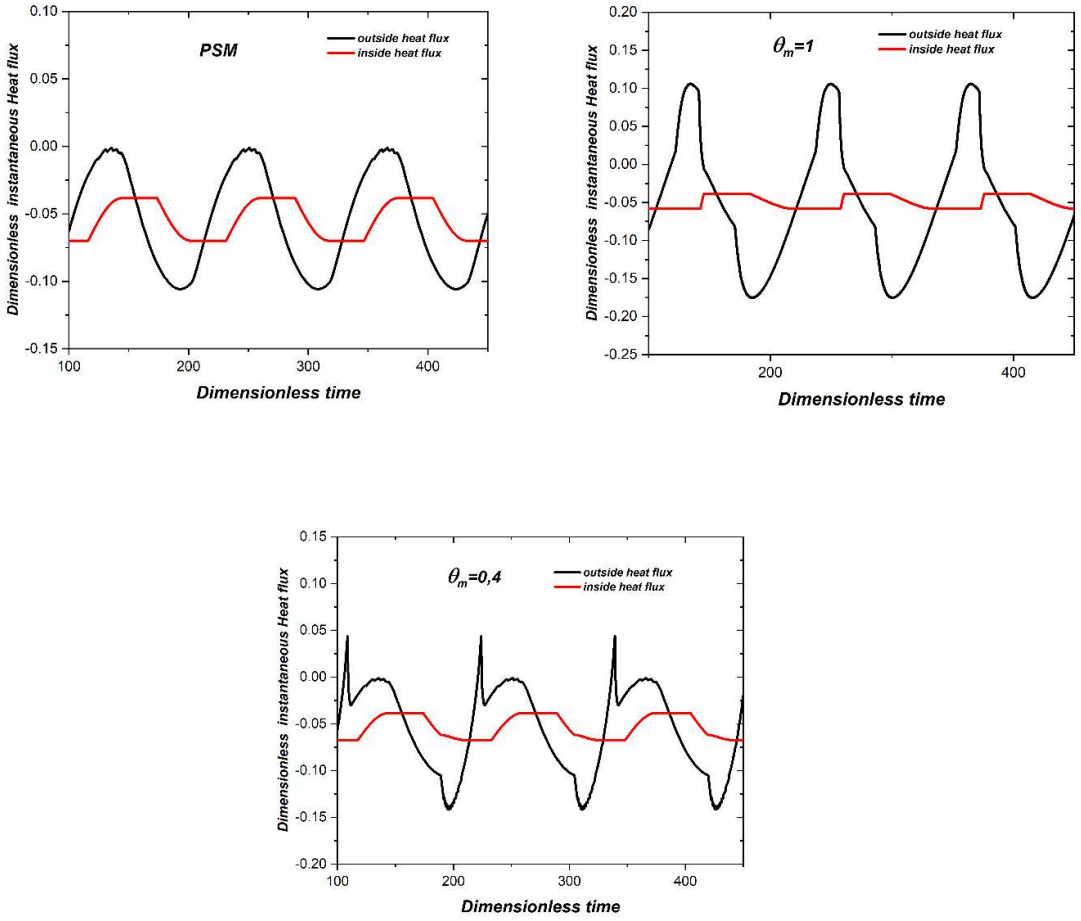

Figure 3.6 Heat flux evolution in winter for cases: $\boldsymbol{\theta_m = 0.4}$, $\boldsymbol{\theta_m = 1}$, and PSM.

3.5.3 Kinetic of phase change fronts

According to Figure 3.7, both solidification and fusion phase change processes are detected based on the instantaneous external stimuli. When considering ($\theta_m = 2.4$), two distinct phase change interfaces become evident. The initial front initiates at ($S_{out,in}$) surface,

near the outside, and progresses towards the center of the PCM during the period of charging, undergoing solidification. During the operating phase, the front moves within the PCM medium through fusion due to the external excitation. Both external and internal stimuli lead to the formation of the second phase change interface within the medium (Sm). In the charging (solidification) period, this front moves towards the external surface of the phase change material (PCM) layer, while in the operating period (fusion), it moves in the opposite direction.

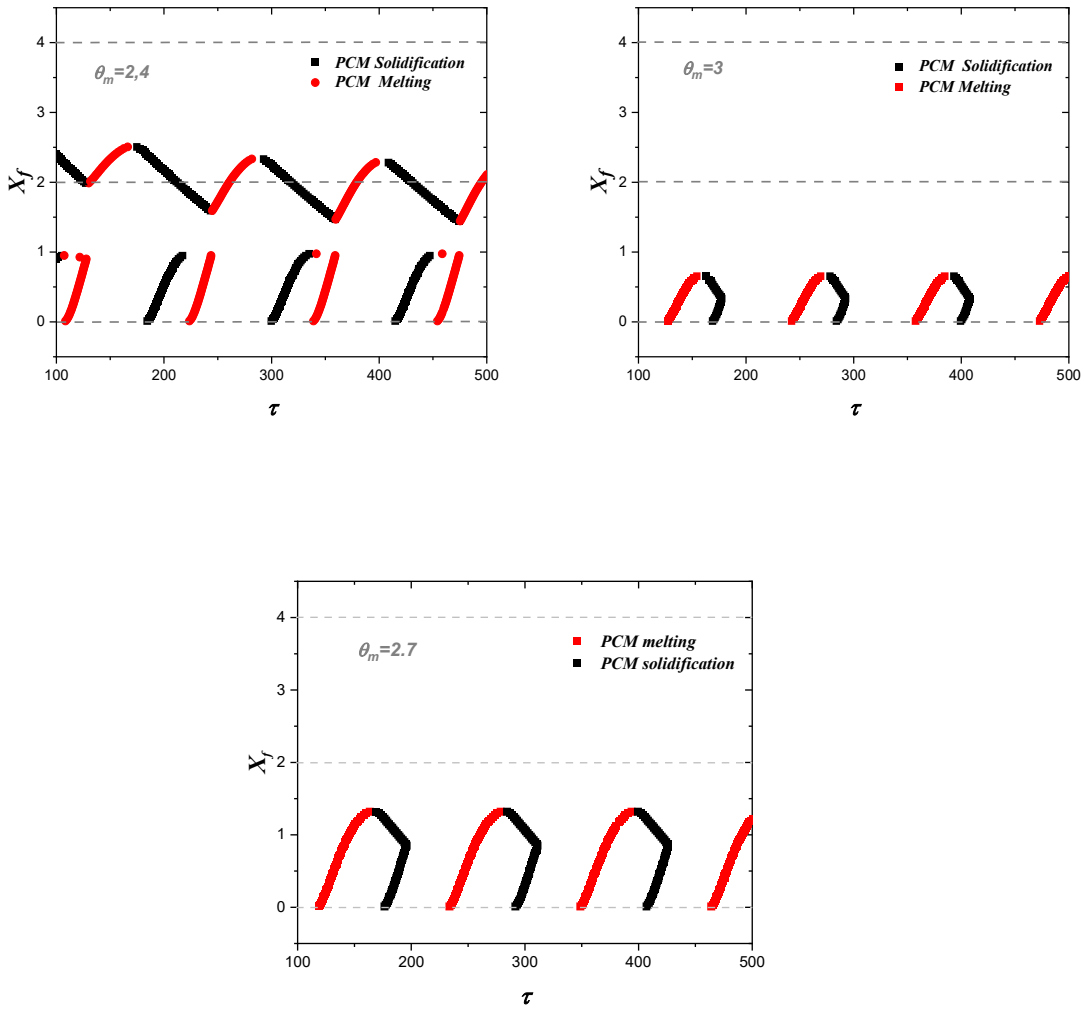

Figure 3.7 Front position evolution of melting temperatures in summer for melting temperatures: $\boldsymbol{\theta_{m2} = 2.4}$, $\boldsymbol{\theta_{m2} = 2.7\ and}$, $\boldsymbol{\theta_{m2} = 3}$.

For ($\theta_m = 2.7$) and ($\theta_m = 3$), a single phase change interface is visible, originating from the surface near the exterior and advancing towards the medium. The nature of the phase transition (either solidification or fusion) depends on the external excitation. Unlike the case of ($\theta_m = 2.4$), the combined effect of external and internal excitations prevents the medium zone of the PCM from reaching the phase change point, be it ($\theta_m = 2.7$) or ($\theta_m = 3$). Furthermore, the phase change front is able to reach the region closer to the PCM medium more effectively for ($\theta_m = 2.7$) compared to ($\theta_m = 3$).

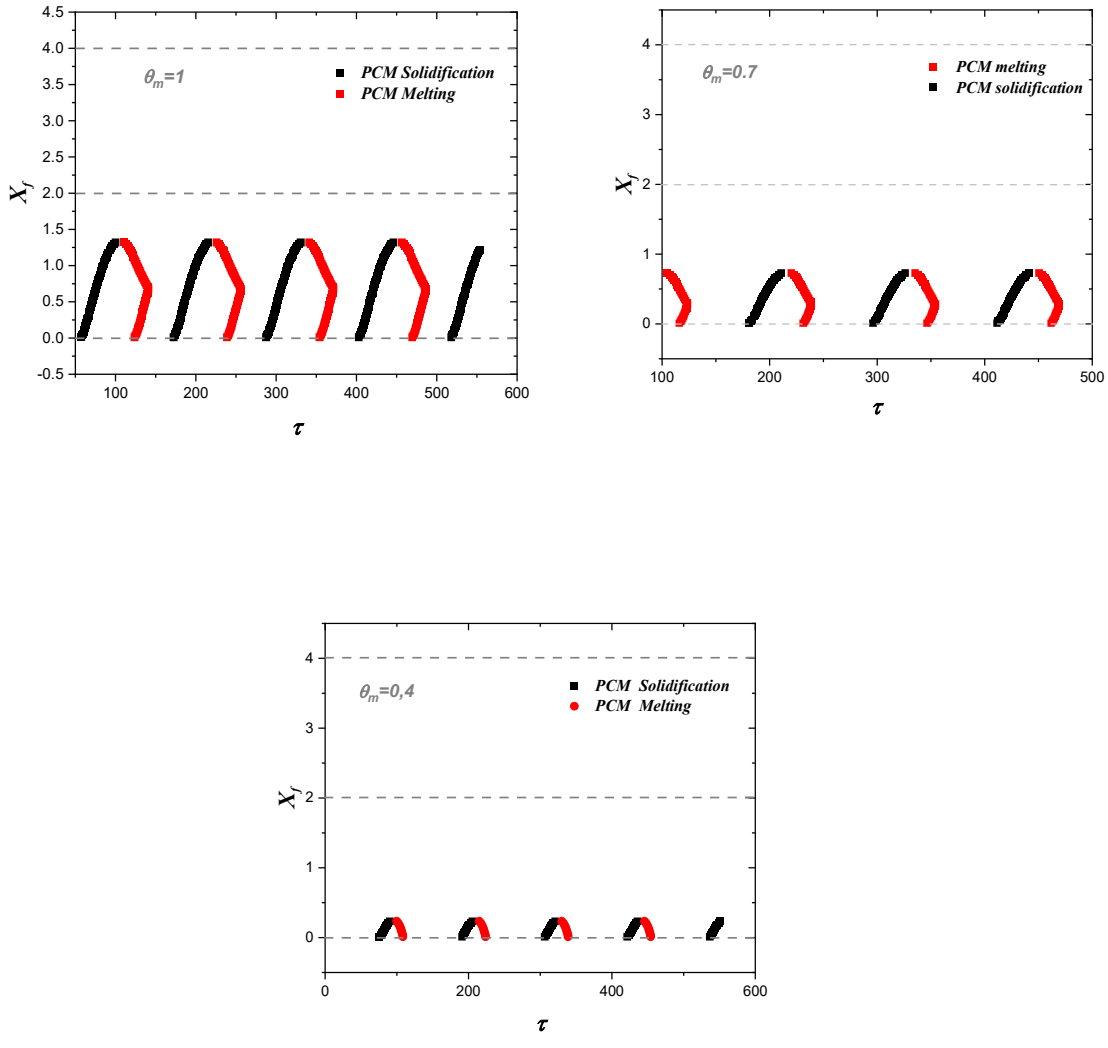

Figure 3.8 Front position evolution of melting temperatures in winter for melting temperatures: $\boldsymbol{\theta_{m2} = 0.4}$, $\boldsymbol{\theta_{m2} = 0.7}$ ***and*** , $\boldsymbol{\theta_{m2} = 1}$.

In the winter scenario, as depicted in Figure 3.8, when the phase change temperatures of ($\theta_m = 1$), ($\theta_m = 0.7$) or ($\theta_m = 0.4$), the phase change material (PCM) layer successfully attains the phase change point. At this point, a single phase change front appears and initiates its movement from the surface ($S_{out,in}$), situated near the exterior, towards the center of the phase change material (PCM) layer. Within the charging period, the front progresses using the fusion operation, while throughout the discharge phase, it proceeds via the solidification operation. Furthermore, it is noted that increasing θ_m allows the phase change front to reach points deeper in the PCM.

3.5.4 Operating PCM fraction

In Figure 3.9A, it can be observed that during the summer season, the largest portion of the PCM in operation (46.75%) could be achieved for ($\theta_m = 2.4$). This last is in proximity to the temperature of the indoor ambient and is more suitable for the external excitation experienced during summer. In this case, the phase change process occurs in two distinct regions, adjacent to the exterior and inside the phase change material (PCM) layer. In contrast, for ($\theta_m = 3$), a limited phase transition process is evident, accompanied by an operating PCM fraction of 16.5%. Conversely, with ($\theta_m = 2.7$), the proportion of the PCM in operation attains 33%.

Similarly, in the winter season (Figure 3.9B), the largest portion of the PCM in operation is observed for ($\theta_m = 1$), which corresponds to the melting temperature closest to the inside ambient temperature. This proximity enables the PCM layer to undergo a substantial phase change process, with an operating fraction of 33%. In comparison, for ($\theta_m = 0.7$), the operating PCM fraction is 18.25%. However, when considering ($\theta_m = 0.4$), which is close to the minimum outside temperature during winter, the phase change is weakest, with an operating fraction of 5.75%. Consequently, these findings emphasize the significance of the melting temperature selection in determining the effectiveness of the phase change process.

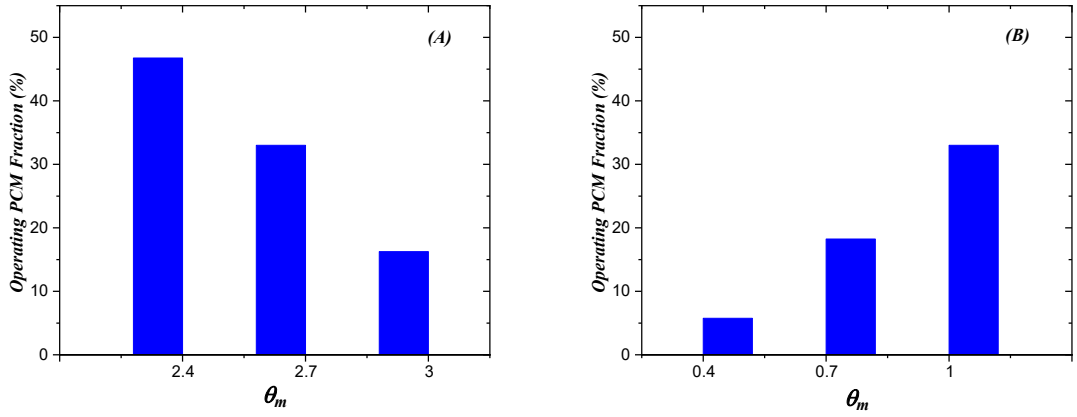

Figure 3.9 Operating PCM fraction: (A) in summer, (B) in winter.

3.5.5 Phase change dimensionless duration for charging /discharging cycles

During the summer season, Figure 3.10A shows the charging and discharging phases of the phase change material (PCM) layer, with the charging period indicating the solidification phase and the discharging period representing the melting phase. As per Hamad [92] as far as the discharging duration is longer the efficiency of the PCM is higher. It is seen that for $(\theta_m = 2.4)$, the discharging duration is long $(\Delta\tau_{discharging} = 57.91)$, due to the phase change process which is well occurred. In contrary, the case where the phase change occurs weakly $(\theta_m = 3)$, the discharging time is short $(\Delta\tau_{dischargin} = 27.17)$. Further, for $(\theta_m = 3)$ the discharging time is short $(\Delta\tau_{discharging} = 45.07)$. It is depicted in this case that where the operating PCM fraction is high the discharging duration is long and vice versa. Also It is seen that in cases where the phase change process is effectively accomplished, the PCM requires a longer duration to reach full charge compared to the required time for discharging period, likewise for $(\theta_m = 2.4)$, the charging needed time was $(\Delta\tau_{charging} = 68.37)$. Conversely, for weak phase change process case the discharging time is longer than charging duration, like $(\theta_m = 3)$, the charging time is short $(\Delta\tau_{charging} = 14.63)$.

The same for the winter season (Figure 3.10B), for $(\theta_m = 1)$, the discharging duration is long, because of the successful occurrence of the phase change process $(\Delta\tau_{discharging} = 43.01)$. In contrary, the scenario with a limited phase change$(\theta_m = 0.4)$, the discharging

time is short $(\Delta\tau_{discharging} = 14.48)$. however, the discharging needed time for$(\theta_m = 0.7)$, where $(\Delta\tau_{discharging} = 29.81)$. As well as the charging duration, which is increases with increasing the proportion of the PCM in operation, $\Delta\tau_{charging} = 8.81$ for $(\theta_m = 0.4)$, while it was $\Delta\tau_{charging} = 30.29$ for $(\theta_m = 1)$. Also It is seen that the PCM needs more time in order to be fully charged compared to the time needed for discharging cycle.

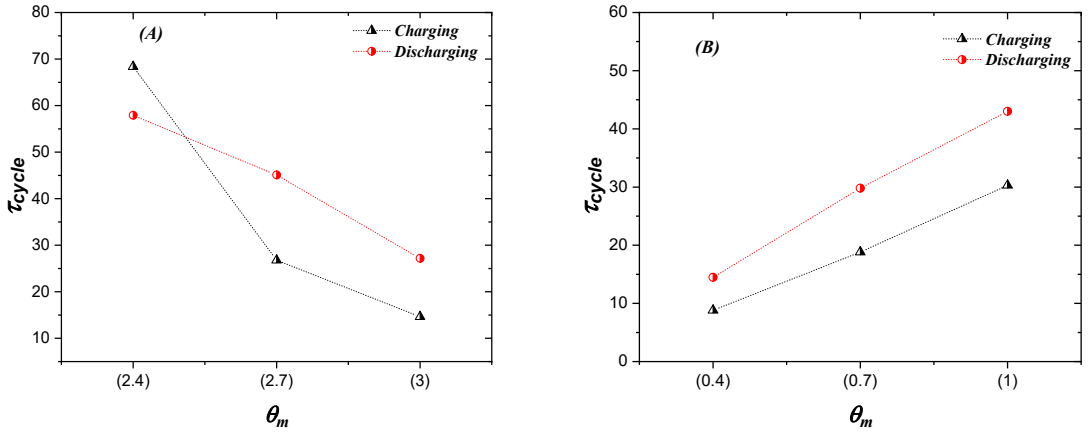

Figure 3.10 Dimensionless operating duration of phase change during charging and discharging cycles in summer (A) and winter (B).

3.5.6 Heat gained/lost over 1 day and average heat flux over one day

The graph labeled as Figure 3.11A illustrates the average of the dimensionless heat flux throughout a summer day, including both periods, nighttime (charging) and daylight (discharging). Surprising results are observed, particularly for melting temperatures of $(\theta_m = 3)$ and $(\theta_m = 2.7)$, which indicate a weak phase change process. These cases show a significant reduction in the median of the absorbed heat flux in comparison to the baseline case (PSM), with a decrease of 19.71% and 20.19% respectively. However, when a strong phase change process is achieved with $(\theta_m = 2.4)$, there is no notable reduction in the mean heat flux transmitted to the indoor environment, only a 4.87% reduction. This can be attributed to the heat emitted from the wall, especially from the phase change material (PCM) layer into the interior during the charging period, which accumulates a significant quantity of heat throughout the operational period. As a result, the mean heat transmitted to the interior remains elevated, exhibiting consistent temperature and heat flux. In contrast, cases

characterized by a limited phase change operation do not accumulate a substantial quantity of heat throughout the operational period, resulting in a reduced heat transfer into the interior within the charging period.

Based on Figure 3.11B, contrary to the results observed during the summer season, the melting temperature that resulted in a substantial proportion of the PCM in operation (indicating an efficient phase transition operation) of ($\theta_m = 1$) shows the most significant decrease in the average heat loss over a day in comparison to the reference case (PSM), with a decrease of 10.29%. On the other hand, for the case where($\theta_m = 0.7$), the reduction in the average heat loss throughout a day in comparison to the baseline scenario is 4.41%. However, in the case of ($\theta_m = 0.4$), when the phase transition operation is not effectively accomplished, there is no reduction in the average lost heat flux. The winter season experiences a less effective phase change process compared to the summer season, resulting in a lower amount of heat required for the purpose of charging the phase change material (PCM) layer. On the other hand, in the summertime, when the phase transition operation is effectively occurring, a greater quantity of heat must be released for charging the phase change material (PCM) layer.

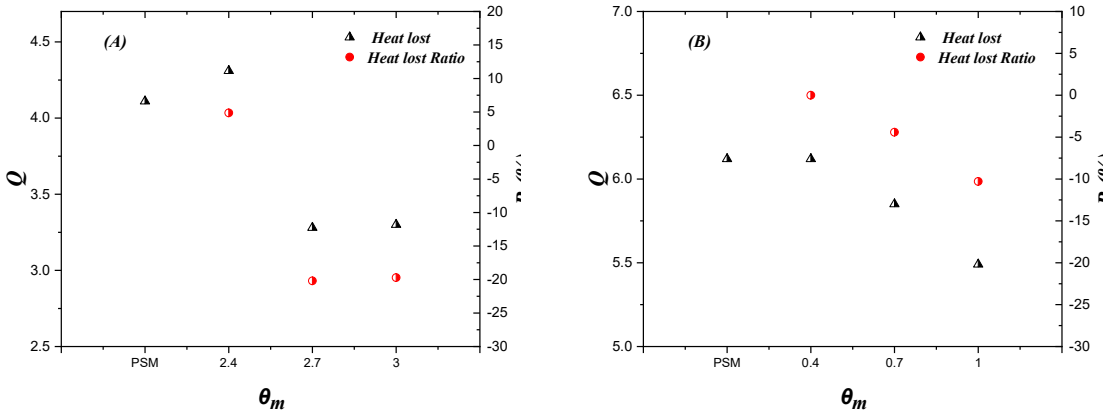

Figure 3.11 Heat gained/lost over one day: (A) in summer, (B) in winter

3.6 Conclusion

The study examined the behavior of a building envelope incorporating a phase change material layer within various seasons, including winter and summer. The findings indicate that:

During both summer seasons, the highest fraction of the operating PCM is achieved for melting temperatures which are close to the inside ambient temperature and more suitable for the external excitation experienced. In which, for summer $\theta_m = 2.4$ provides an operating PCM fraction of 46.75%, while during the winter season $\theta_m = 1$ provides the operating PCM fraction of 33%.

The melting temperatures which offer a high operating PCM fraction, $\theta_m = 2.4$ in summer, and $\theta_m = 1$ in winter, have the longest length of discharging. $(\Delta\tau_{discharging} = 57.91)$ and $(\Delta\tau_{discharging} = 43.01)$, respectively.

The cases with melting temperatures fall within the range of outdoor temperature fluctuations and are in proximity to the indoor comfort temperature (varying with the season) guarantees the PCM wall's optimal annual behavior by effectively smoothing the instantaneous heat flux and reducing its fluctuating amplitude, as well as $\theta_m = 2.4$ and $\theta_m = 1$, for summer and winter respectively. According to several previous works, the significant diminution of the peak and the intensity of the instantaneous heat flux fluctuating within some combinations, allow utilizing a low power HVAC system.

However, cases with melting temperatures fall within the range of outdoor temperature fluctuations and are in proximity to the farthest temperature values (One near the summer's peak temperature, and the other near the winter's lower temperature), guarantees minimizing the energy consumed by the HVAC system in order to keep the inside thermal comfort in summer. Likewise, for $\theta_m = 3$ the consumed energy could be reduced by 19.71% in summer, while during winter with $\theta_m = 1$ which is the melting temperatures include in the field of the external temperature fluctuating and in proximity to the inside comfort temperature, the consumed energy could be reduced by 10.29%.

To enhance energy efficiency, the proposed system in this study may necessitate an additional technology or tool capable of directing heat release to the outdoors during the charging cycle in the summer season, rather than into the indoor environment.

Chapter 4 : Investigation of double layered PCM building envelope during charging cycle

4.1 Introduction

The main goal of this research is to showcase and assess the operational effectiveness of the phase change operation within a building's envelope containing double layers of Phase Change Material (PCM). This was achieved by showcasing the manner in which cold (or heat) is stored through either sensible or latent heat mechanisms, while also investigating the dynamics of phase change fronts. The research further delved into exploring the impact of employing two distinct PCM layers, differing in terms of either their melting temperatures or latent heats. Moreover, the investigation assessed the consequences of the variation between the melting temperatures $|\theta_{m1}-\theta_{m2}|$ and latent heats $|Ste_1- Ste_2|$ of the two PCM layers, considering a wide range of combinations $(\theta_{m1}, \theta_{m2})$ and (Ste_1, Ste_2). Additionally, the study examined the time required to reach the limit point of solidification varying with disparities in temperature and latent heat $|\theta_{m1}-\theta_{m2}|$ and $|Ste_1- Ste_2|$. Furthermore, the investigation analyzed the heat loss during the charging cycle.

4.2 Physical problem

To model the building envelope's behavior during the PCM charging cycle, a wall consisting of four layers is used, as illustrated in Figure 4.1, consisting of two solid concrete layers on the exterior and interior, with two phase change material (PCM) layers situated at the core of the building envelope, experiencing phase change through solidification. The interaction among the various layers occurs at the boundaries: PCM2-solid inside $(S_{in,in})$, PCM2-PCM1 (S_m), PCM1-solid outside $(S_{out,in})$. The interior convective condition assumes varying values, including both hot and cold, represented as $(h_{in}, T_{\infty,in})$, while the exterior convective condition remains consistently cold, specified as $(h_{out}, T_{\infty,out})$. To facilitate the solidification operation in all numerical simulations, it is imperative to maintain the condition $(T_{\infty,out} < T_m)$, where T_m represents the phase change temperature.

4.3 Modeling and governing equations

The simplifying assumptions employed in this study include:

- The volume of the multi-layered wall remains constant.
- Both solid layers act as passive conductors.

- Natural convection within the liquid PCM is not considered.
- Heat transfer is assumed to be one-dimensional.
- The PCM layers envelope is assumed to be thin and to possess high thermal conductivity to disregard its thermal resistance.
- The temperature and heat transfer coefficient of the surrounding convective fluids are held constant.
- For the PCM layers, properties of the solid and liquid phases are assumed to be identical.

With these assumptions in place, the physical model is described by the unsteady one-dimensional heat equation

Subsequently, we refer to the inside concrete layer as 'solid in,' which is exposed to internal convective conditions, and to the outside concrete layer as 'solid out,' subjected to external cold convective conditions.

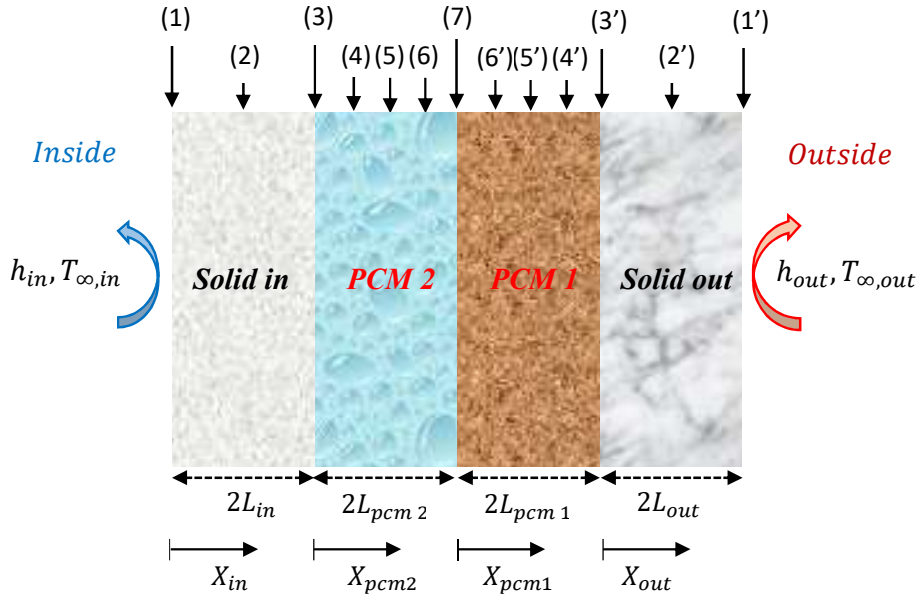

Figure 4.1 Shape of the wall, coordinates systems and selected surfaces

(3) $S_{in,out}$, (1') $S_{out,out}$, (2) $S_{in,1/2}$, (2') $S_{out,1/2}$, (3) $S_{in,in}$, (3') $S_{out,in}$, (4) $S_{pcm\,2,1/4}$, (4') $S_{pcm\,1,1/4}$, (5) $S_{pcm\,2,1/2}$, (5') $S_{pcm\,1,1/2}$, (6) $S_{pcm\,2,3/4}$, (6') $S_{pcm\,1,3/4}$, (7) S_m

Phase change material (PCM1 and PCM2):

$$\begin{cases} Liquid\ region: T > T_m: \rho_l C_l \frac{\partial T_l}{\partial t} = \frac{\partial}{\partial x}\left(k_l \frac{\partial T_l}{\partial x}\right) \\ Solid\ region: T < T_m: \rho_s C_s \frac{\partial T_s}{\partial t} = \frac{\partial}{\partial x}\left(k_s \frac{\partial T_s}{\partial x}\right) \end{cases} \quad (4.1)$$

Solid in and out:

$$\rho_{in} C_{in} \frac{\partial T_{in}}{\partial t} = \frac{\partial}{\partial x}\left(k_{in} \frac{\partial T_{in}}{\partial x}\right) \quad (4.2)$$

$$\rho_{out} C_{out} \frac{\partial T_{out}}{\partial t} = \frac{\partial}{\partial x}\left(k_{out} \frac{\partial T_{out}}{\partial x}\right) \quad (4.3)$$

4.3.1 Initial and boundary conditions

At t = 0, all layers of the wall share the same initial temperature, signifying that the wall is in an initial state of thermal equilibrium. This initial condition is defined as follows:

$$T_1(x_1, 0) = T_2(x_2, 0) = T_{in}(x_{in}, 0) = T_{out}(x_{out}, 0) = T_i \quad (4.4)$$

The boundary conditions on surfaces $(S_{out,out})$, $(S_{out,in})$, (S_m), $(S_{in,in})$, $(S_{in,out})$ are presented below:

At the outer surface of the solid outer layer $(S_{out,out})$

$$-k_{out} \left.\frac{\partial T_{out}}{\partial x_{out}}\right|_{x_{out}=2L_{out}} = h_{out}\left(T_{out}|_{X_{out}=2L_{out}} - T_{\infty,out}\right) \quad (4.5)$$

At the inner surface of the solid outer layer $(S_{out,in})$

$$-k_{1,s} \left.\frac{\partial T_1}{\partial x_1}\right|_{x_1=2L_{pcm1}} = -k_{out} \left.\frac{\partial T_{out}}{\partial x_{out}}\right|_{x_{out}=0} \quad (4.6)$$

At interface PCM1-PCM2 (S_m)

$$-k_{1,s}\frac{\partial T_1}{\partial x_1}\bigg|_{x_1=0} = -k_{2,s}\frac{\partial T_2}{\partial x_2}\bigg|_{x_2=2L_{pcm2}} \tag{4.7}$$

At the inner surface of the solid inner layer ($S_{in,in}$)

$$-k_{2,s}\frac{\partial T_2}{\partial x_2}\bigg|_{x_2=0} = -k_{in}\frac{\partial T_{in}}{\partial x_{in}}\bigg|_{x_{in}=2L_{in}} \tag{4.8}$$

At the outer surface of the solid inner layer ($S_{in,out}$)

$$-k_{in}\frac{\partial T_{in}}{\partial x_{in}}\bigg|_{x_{in}=0} = h_{in}\left(T_{\infty,in} - T_{in}|_{X_{in}=0}\right) \tag{4.9}$$

Where T is the temperature, K the thermal conductivity and the x axial position. The indexes in and out relate respectively to the inner or outer solid layer.

4.3.2 Dimensionless parameters

To facilitate the numerical analysis and identify the key physical factors that influence thermal heat transfer combined with phase change in the two PCM layers, dimensionless parameters are employed. The spatial coordinate and time are represented as per Arfi and Mezaache [81].

$$X_k = \frac{x_k}{L_k} \;\; ; \;\; \tau = \frac{\alpha_{1,s}}{L_1^2}t \tag{4.10}$$

The dimensionless time, denoted as τ, is established using the physical properties of the reference phase change material PCM2. In this context, *x* represents the spatial coordinate, and the subscript '*k*' pertains to the solid mediums 'in' and 'out,' as well as PCM 1 and PCM 2 (where *k* can take values of *1, 2, in*, or *out*). The dimensionless temperature and enthalpy are defined as follows [82]:

$$\theta = \frac{T - T_{\infty,out}}{T_i - T_{\infty,out}} \quad ; \quad H = \frac{\hbar}{\hbar_{ref}} \tag{4.11}$$

It's important to note that with this chosen dimensionless temperature, the melting temperature falls within the range $0 \leq \theta_{m,k} \leq 1$ (where $(T_{\infty,out} \leq T_{m,k} \leq T_i)$. The external cold convective temperature corresponds to $\theta_{\infty,out} = 0$ $(T = T_{\infty,out})$, while the internal convective temperature ranges from $\theta_{\infty,in} \geq 0$ $(T_{\infty,in} \geq T_{\infty,out})$. As a result, various physical scenarios can be examined:

$$\begin{cases} \theta_{\infty,in} = 0 \ (T_{\infty,in} = T_{\infty,out}) \\ \theta_{\infty,in} < 1 \ (T_{\infty,in} < T_i) \\ \theta_{\infty,in} = 1 \ (T_{\infty,in} = T_i) \\ \theta_{\infty,in} > 1 \ (T_{\infty,in} > T_i) \end{cases} \tag{4.12}$$

The primary dimensionless parameters that govern the system are the Biot number, Stefan number, and melting temperature, defined as follows:

$$Bi_{out} = \frac{h_{out} L_{out}}{k_{out}} \quad ; \quad Bi_{in} = \frac{h_{in} L_{in}}{k_{in}} \quad ; \; Ste1 = \frac{\hbar_{ref,1}}{\rho_{ref,1} L_{f,1}} \; ; \; Ste2 = \frac{\hbar_{ref,2}}{\rho_{ref,2} L_{f,2}} \tag{4.13}$$

$$\theta_{m,1} = \frac{T_{m,1} - T_{\infty,out}}{T_i - T_{\infty,out}} \quad ; \quad \theta_{m,2} = \frac{T_{m,2} - T_{\infty,out}}{T_i - T_{\infty,out}} \tag{4.14}$$

These are the dimensionless heat capacity and thermal conductivity expressions

$$K_k = \frac{k_k}{k_{k,s}} \quad ; \quad C_k = \frac{c_k}{c_{k,s}} \tag{4.15}$$

4.3.3 Dimensionless heat equations

The model equations are written using the previously mentioned dimensionless parameters and assumptions. The issue of phase transition and moving fronts is solved for PCM layers using the enthalpy formulation variable. The generalized one-dimensional heat transfer equation describes how heat moves across the various wall layers [81,83]:

$$\frac{\partial H_k}{\partial \tau} = f_k \frac{\partial}{\partial X_k}\left(K_k \frac{\partial \theta}{\partial X_k}\right) \tag{4.16}$$

It is possible to conclude the following from the definition of the dimensionless time τ:

$$f_k = \frac{\alpha_{k,s}}{\alpha_{1,s}}\left(\frac{L_1}{L_k}\right)^2 \tag{4.17}$$

The correlations linking temperature and enthalpy for PCM materials are provided in accordance with the work of [84,85]:

$$H_k = \begin{cases} C_k(\theta_k - \theta_{m,k}) \\ C_k(\theta_k - \theta_{m,k}) + 1/Ste_k \end{cases} \text{ for } \begin{cases} \theta_k < \theta_{m,k} \\ \theta_k > \theta_{m,k} \end{cases} \tag{4.18}$$

$$\theta_k = \begin{cases} H_{k+}\theta_{m,k} \\ \theta_{m,k} \\ (H_k - 1/Ste_k)/C_k + \theta_{m,k} \end{cases} \text{ for } \begin{cases} H_k < 0 \\ 0 \le H_k \le 1/Ste_k \\ H_k > 1/Ste_k \end{cases} \tag{4.19}$$

The link between enthalpy and temperature is easily described for the two solid layers (outside) and (inside) by:

$$H_{out} = C_{out}\theta_{out}\ ; H_{in} = C_{in}\theta_{in} \tag{4.20}$$

4.3.4 Dimensionless thermal boundary conditions

At t = 0, all layers of the wall are initially at the same temperature, T_i, establishing thermal equilibrium within the wall. The initial dimensionless condition is expressed as $\theta(X_k, 0) = 1$. The boundary conditions are detailed below:

At the outer surface of the solid outer layer ($S_{out,out}$)

$$K_{out}\frac{\partial\theta}{\partial X_{out}}\Big|_{X_{out}=2} = -Bi_{out}\theta_{out}|_{X_{out}=2} \tag{4.21}$$

At the inner surface of the solid outer layer ($S_{out,in}$)

$$K_1\frac{\partial\theta}{\partial X_1}\Big|_{X_1=2} = \frac{L_1}{L_{out}}\frac{k_{out}}{k_{1,s}}K_{out}\frac{\partial\theta}{\partial X_{out}}\Big|_{X_{out}=0} \tag{4.22}$$

At interface PCM1-PCM2 (S_m)

$$K_1\frac{\partial\theta}{\partial X_1}\Big|_{X_1=0} = \frac{L_1}{L_2}\frac{k_{2,s}}{k_{1,s}}K_2\frac{\partial\theta}{\partial X_2}\Big|_{X_2=2} \tag{4.23}$$

At the inner surface of the solid inner layer ($S_{in,in}$)

$$K_2\frac{\partial\theta}{\partial X_2}\Big|_{X_2=0} = \frac{L_2}{L_{in}}\frac{k_{in}}{k_{2,s}}K_{in}\frac{\partial\theta}{\partial X_{in}}\Big|_{X_{in}=2} \tag{4.24}$$

At the outer surface of the solid inner layer ($S_{in,out}$)

$$K_{in}\frac{\partial\theta}{\partial X_{in}}\Big|_{X_{in}=0} = Bi_{in}\left(\theta|_{X_{in}=0} - \theta_{\infty,in}\right) \tag{4.25}$$

4.4 Numerical solution

The finite-volume method is employed to solve the physical model representing the phenomenon [86,87].

4.4.1 Mesh

The governing equations for the various wall layers are discretized by employing a consistent meshing approach for each individual layer. The spatial interval, denoting the space between two internal nodes, is marked as ΔX. Each node signifies the control volume center, with the left and right sides referred to as 'w' and 'e,' respectively. The neighboring nodes are designated as 'W' and 'E.

4.4.2 Discretization of the equations

As it is mentioned above, the discretized equations govern the various layers of the wall are carried out through the finite volume method with a uniform mesh for each layer. For the two solid layers, the discretized equations are deduced from the general formulation while for the PCM layers, they are obtained basing on the enthalpy formulation. The discretized equations that represent the coupling at the interfaces of the wall layers are derived from the boundary conditions that govern these interfaces. The cumulative count of nodes and spatial increment for the solid in, solid out, PCM1, and PCM2 layers are provided as by $(N_{in}, \Delta X_{in}), (N_{out}, \Delta X_{out}), (N_1, \Delta X_1), (N_2, \Delta X_2)$. Every layer commences and terminates with half control volume. The gradient terms related to the time variable are discretized using an explicit scheme. Consequently, an examination of solution stability and mesh impact has led to the determination of an appropriate mesh configuration, where: $N_{in} = N_{out} = N_1 = N_2 = 81$.

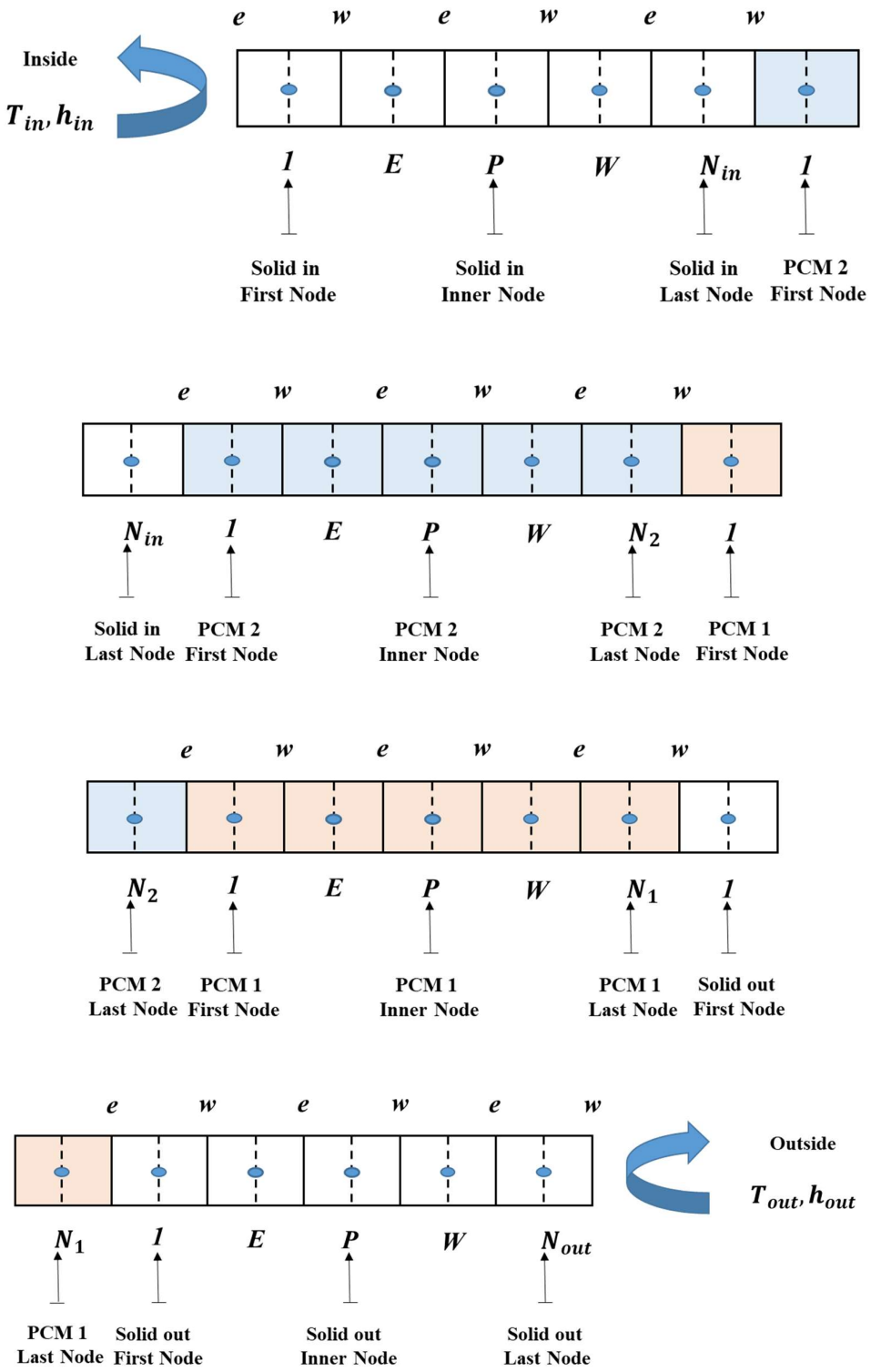

Figure 4.2 The multilayer wall mesh

4.4.2.1 Discretized equations of the inner solid layer

For an interior node

$$\theta_{in,j+1}^{P} = \theta_{in,j}^{P} + f_{in}\frac{\Delta\tau}{X_{in,w}-X_{in,e}}\left(K_{in,w}\frac{\theta_{in,j}^{W}-\theta_{in,j}^{P}}{\Delta X_{in}} - K_{in,e}\frac{\theta_{in,j}^{P}-\theta_{in,j}^{E}}{\Delta X_{in}}\right) \quad (4.26)$$

For the first node

$$\theta_{in,j+1}^{1} = \theta_{in,j}^{1} + f_{in}\frac{\Delta\tau}{X_{in,w}-X_{in,e}}\left(K_{in,w}\frac{\theta_{in,j}^{2}-\theta_{in,j}^{1}}{\Delta X_{in}} - Bi_{in}\left(\theta|_{X_{in}=0,j} - \theta_{\infty,in}\right)\right) \quad (4.27)$$

For the last node

$$\theta_{in,j+1}^{N_{in}} = \theta_{in,j}^{N_{in}} + f_{in}\frac{\Delta\tau}{X_{in,w}-X_{in,e}}\left(\frac{L_{in}}{L_{pcm2}}\frac{k_{2,s}}{k_{in}}K_{2,w}\frac{\theta_{2,j}^{1}-\theta|_{X_{in}=2,j}}{\Delta X_2/_2} - K_{in,e}\frac{\theta_{in,j}^{N_{in}}-\theta_{in,j}^{N_{in}-1}}{\Delta X_{in}}\right) \quad (4.28)$$

4.4.2.2 Discretized equations of the PCM2:

For an interior node

$$\mathrm{H}_{2,j+1}^{P} = \mathrm{H}_{2,j}^{P} + f_2\frac{\Delta\tau}{X_{2,w}-X_{2,e}}\left(K_{2,w}\frac{\theta_{2,j}^{W}-\theta_{2,j}^{P}}{\Delta X_2} - K_{2,e}\frac{\theta_{2,j}^{P}-\theta_{2,j}^{E}}{\Delta X_2}\right) \quad (4.29)$$

For the first node

$$\mathrm{H}_{2,j+1}^{1} = \mathrm{H}_{2,j}^{1} + f_2\frac{\Delta\tau}{X_{2,w}-X_{2,e}}\left(K_{2,w}\frac{\theta_{2,j}^{2}-\theta_{2,j}^{1}}{\Delta X_2} - \frac{L_{pcm2}}{L_{in}}\frac{k_{in}}{k_{2,s}}K_{in,w}\frac{\theta|_{X_2=0,j}-\theta_{in,j}^{N_{in}}}{\Delta X_{in}/_2}\right) \quad (4.30)$$

For the last node

$$\mathrm{H}_{2,j+1}^{N_2} = \mathrm{H}_{2,j}^{N_2} + f_2\frac{\Delta\tau}{X_{2,w}-X_{2,e}}\left(\frac{L_{pcm2}}{L_{pcm1}}\frac{k_{1,s}}{k_{2,s}}K_{1,w}\frac{\theta_{1,j}^{1}-\theta|_{X_1=0,j}}{\Delta X_1/_2} - K_{2,e}\frac{\theta_{2,j}^{N_2}-\theta_{2,j}^{N_2-1}}{\Delta X_2}\right) \quad (4.31)$$

4.4.2.3 Discretized equations of the PCM1:

For an interior node

$$\mathrm{H}_{1,j+1}^{P} = \mathrm{H}_{1,j}^{P} + f_1\frac{\Delta\tau}{X_{1,w}-X_{1,e}}\left(K_{1,w}\frac{\theta_{1,j}^{W}-\theta_{1,j}^{P}}{\Delta X_1} - K_{1,e}\frac{\theta_{1,j}^{P}-\theta_{1,j}^{E}}{\Delta X_1}\right) \quad (4.32)$$

For the first node

$$H_{1,j+1}^{1} = H_{1,j}^{1} + f_1 \frac{\Delta\tau}{X_{1,w}-X_{1,e}}\left(K_{1,w}\frac{\theta_{1,j}^{2}-\theta_{1,j}^{1}}{\Delta X_1} - \frac{L_{pcm1}}{L_{pcm2}}\frac{k_{2,s}}{k_{1,s}}K_{2,w}\frac{\theta|_{X_1=0,j}-\theta_{2,j}^{N_2}}{\Delta X_2/_2}\right) \quad (4.33)$$

For the last node

$$H_{1,j+1}^{N1} = H_{1,j}^{N1} + f_1 \frac{\Delta\tau}{X_{1,w}-X_{1,e}}\left(\frac{L_{pcm1}}{L_{out}}\frac{k_{out}}{k_{1,s}}K_{out,w}\frac{\theta_{out,j}^{1}-\theta|_{X_{out}=0,j}}{\Delta X_{out}/_2} - K_{1,e}\frac{\theta_{1,j}^{N_1}-\theta_{1,j}^{N_1-1}}{\Delta X_1}\right) \quad (4.34)$$

4.4.2.4 Discretized equations of the outer solid layer:

For an interior node

$$\theta_{out,j+1}^{P} = \theta_{out,j}^{P} + f_{out}\frac{\Delta\tau}{X_{out,w}-X_{out,e}}\left(K_{out,w}\frac{\theta_{out,j}^{W}-\theta_{out,j}^{P}}{\Delta X_{out}} - K_{out,e}\frac{\theta_{out,j}^{P}-\theta_{out,j}^{E}}{\Delta X_{out}}\right) \quad (4.35)$$

For the first node

$$\theta_{out,j+1}^{1} = \theta_{out,j}^{1} + f_{out}\frac{\Delta\tau}{X_{out,w}-X_{out,e}}\left(K_{out,w}\frac{\theta_{out,j}^{2}-\theta_{out,j}^{1}}{\Delta X_{out}} - \frac{L_{out}}{L_{pcm1}}\frac{k_{1,s}}{k_{out}}K_{1,w}\frac{\theta|_{X_{out}=0,j}-\theta_{1,j}^{N_1}}{\Delta X_1/_2}\right) \quad (4.36)$$

For the last node

$$\theta_{out,j+1}^{N_{out}} = \theta_{out,j}^{N_{out}} + f_{out}\frac{\Delta\tau}{X_{out,w}-X_{out,e}}\left(-Bi_{out}\theta_{out}|_{X_{out}=2} - K_{out}\frac{\theta_{out,j}^{N_{out}}-\theta_{out,j}^{N_{out}-1}}{\Delta X_{out}}\right) \quad (4.37)$$

4.4.2.5 Determination of the solid-liquid front position

For figuring out where the solid-liquid front located in the PCM layer, the following equation represents the total energy present in a control volume with center node i [83]:

$$H^i V_e^i = \left[(\theta^i - \theta_m)V_s^i + \left(C(\theta^i - \theta_m) + \frac{1}{Ste}\right)V_l^i\right] \quad (4.38)$$

In this context, V_e^i, V_s^i, V_l^i represent, the volume of the control volume, expressed in dimensionless units, the fraction of the PCM phase that is in a solid state and the fraction of the PCM phase that is in a liquid state, respectively. When a control volume experiences a phase change with $\theta^i = \theta_m$, the equation transforms to:

$$H^i V_e^i = (1/Ste)V_l^i \quad \text{or} \quad H^i = (1/Ste)V_l^i/V_e^i \quad (4.39)$$

The value of the enthalpy when the solidification front reaches the node i, is as follows:

$$H_c^i = 1/(2Ste) \tag{4.40}$$

This equation serves as a criterion for managing the front's position. To determine the solidification time at a specific node i, we examine two consecutive time instants, $\tau(j)$ and $\tau(j+1)$.

If $H^i(j+1) \leq H_c \leq H^i(j)$, then the solidification process takes place at a specific moment τ_{sol} within the time range of $\tau(j)$ to $\tau(j+1)$, and this moment can be determined using interpolation, $\tau(j) \leq \tau_{\text{sol}} \leq \tau(j+1)$.

The enthalpy is supposed to vary linearly across the whole time range. The equation for the solidification time of node i is: $\tau^i = (j+X)\Delta\tau$, Where X is determined through linear interpolation in the time domain, thus [83]:

$$X = \frac{H_c - H^i(j+1)}{H^i(j) - H^i(j+1)} \quad ; \quad \tau^i = \left(j + \frac{H_c - H^i(j+1)}{H^i(j) - H^i(j+1)}\right)\Delta\tau \tag{4.41}$$

4.5 Validation

Firstly, by comparing it to the analytical benchmark provided by Neumann, the numerical solution is validated. (**Figure 4.3A**) [89,88], which addresses the solidification or melting process of a pure PCM semi-infinite media under conditions of insulation on all other sides, constant temperature on one surface, and assuming constant thermophysical characteristics (Stefan problem).

The following solution dictates the location of the phase change interface:

$$s(t) = 2\lambda\sqrt{\alpha_l t}$$

With λ is the root of the subsequent transcendental equation [89]:

$$\lambda \exp(\lambda^2)\, erf(\lambda) = Ste/\sqrt{\pi}$$

In order to adapt our design to the Stefan problem, it is assumed that both PCM layers are made of the same material and have constant physical characteristics (ρ_l , c_l , k_l , α_l). In order to address the Stefan problem, we select solid layers whose thicknesses and thermophysical properties enable only the PCM layer to be considered for heat transfer [90]. Therefore, solid layers must have extremely low thicknesses, and thermal diffusivity must be sufficient high compared to PCM: ($L_{solid} \ll L_{pcm}$), ($\alpha_{solid} \gg \alpha_{pcm}$) .

In the comparative illustration depicted in Figure 2A, tetradecane paraffin $C_{14}H_{30}$ PCM and solid copper layers have been selected. The wall design includes a PCM layer with a thickness of 0.08 meters, positioned between two solid layers, each with a thickness of 0.01 meters. At the onset, the PCM medium is in a liquid state with a temperature of $T_i = T_m = 278.5$ K, which corresponds to the melting temperature, The solid layer 1's left side is maintained at a steady temperature of 268.5 K, whereas the external side of solid layer 2 is presumed to be thermally isolated. The copper properties are $k = 390\ \mathrm{W.m^{-1}.K^{-1}}$, $c = 385\ \mathrm{J.kg^{-1}.K^{-1}}$, $\rho = 8920\ \mathrm{kg.m^{-3}}$.

For the second validation, we assess our results by comparing them to the experimental findings in the study conducted by Zhong et al. [93]. Fig. 6 in the work of Zhong et al. [93] illustrates the environement temperature and solar radiation data. While Table 2 in the research by Zhong et al. [93] provides the material's thermophysical characteristics. Nonetheless, the optical characteristics of both glass and PCM are sourced from Li et al. [40]. The simulation was iterated until a periodic state was achieved, following the method described by Li et al. [40]. This periodic state typically takes two time periods, equivalent to 2 days in order to be accomplished.

Figure 4.3B displays the comparaison between the numerical outcomes obtained in this study and the experimental investigation by Zhong et al. [93] regarding the heat flux (excluding transmitted solar radiation) at the inner surface of PCM-filled double-glazing units. Overall, it's evident that the numerical findings align closely with the experimental results. The disparities in the outcomes can be attributed to variations in phase change temperatures. In the study by et al. [93], the PCM has distinct melting and solidification temperatures ($T_m = 21\ ^\circ\mathrm{C}$, $T_s = 13.5\ ^\circ\mathrm{C}$), whereas our current numerical model employs a single temperature for both solidification and melting (an averaged phase change

temperature $T_m = T_s = 18\,°C$). Moreover, the optical characteristics of the PCM, which contribute to a significant numerical discrepancy, are not precisely attainable (Li et al. [40]). Nonetheless, radiation transfer is a crucial factor in this heat transfer mechanism.

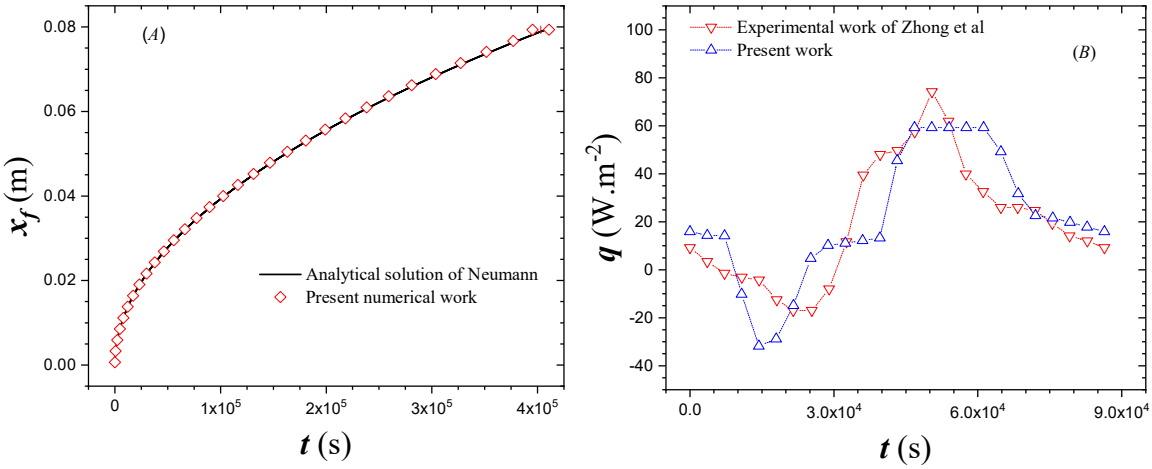

Figure 4.3 Comparison between the current study and existing literature: (A) Time-dependent phase change front position, (B) heat flux density at the inner surface of the double-glazing filled with PCM.

4.6 Results and discussion

4.6.1 Studied cases

As a part of the PCMs charging cycle for the summer, three different scenarios represent a variety of building types and climate zones. For example, during the night and in certain climate zones, residential buildings' interior temperatures may be equivalent to the ambient temperature outside. ($T_{\infty,in} = T_{\infty,out}$), this situation is depicted by ($\theta_{\infty,in} = 0$). However, in certain buildings with significant thermal loads, such as in kitchens, baths, and other rooms, the ambient temperature inside the building is greater than the ambient temperature outdoors the building during the charging period (at night) ($T_{\infty,in} > T_{\infty,out}$), this situation is depicted by ($\theta_{\infty,in} = 1.2$). Additionally, after the running cycle and just before the charging cycle starts, the temperature throughout the wall might be close to the interior ambient temperature ($T_{\infty,in} = T_{inital}$), in some climate zones, this case is represented by ($\theta_{\infty,in} = 1$).

4.6.2 Enthalpy and temperature evolution

The temperature and enthalpy evolution findings that are shown were achieved under the following conditions: both PCM layers melting temperatures ranges between several values (θ_{m1}, θ_{m2}), as well as the latent heats (Ste_1, Ste_2), ($Bi_{in} = Bi_{out} = 4.5$) . The two solid layers have the same thickness ($f_{in} = f_{out} = 4.43$).

4.6.2.1 Case 1 ($\boldsymbol{\theta_{\infty,in} = 0}$)

Fig. 4.4 illustrates the variations in enthalpy and temperature over dimensionless time across the four layers. The figure also indicates the phase change instances and positions throughout the wall for the combinations of ($\theta_{m1} = 0.7, \theta_{m2} = 0.5$), and ($\theta_{m1} = 0.5, \theta_{m2} = 0.7$). During these instances, the temperature remains constant at the solidification temperature, and there is a sudden decrease in enthalpy. This abrupt change signifies the solidification process, characterized by a negative enthalpy change indicating heat removal from the system. Conversely, during melting, the enthalpy change is positive, indicating heat addition to the system. The shift between the liquid and solid states (and conversely during melting) occurs when the enthalpy undergoes an abrupt shift from a positive value to a negative one. During these instances, energy is released through the latent heat process (cold storage). Beyond these instances, the accumulated cold is evident through a noticeable reduction in material temperature (sensible storage).

As is widely recognized, sensible heat pertains to the thermal energy needed to alter the temperature of a substance without inducing a change in its phase. In contrast, latent heat represents the amount of thermal energy needed to initiate a phase change without affecting the substance's temperature. In both cases, ($\theta_{m1} = 0.7, \theta_{m2} = 0.5$) and ($\theta_{m1} = 0.5, \theta_{m2} = 0.7$), complete solidification is observed, indicating that storing cold via latent heat method is appeared in both layers of the PCM. Furthermore, it is evident that phase change material PCM layers with identical phase change temperatures within the two combinations, ($\theta_{m1} = 0.7, \theta_{m2} = 0.5$) and ($\theta_{m1} = 0.5, \theta_{m2} = 0.7$), exhibit similar temperature and enthalpy behaviors. This similarity arises from the boundary conditions, geometric symmetry, as well as various thermophysical characteristics, such as ($\theta_{\infty,in} = \theta_{\infty,out} = 0$, $Bi_{in} = Bi_{out} = 4.5$), and ($Ste_1 = Ste_2 = 0.1$).

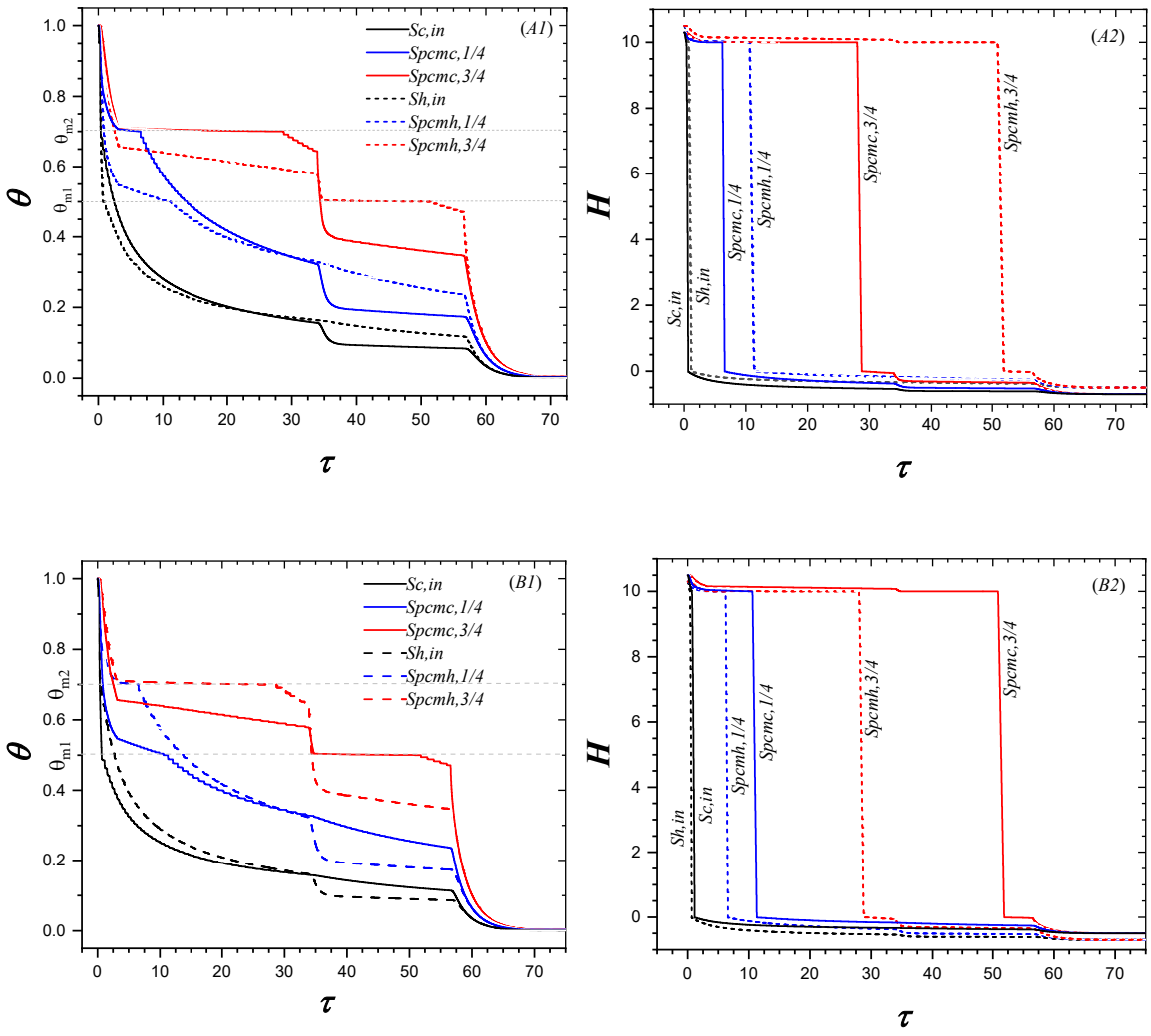

Figure 4.4 Temperature and Enthalpy Progression for the combination: (A1,A2) ($\boldsymbol{\theta_{m1} = 0.7, \theta_{m2} = 0.5}$) , (B1,B2) ($\boldsymbol{\theta_{m1} = 0.5, \theta_{m2} = 0.7}$)

4.6.2.2 Case 2 ($\boldsymbol{\theta_{\infty,in} = 1}$)

Based on Figure 4.5, it is evident that for $\theta_{m1} = 0.7$, the phase change material layer PCM1, positioned nearest to the outdoor cold ambient $\theta_{\infty,in} = 0$, reaches the solidification point more quickly compared to the situation when $\theta_{m1} = 0.5$. The same trend is observed for the frozen section of the phase change material layer (PCM 2), which is closer to the excitation $\theta_{\infty,in} = 1$. Consequently, the solidification process within the second phase change material layer (PCM 2) takes place partially in both scenarios, ($\theta_{m1} = 0.7, \theta_{m2} = 0.5$),

and ($\theta_{m1} = 0.5, \theta_{m2} = 0.7$). Furthermore, in the second case ($\theta_{m1} = 0.5, \theta_{m2} = 0.7$), The depth of the PCM that has been solidified is larger. This is attributed to the higher solidification temperature $\theta_{m2} = 0.7$, which allows for more PCM within this zone (in proximity to indoor ambient $\theta_{\infty,in} = 1$) to reach the solidification point. In contrast, in the case of $\theta_{m2} = 0.5$, the external cold excitation and the initial temperature (which is higher than the solidification temperature) lead to a reduction in the temperature gradient along the PCM layer. Consequently, the PCM with a higher solidification temperature reaches the phase change point faster compared to the one with a lower solidification temperature, resulting in a higher solid fraction (assuming both PCMs have the same latent heat). It is worth mentioning that the first phase change material layer (PCM 1) has been completely frozen in both cases, whether $\theta_{m1} = 0.7$ or $\theta_{m1} = 0.5$.

While the second phase change material layer (PCM 2) undergoes partial solidification, the storage of cold using latent heat is also partial. In the areas where the phase change point is not reached, the PCM retains its liquid state and achieves cold storage through a sensible reduction in temperature. Both excitations contribute to certain regions reaching the phase change point, enabling cold storage through a combination of sensible and latent heat mechanisms. However, there are other regions that fail to reach the solidification point, causing the PCM to remain in its liquid phase. Consequently, in these regions, cold storage occurs solely through a sensible decrease in temperature.

The first PCM layer undergoes complete solidification, allowing for cold storage in both sensible and latent ways. The occurrence of phase change, characterized by a constant temperature, is observed in regions capable of reaching the phase change point. This phase change also influences the temperature behavior of nearby regions, causing them to remain at a constant temperature momentarily, even if they do not reach the phase change point. This effect is similarly observed at the point $S_{pcm2,3/4}$ when τ = 120, where the enthalpy evolution confirms the absence of phase change within those regions. As we move further away from these regions, the impact of the phase change diminishes gradually. This behavior is also evident at points $S_{in,in}$ and $S_{pcm2,1/4}$ (Figure 4.5.(A1)).

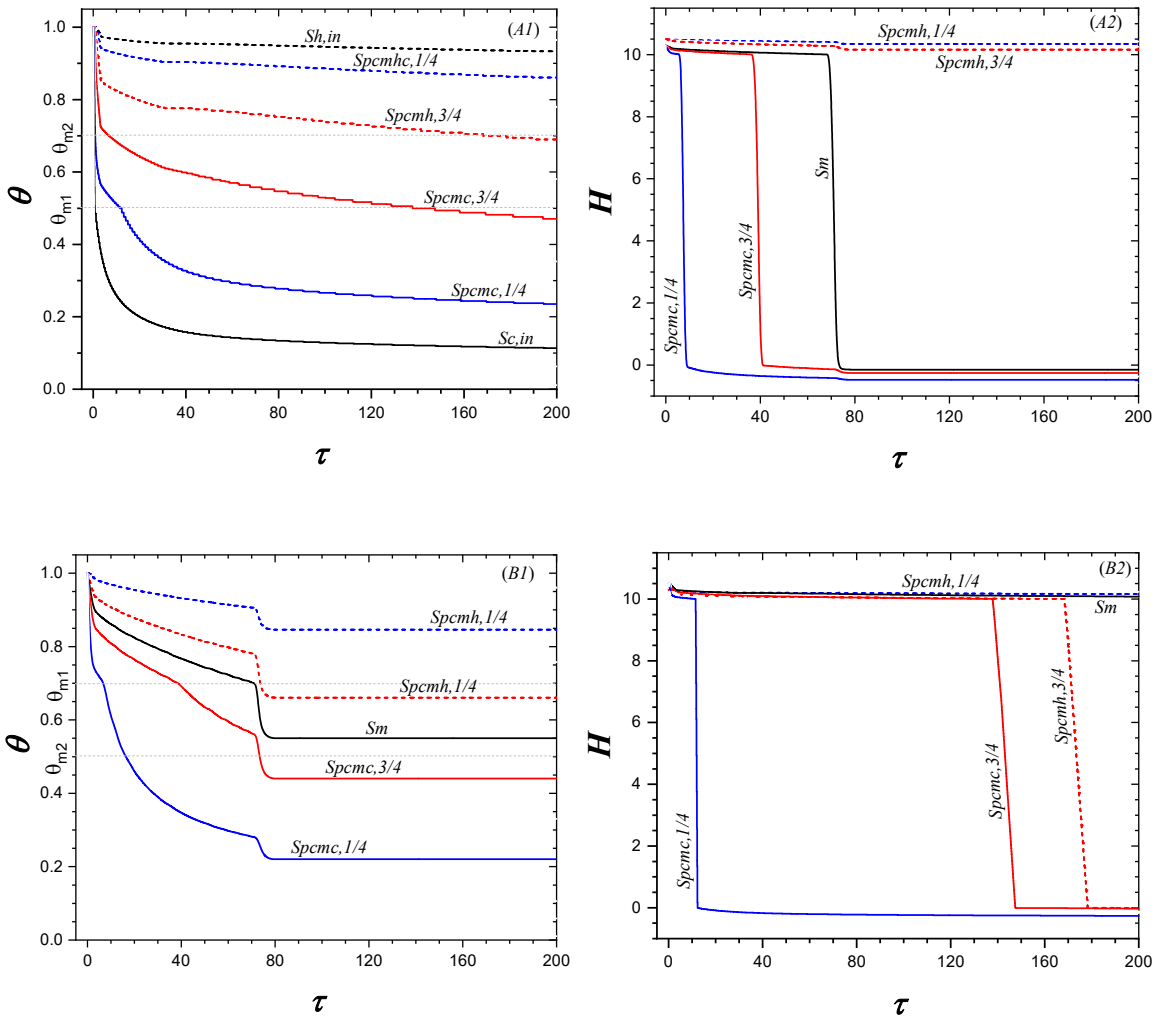

Figure 4.5 Temperature and Enthalpy Progression for the combination: (A1,A2) ($\boldsymbol{\theta_{m1} = 0.7, \theta_{m2} = 0.5}$) , (B1,B2) ($\boldsymbol{\theta_{m1} = 0.5, \theta_{m2} = 0.7}$)

4.6.2.3 Case 3 ($\boldsymbol{\theta_{\infty,in} = 1.2}$)

In relation to Figure 4.6, similar observations can be made for the scenario with the excitation ($\boldsymbol{\theta_{\infty,in} = 1}$). The first PCM layer demonstrates a faster attainment of the solidification point when $\theta_{m1} = 0.7$ compared to $\theta_{m1} = 0.5$. As for the second phase change material layer (PCM 2), only a portion of it reaches the solidification point when $\theta_{m2} = 0.7$, while the remaining portion retained its liquid form. In contrast, for the scenario when $\theta_{m2} = 0.5$, the whole second PCM layer doesn't attain the phase transition threshold because of the influence of the hot excitation ($\boldsymbol{\theta_{\infty,in} = 1.2}$).

Additionally, the enthalpy and temperature profiles within this zone display that the heat is stored through a noticeable temperature rise (sensible way), whereas the other portion accumulates cold by experiencing a significant temperature reduction (sensible way).

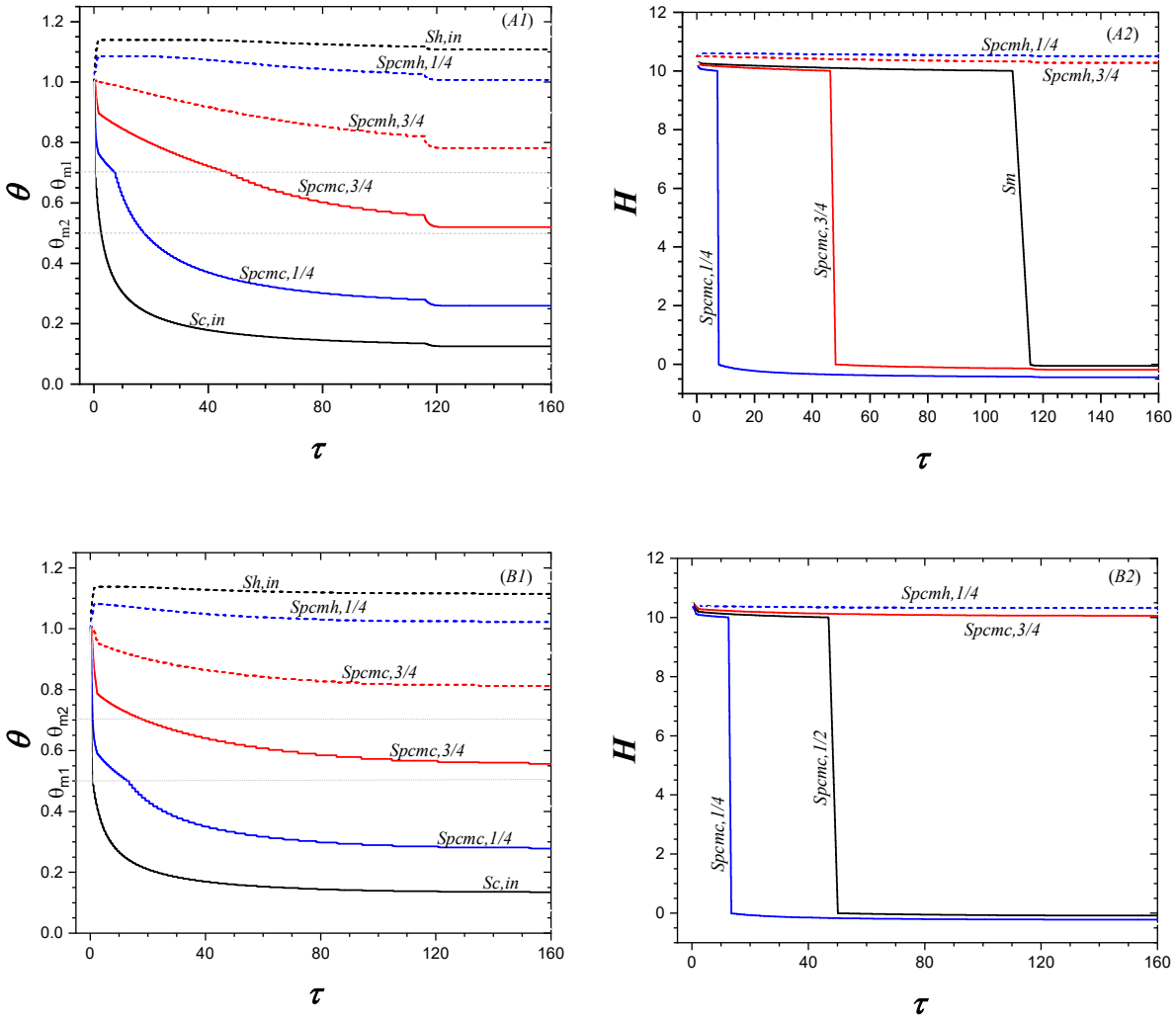

Figure 4.6 Temperature and Enthalpy progression for the combinations: (A1,A2) ($\boldsymbol{\theta_{m1} = 0.7, \theta_{m2} = 0.5}$) , (B1,B2) ($\boldsymbol{\theta_{m1} = 0.5, \theta_{m2} = 0.7}$)

In this case, the first phase change material layer (PCM 2) is completely frozen, enabling it to accumulate cold through latent and sensible means. Likewise, the frozen section of the second phase change material layer (PCM 2), for $\theta_{m2} = 0.7$, also exhibits cold storage in both sensible and latent forms. It is noteworthy that the phase change process influences the

temperature behavior in the neighboring area, but this effect diminishes as we depart further from these areas due to the influence of external excitations.

4.6.3 Front kinetic

4.6.3.1 Melting temperature effect

Figure 4.7(A1) demonstrates that the quantity of phase change interfaces relies on the specific combination of $(\theta_{m1}, \theta_{m2})$. In the case of symmetry $(\theta_{m1} = \theta_{m2})$, two fronts are observed at the interfaces of PCM1-Solid out, and PCM2-Solid in. These fronts move towards the PCM1-PCM2 interface which is the point of intersection, eventually leading to complete solidification. For the other cases $(\theta_{m1} \neq \theta_{m2})$, four phase change fronts are observed. These fronts start at the interfaces and move towards the midpoints of the two phase change material layers, ensuring complete freezing. Notably, the fronts originating from the PCM1-PCM2 interface exhibit a delayed movement in comparison to the other phase transition interfaces. The interface associated with the phase change layer having the lowest phase change point is the slowest to advance. This behavior can be attributed to the diffusion of the cold excitation from the outside, and the dissimilarity between the two phase change points$(\theta_{m1} \neq \theta_{m2})$. These factors create a temperature gradient that facilitates faster solidification near the PCM1-PCM2 interface in the phase change material layer with the higher freezing point compared to other areas within the same phase change material (excluding the area in proximity to the PCM-Solid interface), and more rapid than the other phase change material layer with the lower solidification temperature.

Based on Figure 4.7(B1), the kinetics of the phase transition interfaces indicate that the solidification operation is not fully accomplished. Two distinct phase transition interfaces are observed, with one corresponding to every phase change material layer. The solidification process initiates in the phase change material layer called PCM 1, located closer to the outdoor cold stimulus, commencing at the boundary (PCM1-Solid out) and progressing towards the other phase change material layer (PCM 2). In the case of the phase change material layer (PCM 2), which is in proximity to the indoor ambient $(\theta_{\infty,in} = 1)$, the solidification operation initiates at the PCM1-PCM2 boundary, influenced by the effect of the outdoor cold excitation coming from that direction. Where $(\theta_{\infty,in} = 1)$ denotes that the indoor and initial temperatures are the same, these temperatures are greater than the phase change point. Unlike the scenario when $(\theta_{\infty,in} = 0)$, this time only one external cold stimulus affecting

the system from the outdoor. As the phase change material layer (PCM 1) becomes fully solidified, the solidification front reaches the other phase change material layer (PCM 2), resulting in the appearance of a solidification front that moves from the boundary PCM1-PCM2 towards the boundary PCM2-Solid in.

The movement of the second front (PCM2) occurs later compared to the first front (PCM1), which is in proximity to closer to the outdoor cold ambient. In all combinations, It is noted that, when $\theta_{m2} = 0.5$, the solidification operation does not take place due to the temperature gradient across the entire phase change material layer (PCM 2) is above the phase transition temperature (the internal excitation prevent it from reaching the solidification temperature). Conversely, when $\theta_{m1} = 0.5$, solidification is observed in the phase change material layer PCM 1, despite the low phase transition temperature. This is because the first layer is located near the external cold excitation, allowing it to achieve the phase transition threshold.

Figure 4.7(C1) presents similar observations as mentioned earlier for the case of $\theta_{\infty,in} = 1$. Also, in this case, the solidification operation in the phase change material layer PCM 2 is not observed except when $\theta_{m2} = 0.7$, due to the influence of the indoor ambient (hot) that hinders the phase transition interface. On the other hand, the first phase change material layer has been completely frozen in this case, regardless of the phase change temperature.

4.6.3.2 Stefan number effect

In scenarios when boundary conditions exhibit symmetry, with equal Stefan numbers (Ste_1=Ste_2), Figure 4.7 (A2) demonstrates a symmetry in the kinetics of the solidification fronts. Couple of interfaces could be seen at the boundaries (PCM2-Sol in) and (PCM1-Solid out) and, influenced by the outdoor and indoor cold environments. The two interfaces move towards the boundary PCM1-PCM2, where they meet to ensure complete freezing of the two phase change material layers. It is noteworthy that complete freezing can be accomplished more rapidly with greater Stefan numbers. This can be ascribed to the Stefan number's characterization, indicating the proportion of sensible heat to latent heat. A lower Stefan

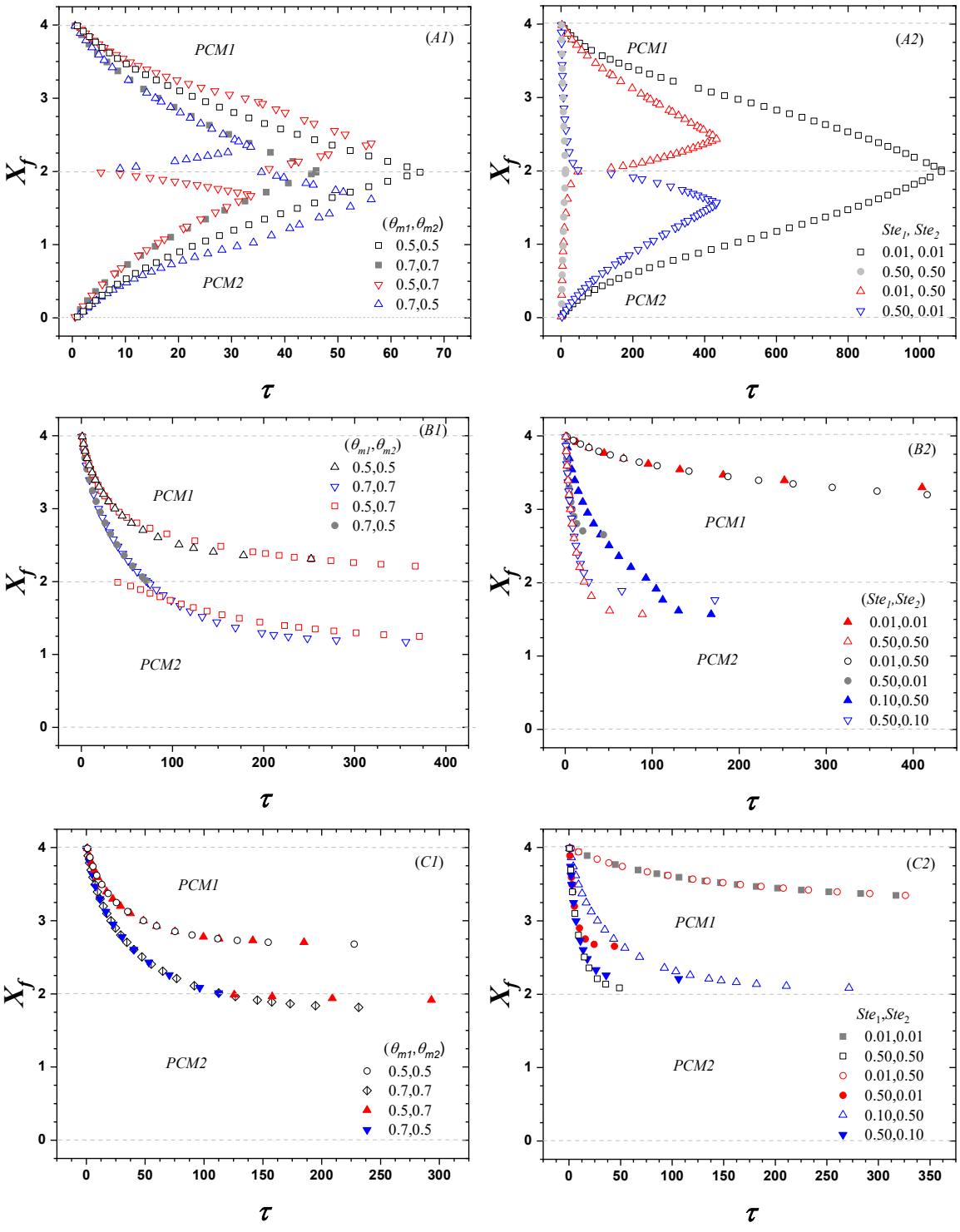

Figure 4.7 Front position progression across various melting temperatures and Stefan numbers: (A1, A2) $\boldsymbol{\theta_{\infty,in} = 0}$, (B1, B2) $\boldsymbol{\theta_{\infty,in} = 1}$, (C1, C2) $\boldsymbol{\theta_{\infty,in} = 1.2}$

number indicates a greater percentage of energy stored as latent heat in contrast to sensible heat, and conversely. Therefore, in cases with a low Stefan number, more time is required to

store or release a larger amount of heat to simplify the phase transition operation. The other curves represent cases where ($Ste_1 \neq Ste_2$) and exhibit three solidification fronts. The phase change material layer with the lower Stefan number shows two solidification fronts. The initial interface commences at the PCM1-Solid out (or PCM2-Solid in) boundary, in proximity to the outdoor cold ambiance, prior to the other front, which is a continuation of the interface originating from the other phase change material layer with the greater Stefan number and advancing toward the PCM1-PCM2 boundary. The phase change material layer with the higher Stefan number displays a single solidification front, progressing from the boundaries (PCM2-Solid in) or (PCM1-Solid out) towards the boundary PCM1-PCM2. Complete frozen is achieved in all these cases.

In Figure 4.7(B2), it is observed that regardless of the combination of Stefan numbers ($Ste_1 - Ste_2$), only one solidification front is visible, commencing at the boundary (PCM1-Solid out) in close proximity to the surface exposed to the outdoor cold stimulus and moving towards the other phase change material layer (PCM 2). Notably, If, in any case, one of the phase change material layers has the minimum Stefan number ($Ste_1 = Ste_2 = 0.01$), the solidification process remains incomplete in the first PCM layer, while the phase change point is not reached in the second PCM layer. As mentioned earlier, a low Stefan number signifies that a larger quantity of energy needs to be liberated to attain the solidification threshold. In alternative scenarios, complete freezing is evident within the phase change material layer (PCM 1), additionally, a continuation of the initial solidification front (indicative of the cold stimulus) extends into the second phase change material layer (PCM 2), advancing from the PCM1-PCM2 boundary toward the PCM2-Solid in boundary. Hence, the freezing of the phase change material layer (PCM 2) remains incomplete. Also it is evident that a higher Stefan number enables more rapid solidification operation in the phase change material layer (PCM 1). Regarding the second PCM layer, a higher Stefan number results in a larger quantity of frozen phase change material. the higher Stefan number signifies less quantity of energy storage (released) by latent heat in comparison to energy storage (released) by sensible heat, leading to a rapid solidification operation and a greater portion of phase change material reaching the freezing threshold.

Based on Figure 4.7(C2), it can be observed that the phase change material layer (PCM 2) does not undergo the solidification operation because of the presence of the indoor hot

ambiance near the boundary PCM2-Solid in. Throughout the entire phase change material layer PCM 2, the influence of the outside cold environment from the opposite direction is diminished. Additionally, it is evident that the freezing of the phase change material layer PCM 1 remains incomplete. As previously stated, a higher Stefan number enables faster freezing within the phase change material layer PCM 1, resulting in a greater quantity of frozen phase change material, and conversely. The Stefan number signifies the proportion of the energy storage (release) by sensible heat way and energy storage (release) by latent heat way, with an inverse relationship to latent heat. Thus, a high Stefan number implies a low amount of latent heat. In cases where the melting temperatures are the same, A high Stefan number (indicating low latent heat) implies that the substance requires a lower quantity of heat to be released in order to achieve its freezing threshold, as opposed to a low Stefan number (indicating high latent heat). Consequently, the solidification operation occurs more rapidly and results in a larger quantity of solidified matter.

4.6.4 Solid fraction

When $\theta_{\infty,in} = 0$, it has been discovered that, the solid fraction indicates complete freezing of the two phase change material layers, whatever the combination $(\theta_{m1}, \theta_{m2})$ (Ste_1, Ste_1), this pertains to the symmetrical boundary conditions in which two external cold excitations are present.

4.6.4.1 Melting temperature effect

In the scenario of $\theta_{\infty,in} = 1$ (Figure 4.8), as anticipated, in accordance with the external environment effect, the highest solid fraction is obtained with the highest melting temperature. Furthermore, when the inside phase change material layer PCM 2 layer, which is positioned at a greater distance from the outside cold ambiance, possesses the highest solidification point, it results in a higher portion of solid in contrast to the situation where the outside phase change material layer PCM 1 has the highest solidification point, which is closer to the outdoor cold environment.

Moreover, certain combinations, such as when the phase change material layer PCM 1 has a lower solidification point in comparison to the phase change material layer PCM 2 (e.g. $\theta_{m1} = 0.5, \theta_{m2} = 0.7$), yield approximately identical solid portion such as cases where the two solidification points are set to the highest value (e.g. $\theta_{m1} = 0.7, \theta_{m2} = 0.7$).

Conversely, cases where the phase change material layer PCM 1 has a greater solidification points than the phase change material layer PCM 2 (e.g. $\theta_{m1} = 0.7, \theta_{m2} = 0.5$), result in a lower solid portion in comparison to the situation where the two solidification points are identical and set at the highest value (e.g. $\theta_{m1} = 0.7, \theta_{m2} = 0.7$). This observation can be clarified by considering the gradient of the temperature. Where near the boundary condition $\theta_{\infty,in} = 1$, a greater solidification point is needed to achieve the phase change process (solidification), while a lower melting temperature is sufficient to achieve solidification for the phase change material layer in proximity to the outdoor cold ambiance.

In the situation of $\theta_{\infty,in} = 1.2$ (Figure 4.8), due to the hot excitation, the solidification process is absent in the second PCM layer, except for combinations where $\theta_{m2} = 0.7$. However, in the phase change material layer PCM 1, it is observed that the solid portion increases with the rise in the solidification point. The overall solid portion is closely linked to the increase in the solidification point of the phase change material layer PCM 1, as the freezing operation is limited within the phase change material layer PCM 2.

4.6.4.2 Stefan number effect

In the scenario of $\theta_{\infty,in} = 1$, as depicted in Figure 4.8, the phase change material layer PCM 1 achieves complete freezing for combinations where $Ste_1 = 0.1$ or $Ste_1 = 0.5$. However, within the phase change material layer PCM 2, for situations when $Ste_1 = 0.1$ or $Ste_1 = 0.5$, is observed only a partial freezing. Furthermore, it is seen that the solid fraction of the phase change material layer PCM 1 increases with an increase in the Stefan number of the phase change material layer PCM 2.

In the situation of $\theta_{\infty,in} = 1.2$, as illustrated in Figure 4.8, it can be observed that an increase in the Stefan number Ste_1 leads to a higher solid fraction in the phase change material layer PCM 1. Similarly, the solid portion in the first PCM layer also increases with raising up Stefan number (Ste_2) of the second phase change material layer PCM 2. The combination of ($Ste_1 = 0.5$, $Ste_2 = 0.5$) and ($Ste_1 = 0.1$, $Ste_2 = 0.5$) yields the highest solid fraction.

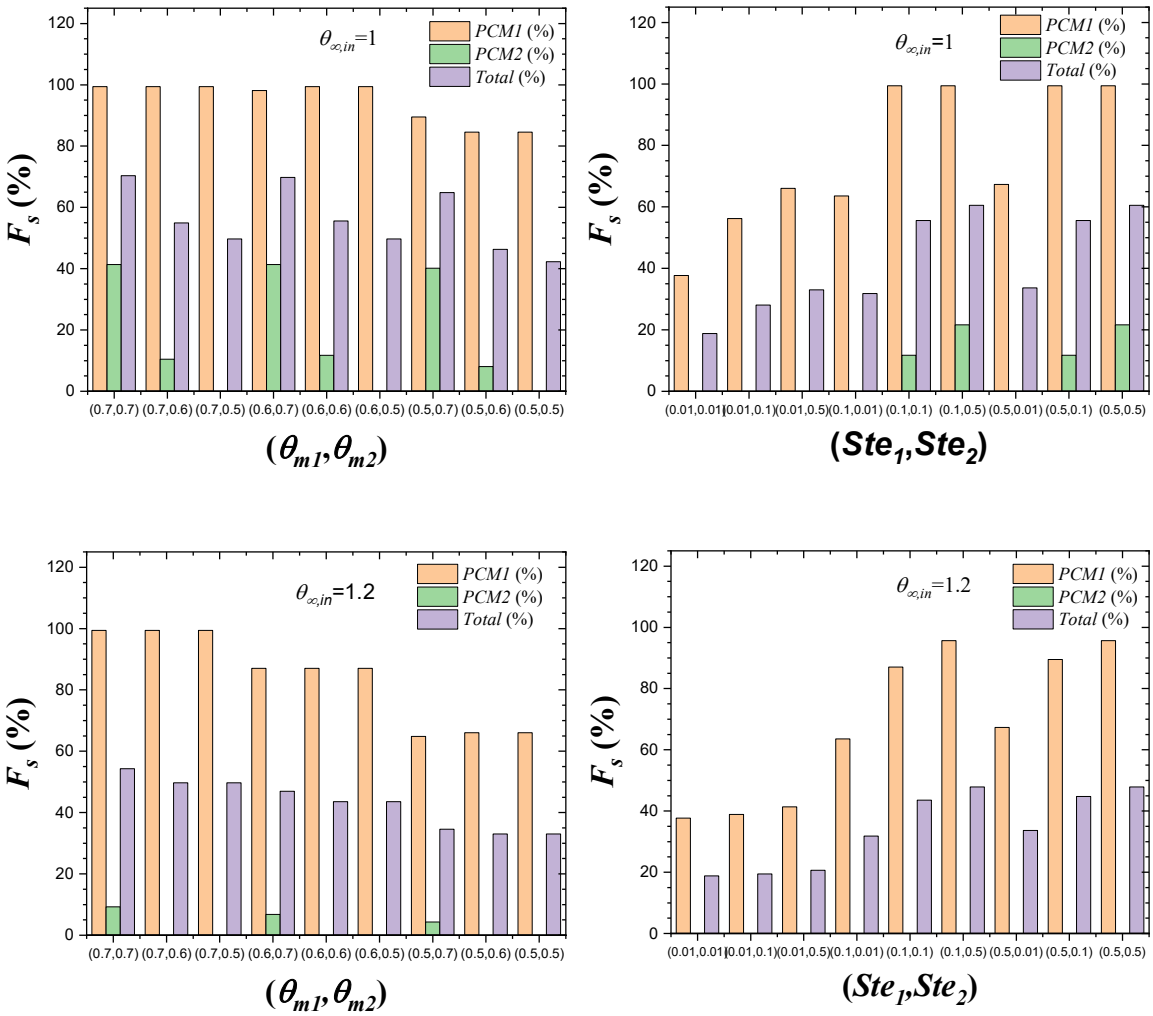

Figure 4.8 Variation in Solid Fraction with Melting Temperatures and Stefan Numbers for different combinations $(\boldsymbol{\theta_{m1}, \theta_{m2}})$ and (Ste_1, Ste_2)

4.6.5 Time needed in order to reach the limit of solidification

4.6.5.1 Melting temperature effect

In the scenario where $\theta_{\infty,in} = 0$, the data presented in Table 4.1 indicates that the duration required to reach the solidification limit point (if applicable) decreases as the melting temperatures (θ_{m1} and θ_{m2}) increase for both PCM layers. Additionally, it is noteworthy that every phase change material layer is impacted by increasing the solidification point of the other phase change material layer. Such as the time needed to reach the limit point of the freezing for one layer diminishes when the melting temperature of the other layer decreases.

In the case of $\theta_{\infty,in} = 1$, the findings from Table 4.1 demonstrate that the time required for the first PCM layer to achieve full solidification or reach the solidification limit point is influenced by the solidification point of the phase change material layer PCM 2. Specifically, a decrease in θ_{m2} results in a shorter duration for achieving the limit of solidification in the phase change material layer PCM 1. Conversely, a decrease in θ_{m1} leads to an increased time required for reaching the limit point of freezing in the phase change material layer PCM 1. It is important to note that the solidification process in this situation is solely driven by the external cold excitation, which is in proximity to the phase change material layer PCM 1.

In the scenario of $\theta_{\infty,in} = 1.2$, the observations from Table 4.1 indicate that the solidification process is predominantly incomplete in the phase change material layer PCM 1 for most combinations. However, solidification is observed within the phase change material layer PCM 2 in combinations where $\theta_{m2} = 0.7$. Due to these circumstances, the required time to achieve the limit of solidification does not follow a consistent pattern of decrease or increase in melting temperature for both PCM layers.

4.6.5.2 Stefan number effect

In the scenario of $\theta_{\infty,in} = 0$, Table 4.2 highlights the influence of raising up Stefan number for two phase change material layer on the required time to reach the solidification limit. It is observed that the time decreases for both layers as the Stefan numbers Ste_1 or Ste_2 increases. The Stefan number signifies the proportion of the storing heat (cold) by the sensible way (cold) storage relative to the storing heat (cold) by the latent way. An increase in the Stefan number indicates a higher quantity storage of heat (cold) by sensible way in contrast to storage of heat (cold) by latent way, resulting in a reduced energy requirement to attain the solidification threshold. Consequently, a reduction in the needed time to achieve complete freezing is noted as the phase change material layers begin to store cold through sensible method and conveys the influence of the outdoor cold stimulus to the adjacent layer, thus, accelerating its reaching to the freezing threshold.

For $\theta_{\infty,in} = 1$, the data in Table 4.2 reveals that the freezing of the phase change material layer PCM 1 remains unfinished in certain combinations, however, it does not take place at all in the phase change material layer PCM 2 if $Ste_1 = 0.01$ or $Ste_2 = 0.01$. Notably, when $Ste_1 = 0.01$, an increase in Ste_2 corresponds to an increase in the time needed to reach the

solidification limit in the phase change material layer PCM 1, corresponding to the augmentation in the solid portion achieved. Conversely, for $Ste_1 = 0.1$ and $Ste_1 = 0.5$, an increase in Ste_2 results in a reduction in the necessary time for both PCM layers to reach the solidification limit. This decrease can be attributed to the fact that, with a constant solid fraction, increasing Ste_2 reduces the quantity of energy that needs to be liberated to attain solidification, consequently shortening the required time for both PCM layers. As for the effect of Ste_1, it is evident that an increase in Ste_1 results in a reduction in the necessary time for the phase change material layer PCM 1 to achieve its solidification limit.

For $\theta_{\infty,in} = 1.2$, according to the information presented in Table 4.2, the process of solidification does not occur within the second PCM layer regardless of the combination, primarily due to the influence of the nearby hot excitation. However, partial solidification is observed within the phase change material layer PCM 1. In terms of the influence of Ste_1 and Ste_2, it is evident that raising up either Ste_1 or Ste_2 leads to a shorter duration required to attain the solidification threshold. This observation aligns with the previous condition $\theta_{\infty,in} = 1$, and can be attributed to similar underlying mechanisms.

Table 4-1 Required Duration to reach the limit of solidification as function of melting temperatures

$(\theta_{m1}, \theta_{m2})$	$\theta_{\infty,in} = 0$		$\theta_{\infty,in} = 1$		$\theta_{\infty,in} = 1.2$	
	PCM1	PCM2	PCM1	PCM2	PCM1	PCM2
(0.7,0.7)	45.36	45.36	70.53	282.96	111.94	112.22
(0.7,0.6)	36.91	49.33	70.54	105.00	111.98	0
(0.7,0.5)	33.07	55.33	70.54	0	111.95	0
(0.6,0.7)	49.33	36.91	157.33	320.04	266.23	175.44
(0.6,0.6)	53.26	53.26	125.01	141.14	214.82	0
(0.6,0.5)	42.52	58.97	125.04	0	215.02	0
(0.5,0.7)	55.33	33.07	365.69	548.22	183.99	167.58
(0.5,0.6)	58.98	42.52	302.55	200.41	226.74	0
(0.5,0.5)	64.52	64.52	251.24	0	226.58	0

Table 4-2 Required Duration to reach the limit of solidification as function of Stephan numbers

(Ste_1, Ste_2)	$\theta_{\infty,in} = 0$		$\theta_{\infty,in} = 1$		$\theta_{\infty,in} = 1.2$	
	PCM1	PCM2	PCM1	PCM2	PCM1	PCM2
(0.01,0.01)	1058.02	1058.02	564,24	0	564.24	0
(0.01,0.10)	450.21	124.02	1527,11	0	615.22	0
(0.01,0.50)	430.99	46.39	1550,11	0	813.09	0
(0.10,0.01)	124.02	450.21	96,88	0	96.88	0
(0.10,0.10)	53.26	53.26	125,01	141.14	214.82	0
(0.10,0.50)	34.05	12.29	98,99	66.04	270.85	0
(0.50,0.01)	46.39	430.99	43,46	0	43.46	0
(0.50,0.10)	12.29	34.05	26,28	141.14	105.85	0
(0.50,0.50)	11.71	11.71	21,36	66.05	48.40	0

4.6.6 Starting Time of solidification

According to tables 5-6, the starting time of freezing for the phase change material layer PCM 1 is roughly the same whatever the combination $(\theta_{m1}, \theta_{m2})$, (Ste_1, Ste_2), because this layer is close to the cold excitation; therefore, we are going to focus within this part on the starting time of freezing for the phase change material layer PCM 2 (the same for the case $\theta_{\infty,in} = 0$ **,** the solidification process start at same time for all combinations).

4.6.6.1 Melting temperature effect

It is shown via Table 5, for the case $\theta_{\infty,in} = 1$, that the decreasing of θ_{m1} leads to increase the starting time of the solidification process through the second PCM layer. Because the diminution of θ_{m1} delays the phase change material layer PCM 1 to achieve the full freezing, and consequently delays the starting of solidification process within the phase change material layer PCM 2 (at the boundary PCM1-PCM2). Likewise, the decreasing of θ_{m2} drives to growing up the starting time of solidification process.

For $\theta_{\infty,in} = 1.2$, the process of solidification appears only when $\theta_{m2} = 0.7$, such as the previous case $\theta_{\infty,in} = 1$ **,** the decreasing of θ_{m1} leads to increase the starting time of the solidification process through the second PCM layer.

Table 4-3 Starting time of solidification as function of melting temperatures

$(\theta_{m1}, \theta_{m2})$	$\theta_{\infty,in} = 0$		$\theta_{\infty,in} = 1$		$\theta_{\infty,in} = 1.2$	
	PCM1	PCM2	PCM1	PCM2	PCM1	PCM2
(0.7,0.7)	0.544	0.54	0.54	73.19	0.54	119.11
(0.7,0.6)	0.544	0.72	0.54	77.33	0.54	0
(0.7,0.5)	0.544	0.96	0.54	0	0.54	0
(0.6,0.7)	0.72	0.54	0.72	58.34	0.72	124.20
(0.6,0.6)	0.72	0.72	0.72	132.22	0.72	0
(0.6,0.5)	0.72	0.96	0.72	0	0.72	0
(0.5,0.7)	0.96	0.54	0.96	40.00	0.96	125.61
(0.5,0.6)	0.96	0.72	0.96	135.40	0.96	0
(0.5,0.5)	0.96	0.96	0.96	0	0.96	0

4.6.6.2 Stefan number effect

For the case $\theta_{\infty,in} = 1$, regarding Table 6, it is seen for $Ste_1 = 0.1$ and $Ste_1 = 0.5$, the increasing of Ste_2 creates a diminution of the starting time of the solidification process. The augmentation of Ste_2 means a diminution of the heat (cold) storage by latent heat comparing to the sensible heat (cold) storage that provides early solidification process launching.

Table 4-4 Starting time of solidification as function of Stefan numbers

(Ste_1, Ste_2)	$\theta_{\infty,in} = 0$		$\theta_{\infty,in} = 1$		$\theta_{\infty,in} = 1.2$	
	PCM1	PCM2	PCM1	PCM2	PCM1	PCM2
(0.01,0.01)	2.20	2.20	2,20	0	2,20	0
(0.01,0.10)	2.17	0.72	2,20	0	2,20	0
(0.01,0.50)	2.16	0.57	2,20	0	2,20	0
(0.10,0.01)	0.72	2.17	0,72	0	0,72	0
(0.10,0.10)	0.72	0.72	0,72	132.22	0,72	0
(0.10,0.50)	0.72	0.57	0,72	101.87	0,72	0
(0.50,0.01)	0.57	2.16	0,57	0	0,57	0
(0.50,0.10)	0.57	0.72	0,57	30.93	0,57	0
(0.50,0.50)	0.57	0.57	0,57	22.73	0,57	0

4.6.7 Heat lost during charging cycle

The total heat lost during charging cycle period is defined as the instantaneous dimensionless heat flux integrated over the time period [91] :

$$Q = \int_0^{\Delta\tau} \dot{Q}\ d\tau \tag{4.42}$$

The definition of the dimensionless heat flux at the external surface of the wall in an instantaneous context is provided by:

$$\dot{Q} = -Bi_{out}\ \ \theta_{out}|_{X_{out}=2} \tag{4.43}$$

In this section, it is presupposed that both PCM layers have completely melted during a prior operational cycle; All points of the wall have an identical initial temperature $\theta_i = 1$, which is equivalent to the ambient temperature on the inside $\theta_{\infty,in} = 1$. The estimated duration of the charging cycle is calculated using a 24-hour real daily period, assuming that the charging cycle takes approximately half a day to complete.

4.6.7.1 Melting temperature effect

Based on Figure 4.9, it was observed that utilizing a charging period of half-day , equivalent to Δτ=57, the combination (*PSM, PSM*) depicting a building envelope with absence of phase change material exhibits the minimum quantity of liberated heat during the charging period. This is attributed to the relatively limited heat storage during the operational period, which takes place in a sensible manner. In contrast, other cases involving PCM layers accumulate heat in a latent manner during the operational period. Moreover, the melting temperature of the phase change material (PCM) layer positioned in proximity to the outdoor ambiance plays a more crucial role in controlling the released heat compared to the melting temperature of the PCM layer located close to the indoor ambiance, primarily due to its proximity to the external stimulus.

Furthermore, based on the kinetic of the phase change front position, it's evident that the inside PCM layer undergoes a feeble freezing operation during this brief charging cycle, with the solid portion remaining constant regardless of the inside PCM layer's solidification point, This results in an equal quantity of heat loss for combinations that share the same solidification point of the outer PCM layer, Subsequently, combinations with identical θ_{m1}

values yield the same proportion of additional heat released. For example, both combinations ($\theta_{m1} = 0.6, \theta_{m2} = 0.5$) and ($\theta_{m1} = 0.6, \theta_{m2} = 0.7$) achieve 15%.

Furthermore, based on the kinetic of the phase change front position analysis, it is observed that the inside phase change material layer (PCM) undergoes a limited freezing operation during the duration of charging. Regardless of the melting temperature of the inner PCM layer, the solid fraction remains constant, resulting in a consistent amount of heat loss for combinations that share the same phase change point for the outside PCM layer. Consequently, combinations with the same θ_{m1} (solidification point of the outside phase change material layer) exhibit an equal ratio of additional heat released. For example, both combinations ($\theta_{m1} = 0.6, \theta_{m2} = 0.5$) and ($\theta_{m1} = 0.6, \theta_{m2} = 0.7$) achieve a 15% increase in heat release.

Nevertheless, it is worth mentioning that the amount of heat lost diminishes as the solidification point of the outer phase change material (PCM) layer, θ_{m1}, decreases. Similarly, the combination ($\theta_{m1} = 0.7, \theta_{m2} = 0.5$) releases an additional 18% of heat compared to the reference case (PSM, PSM). In contrast, the combination ($\theta_{m1} = 0.5, \theta_{m2} = 0.7$) achieves a 13% increase. This can be attributed to the solidification process significantly decreasing as the freezing point of the outside phase change material layer decreases, resulting in a decrease in cold (heat) storage by latent heat way. In comparison to cold (heat) storage by sensible heat way, the first manner offers the benefit of higher density of energy. Consequently, reducing the solidification point of the outside phase change material layer leads to a decrease in the released heat.

4.6.7.2 *Ste* number effect

According to Figure 8, combinations with a high latent heat in the outer layer (Ste_1=0.01) exhibit a higher amount of liberated heat during the charging period compared to the reference combination (PSM, PSM). Despite having a reduced solid portion in contrast to other cases, these high latent heat combinations show a supplementary heat release ratio of 150% in comparison to the baseline scenario. On the other hand, combinations with a low latent heat in the outer layer (Ste_1=0.1, 0.5) generally demonstrate a reduced heat release quantity Throughout a half-day charging period compared to the combination (*PSM, PSM*).

For example, in the combination ($Ste_1 = 0.5, Ste_2 = 0.1$), the liberated heat ratio was 10% lower than the baseline case.

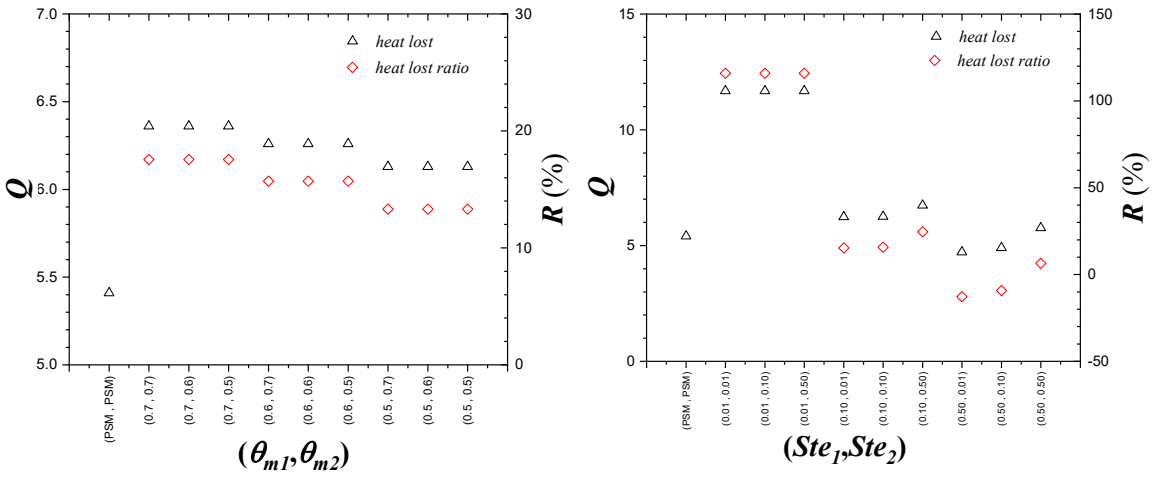

Figure 4.9 Heat loss and heat release ratio as a function of melting temperatures and Stefan numbers for various combinations ($\boldsymbol{\theta_{m1}, \theta_{m2}}$) and ($Ste_1$, Ste_2) during the charging cycle

This can be attributed to the relatively low quantity of accumulated heat within the operational period in combinations where Ste_1=0.1 and 0.5, compared to combinations with Ste_1=0.01 (high latent heat) and the reference combination (PSM, PSM). In the latter case, the heat storage occurs in a sensible manner, while combinations involving phase change materials store heat in a latent manner (either low or high depending on the PCM's latent heat). Furthermore, reducing the latent heat of the outside phase change material layer (PCM) results in a decrease in the heat released. Similarly, increasing Ste2, which indicates a decrease in the latent heat of the inside phase change material layer (PCM), drives to raising up in the liberated heat and the solid portion. For example, in the combination (Ste_1=0.1, Ste_2=0.01), the liberated heat ratio was 15%, whereas for (Ste_1=0.1, Ste_2=0.5), it was 25%.

4.7 Conclusion

The objective of this study is to demonstrate how the interaction between both inner and outer PCM layers influences the overall performance of the building envelope under various conditions, including building type and climate zone. By considering the points illustrated

below, we can determine whether PCMs with varying melting temperatures or latent heat can enhance the performance of the building envelope:

The analysis of solid fraction indicates the following:

Combinations where the melting temperature of the second (inner) PCM layer is higher or equal to that of the first (outer) PCM layer exhibit the highest solid fraction. For example:

- When the inside ambient temperature is higher than the outside temperature ($T_{\infty,in} > T_{\infty,out}$), the combination ($\theta_{m1} = 0.6, \theta_{m2} = 0.7$) achieved a solid fraction of 47%, whereas the combination ($\theta_{m1} = 0.6, \theta_{m2} = 0.5$) had a solid fraction of 43.5%.
- Similarly, when the inside ambient temperature is equal to the wall's initial temperature ($T_{\infty,in} = T_{inital} > T_{\infty,out}$), the combination ($\theta_{m1} = 0.6, \theta_{m2} = 0.7$ resulted in a solid fraction of 70%, while the combination ($\theta_{m1} = 0.6, \theta_{m2} = 0.5$) reached 50%.

Combinations where the latent heat of the second (inner) PCM layer is lower or equal to that of the first (outer) PCM layer demonstrate a high solid fraction. For instance:

- When the inside ambient temperature is higher than the outside temperature ($T_{\infty,in} > T_{\infty,out}$), the combination ($Ste_1 = 0.1, Ste_2 = 0.5$) exhibited a solid fraction of 48%, whereas the combination ($Ste_1 = 0.1, Ste_2 = 0.01$) had a solid fraction of 32%.
- Similarly, when the inside ambient temperature is equal to the wall's initial temperature ($T_{\infty,in} = T_{inital} > T_{\infty,out}$), the combination ($Ste_1 = 0.1, Ste_2 = 0.5$) resulted in a solid fraction of 60%, while the combination ($Ste_1 = 0.1, Ste_2 = 0.01$) reached 32%.

Regarding the time needed to reach the limit point of solidification, the following observations were made:

- The time required decreases as the melting temperature of the other PCM layer decreases.
- Decreasing θ_{m1} (melting temperature of the first PCM layer) leads to an increase in the time needed to reach the limit point of solidification in that layer.
- Reducing the latent heat of the second PCM layer results in a decrease in the required time to reach the limit point of solidification in both PCM layers.

The examination of the heat released ratio reveals the following:

- The melting temperature of the outer PCM layer serves as the primary factor controlling the amount of heat lost, primarily due to its proximity to the external excitation. Where increasing θ_{m1} results in a higher heat loss. For example, the combination ($\theta_{m1} = 0.7, \theta_{m2} = 0.5$ releases an extra heat ratio of 18% compared to the reference case (*PSM, PSM*), while the combination ($\theta_{m1} = 0.5, \theta_{m2} = 0.7$) achieves 13%.
- Conversely, the melting temperature of the inner PCM layer does not significantly affect the amount of heat released, as it is commonly chosen to be suitable with the other season. Where combinations with the same θ_{m1} provide an identical ratio of extra heat released. For instance, both combinations ($\theta_{m1} = 0.6, \theta_{m2} = 0.5$) and ($\theta_{m1} = 0.6, \theta_{m2} = 0.7$) achieve a 15% increase in heat release.

As a result, for effective charging of the PCM layer with a melting temperature suitable for the specified season, it is advisable to place it in close proximity to the external excitation.

- To ensure efficient charging of PCM layers, it is preferable for the latent heat of the inner PCM layer, which is farthest from the external excitation, to be lower than the latent heat of the outer PCM layer (which is closest to the outside). This can be achieved by having a higher Stefan number for the inner layer Ste_2 compared to the outer layer Ste_1. This arrangement promotes a stronger solidification process with a higher solid fraction, resulting in a greater amount of heat being released. For example, in the combination ($Ste_1 = 0.1, Ste_2 = 0.01$), the heat released ratio was 15%, while for ($Ste_1 = 0.1, Ste_2 = 0.5$), it was 25%. Additionally, increasing the latent heat of the outer PCM layer enhances the ratio of heat released.

However, when optimizing both melting temperatures and latent heats, it is crucial to consider the overall performance of the wall and the heat gained during the operating cycle. This comprehensive approach ensures that the chosen parameters effectively meet the desired objectives.

Chapter 5 : Analysis of a dynamic double layer PCM enhancing building envelope

5.1 Introduction

The purpose of this part is to examine the influence of two movable Phase Change Material layers (PCM) integrated into a building envelope. every layer is intended for a particular season (either winter or summer). These layers can interchange positions based on the optimal arrangement for the given season. Various combinations of melting temperatures $(\theta_{m1}, \theta_{m2})$ are proposed, and the performance of the envelope is investigated during the two seasons. The analysis encompasses the temperature and enthalpy changes, along with the progression of phase change fronts (melting or solidification) of the PCM. Additionally, it assesses the proportion of operational PCM throughout every season, the duration of charging and discharging cycles for the PCM, and the temporal variation of heat flux.

5.2 Problems and methods

Figure 4.1 demonstrates the proposed technology, a four layers wall containing two layers of concrete and two dynamic PCM layers with varying phase change temperatures $(\theta_{m1}, \theta_{m2})$, the two PCM layers, referred to as PCM A and PCM B, can potentially shift their locations between each other, from position 1 to position 2 or from 2 to 1, according to the optimal season of each PCM. The external wall side experiences a convective heat exchange with a temperature that varies sinusoidally in accordance with the season, whether it's summer or winter (T_{out}, h_{out}), while the inner surface interacts with the indoor environment at a consistent temperature(T_{in}, h_{in}). The HVAC system is employed to regulate and maintain the indoor ambient temperature at the designated thermostat set point. The sinusoidal outdoor temperature pattern aligns with a 24-hour cycle, simulating the real outdoor temperature [94]. The modeled wall structure represents a typical North African building envelope (two layers of concrete divided by insulating material), in this study, the insulation is substituted with two dynamic phase change material layers. For the practical utilization of this envisioned system, the PCM layers might be integrated in a shape-stabilized form within a polymeric matrix, similar to the approach introduced by Barreneche et al. [95] and as suggested by De Gracia [80] for application in a movable layers system. There is the option of using either manual or mechanical rollers to shift the polymeric sheet, and, as a result, adjust the positioning of the

PCM. The electrical energy consumption of these mechanical rollers is disregarded because of their brief operational duration [80].

5.3 Modeling and governing equations

As previously mentioned, the heat transfer within the studied configuration is primarily governed by conduction, with phase change occurring within the two PCM layers.

The simplifying assumptions employed in this study include:

- The volume of the multi-layered wall remains constant.
- Both solid layers act as passive conductors.
- Natural convection within the liquid PCM is not considered.
- Heat transfer is assumed to be one-dimensional.
- The PCM layers envelope is assumed to be thin and to possess high thermal conductivity to disregard its thermal resistance.
- The temperature and heat transfer coefficient of the surrounding convective fluids are held constant.
- For the PCM layers, properties of the solid and liquid phases are assumed to be identical.

With these assumptions in place, the physical model is described by the unsteady one-dimensional heat equation.

Subsequently, we refer to the inside concrete layer as 'solid in,' which is exposed to internal convective conditions, and to the outside concrete layer as 'solid out,' subjected to external cold convective conditions. where equations are in general form within concrete layers, and in enthalpy form depicting the PCM layers [81].

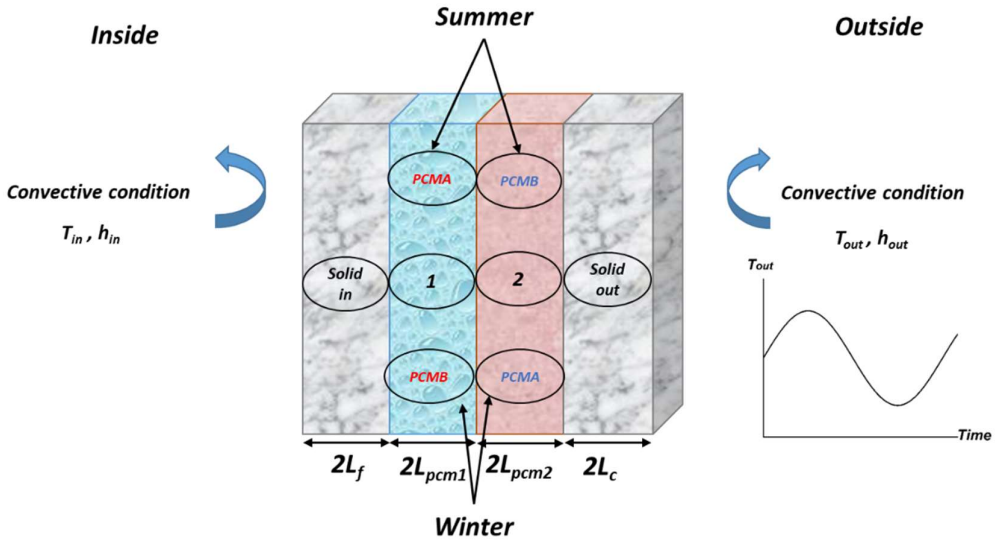

Figure 5.1 Sketch up of the proposed system

Phase change material (PCM1 and PCM2):

$$\begin{cases} Liquid\ region: T > T_m: \rho_l C_l \frac{\partial T_l}{\partial t} = \frac{\partial}{\partial x}\left(k_l \frac{\partial T_l}{\partial x}\right) \\ Solid\ region: T < T_m: \rho_s C_s \frac{\partial T_s}{\partial t} = \frac{\partial}{\partial x}\left(k_s \frac{\partial T_s}{\partial x}\right) \end{cases} \quad (5.1)$$

Solid in and out:

$$\rho_{in} C_{in} \frac{\partial T_{in}}{\partial t} = \frac{\partial}{\partial x}\left(k_{in} \frac{\partial T_{in}}{\partial x}\right) \quad (5.2)$$

$$\rho_{out} C_{out} \frac{\partial T_{out}}{\partial t} = \frac{\partial}{\partial x}\left(k_{out} \frac{\partial T_{out}}{\partial x}\right) \quad (5.3)$$

5.3.1 Initial and boundary conditions

At t = 0, all layers of the wall share the same initial temperature, signifying that the wall is in an initial state of thermal equilibrium. This initial condition is defined as follows:

$$T_1(x_1, 0) = T_2(x_2, 0) = T_{in}(x_{in}, 0) = T_{out}(x_{out}, 0) = T_i \quad (5.4)$$

The boundary conditions on surfaces $(S_{out,out})$, $(S_{out,in})$, (S_m), $(S_{in,in})$, $(S_{in,out})$ are presented below:

At the outer surface of the solid outer layer $(S_{out,out})$

$$-k_{out}\left.\frac{\partial T_{out}}{\partial x_{out}}\right|_{x_{out}=2L_{out}} = h_{out}\left(T_{out}|_{X_{out}=2L_{out}} - T_{\infty,out}\right) \quad (5.5)$$

At the inner surface of the solid outer layer ($S_{out,in}$)

$$-k_{2,s}\left.\frac{\partial T_2}{\partial x_2}\right|_{x_2=2L_{pcm2}} = -k_{out}\left.\frac{\partial T_{out}}{\partial x_{out}}\right|_{x_{out}=0} \quad (5.6)$$

At interface PCM1-PCM2 (S_m)

$$-k_{1,s}\left.\frac{\partial T_1}{\partial x_1}\right|_{x_1=0} = -k_{2,s}\left.\frac{\partial T_2}{\partial x_2}\right|_{x_2=2L_{pcm2}} \quad (5.7)$$

At the inner surface of the solid inner layer ($S_{in,in}$)

$$-k_{1,s}\left.\frac{\partial T_1}{\partial x_1}\right|_{x_1=0} = -k_{in}\left.\frac{\partial T_{in}}{\partial x_{in}}\right|_{x_{in}=2L_{in}} \quad (5.8)$$

At the outer surface of the solid inner layer ($S_{in,out}$)

$$-k_{in}\left.\frac{\partial T_{in}}{\partial x_{in}}\right|_{x_{in}=0} = h_{in}\left(T_{\infty,in} - T_{in}|_{X_{in}=0}\right) \quad (5.9)$$

Where T is the temperature, K the thermal conductivity and the x axial position. The indexes in and out relate respectively to the inner or outer solid layer.

5.3.2 Dimensionless parameters

To facilitate the numerical analysis and identify the key physical factors that influence thermal heat transfer combined with phase change in the two PCM layers, dimensionless

parameters are employed. The spatial coordinate and time are represented as per Arfi and Mezaache [81] :

$$X_k = \frac{x_k}{L_k} \quad \tau = \frac{\alpha_{1,s}}{L_1^2} t \tag{5.10}$$

The lowest winter temperature, $T_{out,min}$, is selected as the reference temperature during the dimensioning of physical quantities. in order to ensure that all dimensionless temperatures are up to zero ($\theta > 0$). The dimensionless temperature and enthalpy are defined as follows [82]:

$$\theta = \frac{T - T_{out,min}}{T_i - T_{out,min}} \quad H = \frac{\hbar}{\hbar_{ref}} \tag{5.11}$$

The primary dimensionless parameters that govern the system are the Biot number, Stefan number, and melting temperature, defined as follows:

$$Bi_{out} = \frac{h_{out} L_{out}}{k_{out}} \quad Bi_{in} = \frac{h_{in} L_{in}}{k_{in}} \tag{5.12}$$

$$Ste_1 = \frac{\hbar_1}{\lambda_1} \quad Ste_2 = \frac{\hbar_2}{\lambda_2} \tag{5.13}$$

$$\theta_{m,1} = \frac{T_{m,1} - T_{out,min}}{T_i - T_{out,min}} \quad \theta_{m,2} = \frac{T_{m,2} - T_{out,min}}{T_i - T_{out,min}} \tag{5.14}$$

These are the dimensionless heat capacity and thermal conductivity expressions:

$$K_k = \frac{k_k}{k_{k,s}} \quad C_k = \frac{c_k}{c_{k,s}} \tag{5.15}$$

5.3.3 Dimensionless heat equations

The model equations are written using the previously mentioned dimensionless parameters and assumptions. The issue of phase transition and moving fronts is solved for PCM layers using the enthalpy formulation variable. The generalized one-dimensional heat transfer equation describes how heat moves across the various wall layers [81,84].

$$\frac{\partial H_k}{\partial \tau} = f_k \frac{\partial}{\partial X_k}\left(K_k \frac{\partial \theta}{\partial X_k}\right) \tag{5.16}$$

It is possible to conclude the following from the definition of the dimensionless time τ:

$$f_k = \frac{\alpha_{k,s}}{\alpha_{1,s}}\left(\frac{L_1}{L_k}\right)^2 \tag{5.17}$$

The correlations linking temperature and enthalpy for PCM materials are provided in accordance with the previous work [96] :

$$H_k = \begin{cases} C_k(\theta_k - \theta_{m,k}) \\ C_k(\theta_k - \theta_{m,k}) + 1/Ste_k \end{cases} \text{ for } \begin{cases} \theta_k < \theta_{m,k} \\ \theta_k > \theta_{m,k} \end{cases} \tag{5.18}$$

$$\theta_k = \begin{cases} H_{k+}\theta_{m,k} \\ \theta_{m,k} \\ (H_k - 1/Ste_k)/C_k + \theta_{m,k} \end{cases} \text{ for } \begin{cases} H_k < 0 \\ 0 \le H_k \le 1/Ste_k \\ H_k > 1/Ste_k \end{cases} \tag{5.19}$$

The link between enthalpy and temperature is easily described for the two solid layers (outside) and (inside) by $H_{out} = C_{out}\theta_{out}$ and $H_{in} = C_{in}\theta_{in}$.

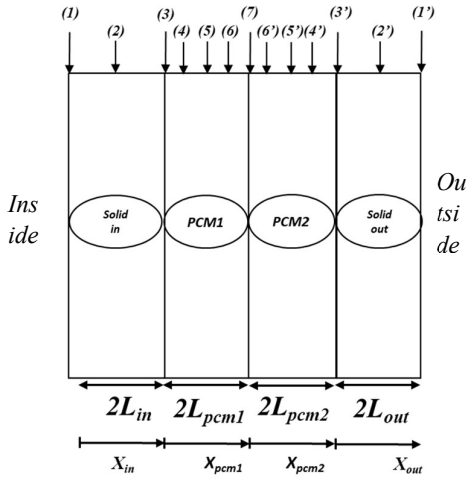

Figure 5.2 Selected surfaces

(1) $S_{in,out}$, (1′) $S_{out,out}$, (2) $S_{in,1/2}$, (2′) $S_{out,1/2}$, (3) $S_{in,in}$, (3′) $S_{out,in}$, (4) $S_{pcm\ 1,1/4}$, (4′) $S_{pcm\ 2,1/4}$, (5) $S_{in,1/2}$, (5′) $S_{out,1/2}$, (6)$S_{in,3/4}$, (6′) $S_{out,3/4}$, (7) S_m

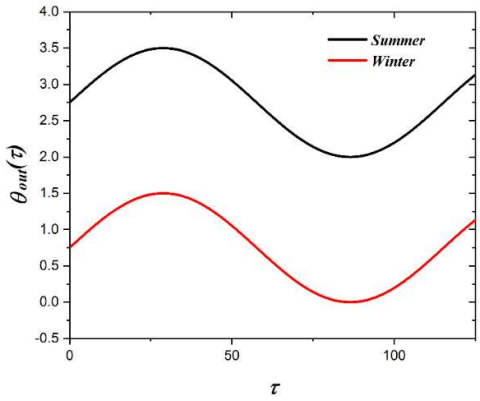

Figure 5.3 Outside dimensionless fluctuate temperature versus time

5.3.4 Dimensionless thermal boundary conditions

Regarding the boundary conditions, they are outlined as follows:

At the outer surface of the solid outer layer ($S_{ou\ ,out}$)

$$\mathrm{K_{out}}\frac{\partial\theta}{\partial \mathrm{X_{out}}}\bigg|_{\mathrm{X_{out}=2}} = \mathrm{Bi_{out}}\left(\theta|_{\mathrm{X_{out}=2}} - \theta_{\infty,\mathrm{out}}\right) \tag{5.20}$$

At the inner surface of the solid outer layer ($S_{out,in}$)

$$K_2 \frac{\partial \theta}{\partial X_2}\Big|_{X_2=2} = \frac{L_2}{L_{out}} \frac{k_{out}}{k_{2,s}} K_{out} \frac{\partial \theta}{\partial X_{out}}\Big|_{X_{out}=0} \tag{5.21}$$

At interface PCM1-PCM2 (S_m)

$$K_1 \frac{\partial \theta}{\partial X_1}\Big|_{X_1=2} = \frac{L_1}{L_2} \frac{k_{2,s}}{k_{1,s}} K_2 \frac{\partial \theta}{\partial X_2}\Big|_{X_2=0} \tag{5.22}$$

At the inner surface of the solid inner layer ($S_{in,in}$)

$$K_1 \frac{\partial \theta}{\partial X_1}\Big|_{X_1=0} = \frac{L_1}{L_{in}} \frac{k_{in}}{k_{1,s}} K_{in} \frac{\partial \theta}{\partial X_{in}}\Big|_{X_{in}=2} \tag{5.23}$$

At the outer surface of the solid inner layer ($S_{in,out}$)

$$K_{in} \frac{\partial \theta}{\partial X_{in}}\Big|_{X_{in}=0} = Bi_{in}(\theta_{\infty,in} - \theta_{in}|_{X_{in}=0}) \tag{5.24}$$

In accordance with meteorological data representing the Mediterranean climate [91], the outdoor ambient temperature $T_{\infty,out}$ varies between 20°C and 35°C in summer, and between 0 °C and 15 °C in winter (Figure 5.3). It is described by the following sinusoidal function $T_{\infty,out} = \bar{T}_{\infty,out} + a'_m \sin(\omega' t)$. Therefore, the dimensionless outdoor temperature is determined by the following equation: $\theta_{\infty,out} = \bar{\theta}_{\infty,out} + a_m \sin(\omega\tau)$, with $a_m = a'_m/(T_i - T_{out,min})$ and $\omega = (L_1^2/\alpha_{1,s})\,\omega'$. In the context of the aforementioned dimensionless investigation, the dimensionless sinusoidal outdoor temperature experiences a range of 2 to 3.5 over the course of one period, particularly during the summer season, conversely, in the winter season, it oscillates between 0 and 1.5, figure 2. The initial

temperature used for calculating dimensionless temperatures in all simulations is set at T_i = 15 °C.

5.4 Numerical solution

The finite-volume method is employed to solve the physical model representing the phenomenon [86,87].

5.4.1 Mesh

The governing equations for the various wall layers are discretized by employing a consistent meshing approach for each individual layer. The spatial interval, denoting the space between two internal nodes, is marked as ΔX. Each node signifies the control volume center, with the left and right sides referred to as 'w' and 'e,' respectively. The neighboring nodes are designated as 'W' and 'E.

As it is mentioned above, the discretized equations govern the various layers of the wall are carried out through the finite volume method with a uniform mesh for each layer. For the two solid layers, the discretized equations are deduced from the general formulation while for the PCM layers, they are obtained basing on the enthalpy formulation. The discretized equations that represent the coupling at the interfaces of the wall layers are derived from the boundary conditions that govern these interfaces. The cumulative count of nodes and spatial increment for the solid in, solid out, PCM1, and PCM2 layers are provided as by $(N_{in}, \Delta X_{in}), (N_{out}, \Delta X_{out}), (N_1, \Delta X_1), (N_2, \Delta X_2)$. Every layer commences and terminates with half control volume. The gradient terms related to the time variable are discretized using an explicit scheme. Consequently, an examination of solution stability and mesh impact has led to the determination of an appropriate mesh configuration, where: $N_{in} = N_{out} = N_1 = N_2 = 81$.

5.4.2 Discretized equations of the inner solid layer

For an interior node

$$\theta_{in,j+1}^{P} = \theta_{in,j}^{P} + f_{in} \frac{\Delta\tau}{X_{in,w} - X_{in,e}} \left(K_{in,w} \frac{\theta_{in,j}^{W} - \theta_{in,j}^{P}}{\Delta X_{in}} - K_{in,e} \frac{\theta_{in,j}^{P} - \theta_{in,j}^{E}}{\Delta X_{in}} \right) \quad (5.25)$$

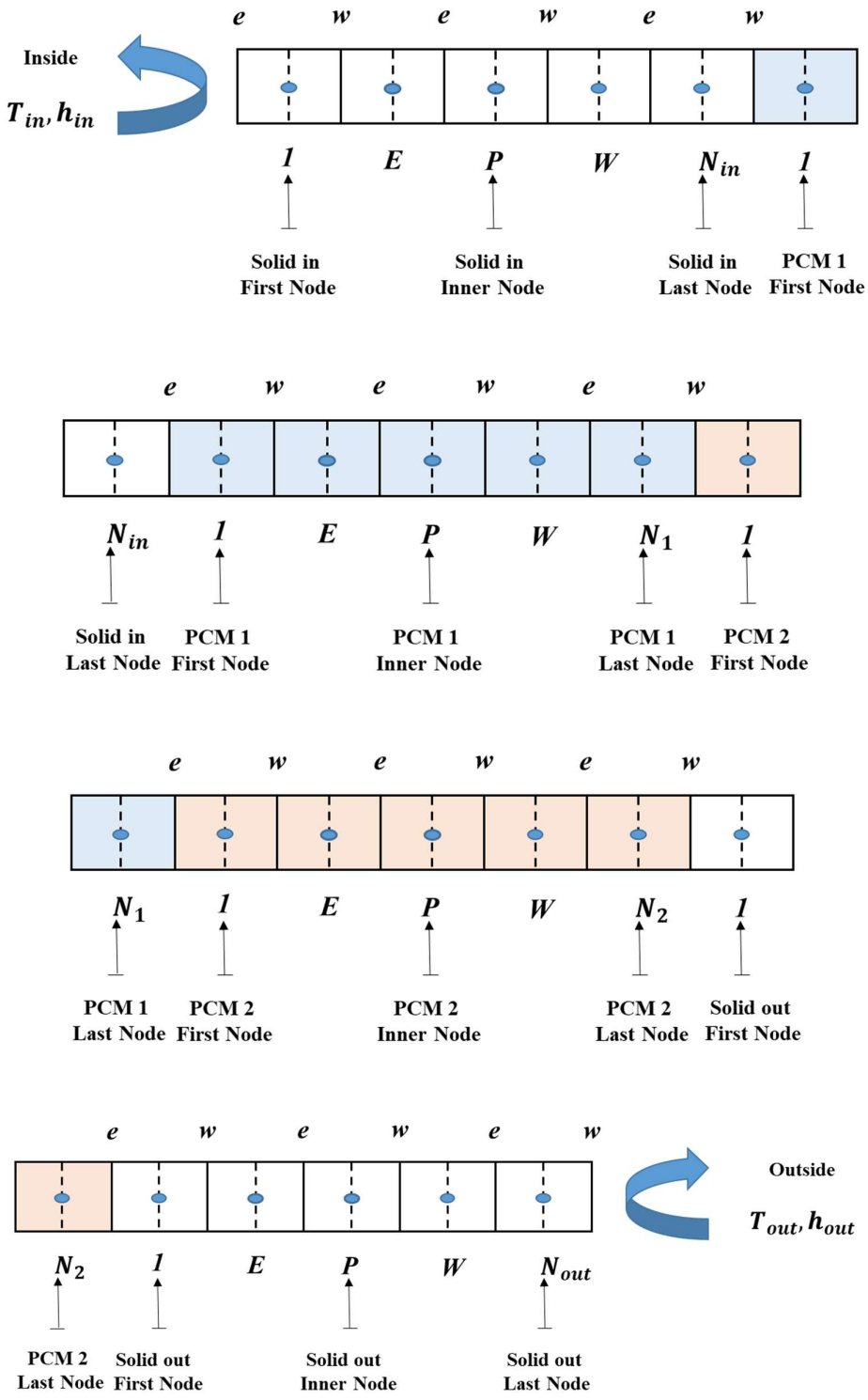

Figure 5.4 The multilayer wall mesh

For the first node

$$\theta^{1}_{in,j+1} = \theta^{1}_{in,j} + f_{in}\frac{\Delta\tau}{X_{in,w}-X_{in,e}}\left(K_{in,w}\frac{\theta^{2}_{in,j}-\theta^{1}_{in,j}}{\Delta X_{in}} - Bi_{in}\left(\theta|_{X_{in}=0,j} - \theta_{\infty,in}\right)\right) \quad (5.26)$$

For the last node

$$\theta^{N_{in}}_{in,j+1} = \theta^{N_{in}}_{in,j} + f_{in}\frac{\Delta\tau}{X_{in,w}-X_{in,e}}\left(\frac{L_{in}}{L_{pcm}}\frac{k_{1,s}}{k_{in}}K_{1,w}\frac{\theta^{1}_{1,j}-\theta|_{X_{in}=2,j}}{\Delta X_1/_2} - K_{in,e}\frac{\theta^{N_{in}}_{in,j}-\theta^{N_{in}-1}_{in,j}}{\Delta X_{in}}\right) \quad (5.27)$$

5.4.3 Discretized equations of the PCM1:

For an interior node

$$\mathrm{H}^{P}_{1,j+1} = \mathrm{H}^{P}_{1,j} + f_1\frac{\Delta\tau}{X_{1,w}-X_{1,e}}\left(K_{1,w}\frac{\theta^{W}_{1,j}-\theta^{P}_{1,j}}{\Delta X_1} - K_{1,e}\frac{\theta^{P}_{1,j}-\theta^{E}_{1,j}}{\Delta X_1}\right) \quad (5.28)$$

For the first node

$$\mathrm{H}^{1}_{1,j+1} = \mathrm{H}^{1}_{1,j} + f_1\frac{\Delta\tau}{X_{1,w}-X_{1,e}}\left(K_{1,w}\frac{\theta^{2}_{1,j}-\theta^{1}_{1,j}}{\Delta X_1} - \frac{L_{pcm1}}{L_{in}}\frac{k_{in}}{k_{1,s}}K_{in,w}\frac{\theta|_{X_1=0,j}-\theta^{N_{in}}_{in,j}}{\Delta X_{in}/_2}\right) \quad (5.29)$$

For the last node

$$\mathrm{H}^{N_1}_{1,j+1} = \mathrm{H}^{N_1}_{1,j} + f_1\frac{\Delta\tau}{X_{1,w}-X_{1,e}}\left(\frac{L_{pcm1}}{L_{pcm2}}\frac{k_{2,s}}{k_{1,s}}K_{2,w}\frac{\theta^{1}_{2,j}-\theta|_{X_2=0,j}}{\Delta X_2/_2} - K_{1,e}\frac{\theta^{N_1}_{1,j}-\theta^{N_1-1}_{1,j}}{\Delta X_1}\right) \quad (5.30)$$

5.4.4 Discretized equations of the PCM2

For an interior node

$$\mathrm{H}^{P}_{2,j+1} = \mathrm{H}^{P}_{2,j} + f_2\frac{\Delta\tau}{X_{2,w}-X_{2,e}}\left(K_{2,w}\frac{\theta^{W}_{2,j}-\theta^{P}_{2,j}}{\Delta X_2} - K_{2,e}\frac{\theta^{P}_{2,j}-\theta^{E}_{2,j}}{\Delta X_2}\right) \quad (5.31)$$

For the first node

$$\mathrm{H}^{1}_{2,j+1} = \mathrm{H}^{1}_{2,j} + f_2\frac{\Delta\tau}{X_{2,w}-X_{2,e}}\left(K_{2,w}\frac{\theta^{2}_{2,j}-\theta^{1}_{2,j}}{\Delta X_2} - \frac{L_{pcm2}}{L_{pcm1}}\frac{k_{1,s}}{k_{2,s}}K_{1,w}\frac{\theta|_{X_2=0,j}-\theta^{N_1}_{1,j}}{\Delta X_1/_2}\right) \quad (5.32)$$

For the last node

$$\mathrm{H}_{2,j+1}^{N_2} = \mathrm{H}_{2,j}^{N_2} + f_2 \frac{\Delta\tau}{X_{2,w}-X_{2,e}} \left(\frac{L_{pc}}{L_{out}} \frac{k_{out}}{k_{2,s}} K_{out,w} \frac{\theta_{out,j}^{1} - \theta|_{X_{out}=0,j}}{\Delta X_{out}/_2} - K_{2,e} \frac{\theta_{2,j}^{N_2} - \theta_{2,j}^{N_2-1}}{\Delta X_2} \right) \quad (5.33)$$

5.4.5 Discretized equations of the outer solid layer:

For an interior node

$$\theta_{out,j+1}^{P} = \theta_{out,j}^{P} + f_{out} \frac{\Delta\tau}{X_{out,w}-X_{out,e}} \left(K_{out,w} \frac{\theta_{out,j}^{W} - \theta_{out,j}^{P}}{\Delta X_{out}} - K_{out,e} \frac{\theta_{out,j}^{P} - \theta_{out,j}^{E}}{\Delta X_{out}} \right) \quad (5.34)$$

For the first node

$$\theta_{out,j+1}^{1} = \theta_{out,j}^{1} + f_{out} \frac{\Delta\tau}{X_{out,w}-X_{out,e}} \left(K_{out,w} \frac{\theta_{out,j}^{2} - \theta_{out,j}^{1}}{\Delta X_{out}} - \frac{L_{out}}{L_{pc}} \frac{k_{2,s}}{k_{out}} K_{2,w} \frac{\theta|_{X_{out}=0,j} - \theta_{2,j}^{N_2}}{\Delta X_2/_2} \right) \quad (5.35)$$

For the last node

$$\theta_{out,j+1}^{N_{out}} = \theta_{out,j}^{N_{out}} + f_{out} \frac{\Delta\tau}{X_{out,w}-X_{out,e}} \left(\mathrm{Bi}_{\mathrm{out}} \left(\theta_{\infty,\mathrm{out}} - \theta|_{\mathrm{X_{out}=2}} \right) - K_{out} \frac{\theta_{out,j}^{N_{out}} - \theta_{out,j}^{N_{out}-1}}{\Delta X_{out}} \right) \quad (5.36)$$

5.4.6 Determination of the solid-liquid front position

For figuring out where the solid-liquid front located in the PCM layer, the following equation represents the total energy present in a control volume with center node i [83]:

$$H^i V_e^i = \left[(\theta^i - \theta_m) V_s^i + \left(C(\theta^i - \theta_m) + \frac{1}{Ste} \right) V_l^i \right] \quad (5.37)$$

In this context, V_e^i, V_s^i, V_l^i represent, the volume of the control volume, expressed in dimensionless units, the fraction of the PCM phase that is in a solid state and the fraction of the PCM phase that is in a liquid state, respectively. When a control volume experiences a phase change with $\theta^i = \theta_m$, the equation transforms to:

$$H^i V_e^i = (1/Ste) V_l^i \quad \text{or} \quad H^i = (1/Ste) V_l^i / V_e^i \quad (5.38)$$

The value of the enthalpy when the solidification front reaches the node i, is as follows:

$$H_c^i = 1/(2Ste) \quad (5.39)$$

This equation serves as a criterion for managing the front's position. To determine the solidification time at a specific node i, we examine two consecutive time instants, $\tau(j)$ and $\tau(j+1)$.

If $H^i(j+1) \leq H_c \leq H^i(j)$, then the solidification process takes place at a specific moment τ_{sol} within the time range of $\tau(j)$ to $\tau(j+1)$, and this moment can be determined using interpolation, $\tau(j) \leq \tau_{\text{sol}} \leq \tau(j+1)$.

The enthalpy is supposed to vary linearly across the whole time range. The equation for the solidification time of node i is: $\tau^i = (j+X)\Delta\tau$, Where X is determined through linear interpolation in the time domain, thus [83]:

$$X = \frac{H_c - H^i(j+1)}{H^i(j) - H^i(j+1)} \quad ; \quad \tau^i = \left(j + \frac{H_c - H^i(j+1)}{H^i(j) - H^i(j+1)}\right)\Delta\tau \tag{5.40}$$

5.5 Numerical outputs

The primary numerical results from the simulation include the evolution of dimensionless temperature and the instantaneous heat flux with respect to dimensionless time for each node, additionally; the simulation provides information about the kinetics of the phase change interfaces. Based on this dataset, various other numerical results have been calculated and are detailed in the subsequent section. Similarly, the active fraction of PCM during every season, the length of the PCM charging and discharging periods, and the average heat flux experienced over a day have been determined.

The cumulative heat absorbed or released during the winter or summer timeframe is calculated by integrating the dimensionless heat flux over the time duration τ_f [91].

$$Q = \int_0^{\tau_f} \dot{Q}\ d\tau \tag{5.41}$$

The definition of the instantaneous dimensionless heat flux at the internal wall side, which interacts with the indoor environment, is as follows:

$$q^* = Bi_{in}(\theta_{\infty,in} - \theta_{in}|_{X_{in}=0}) \tag{5.42}$$

The average dimensionless heat flux, denoted as $\bar{q}$, which is either lost or gained over the winter or summer period, can be obtained by dividing the total heat by the cumulative computed time:

$$\bar{q} = \frac{Q}{\Delta\tau} \tag{5.43}$$

In order to calculate all previous integral, the trapezoidal method which is a method of numerical integration has been used (Strang et al. 2016).

5.6 Results and Discussion

This study explores various combinations $(\theta_{m1}, \theta_{m2})$ beginning with the baseline case (PSM, PSM) in which no PCM layers are present. Many combinations involve distinct phase change temperatures $(\theta_{m1} \neq \theta_{m2})$, while in other cases, both PCM layers share the same phase change temperature $(\theta_{m1} = \theta_{m2})$, representing the scenario of a single PCM layer. The chosen phase change temperatures are strategically placed within the range of the outdoor temperature variations. One of these temperatures aligns with the indoor comfort temperature, while the other corresponds to the outermost limit of the temperature fluctuations in accordance with the season; in the context of the summer outdoor temperature variations, θ_m =2.4 and θ_m =3 are involved, while in the winter outdoor temperature fluctuations, θ_m =0.4 and θ_m =1 are involved.

5.6.1 Temperature evolution

Figure 5.5 illustrates the temporal variation of dimensionless temperature across the four layers, within various combinations. It also highlights the occurrences of phase transitions at various locations throughout the building envelope for the combinations $(\theta_{m1} = 1, \theta_{m2} = 2.4)$ and $(\theta_{m1} = 2.4, \theta_{m2} = 1)$,. These instances are characterized by a constant temperature corresponding to the fusion or freezing points. Throughout these intervals, the PCM experiences either the release or storage of energy using latent heat. Beyond these timeframes, the stored cold or heat becomes evident through a noticeable reduction or rise in the material's

temperature (sensible way). Sensible heat refers to the energy necessary to increase or decrease the temperature of a substance without inducing a phase transition, in contrast, latent heat denotes the quantity of energy required to induce a transition in the phase of a substance without influencing the temperature of the material.

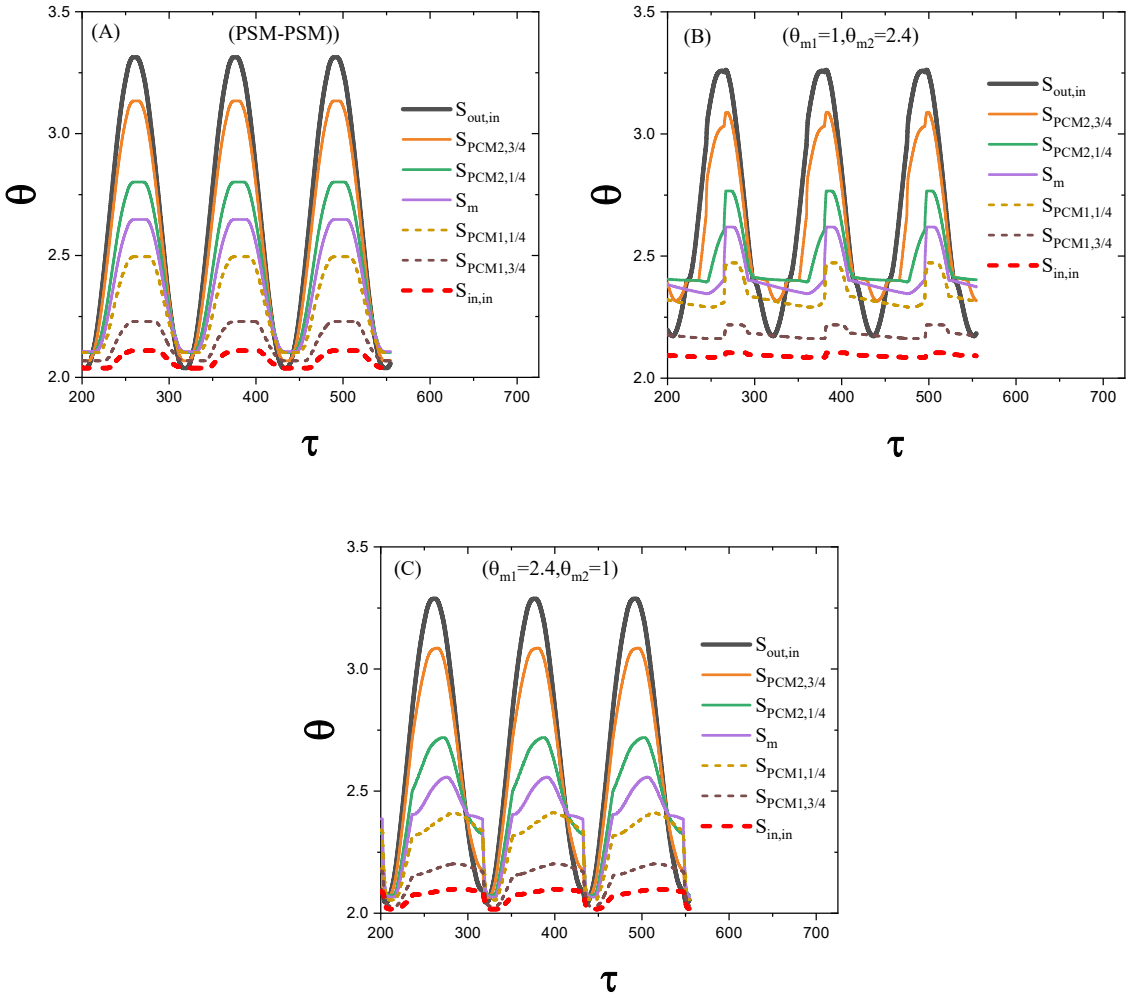

Figure 5.5 Dimensionless temperature evolution in summer for the combinations: (A) $(\boldsymbol{PSM, PSM})$, (B) $(\boldsymbol{\theta_{m1} = 1, \theta_{m2} = 2.4})$, (C) $(\boldsymbol{\theta_{m1} = 2.4, \theta_{m2} = 1})$.

Furthermore, when considering combinations that include PCM layers such as $(\theta_{m1} = 1, \theta_{m2} = 2.4)$ and $(\theta_{m1} = 2.4, \theta_{m2} = 1)$, the temperature evolution demonstrates a reduction in temperature fluctuations across the entire wall compared to the combination without PCM layers (PSM, PSM). This reduction in temperature fluctuation is attributed to the presence of

PCM layers, which help to dampen the impacts of external excitation on the temperature variations within the wall.

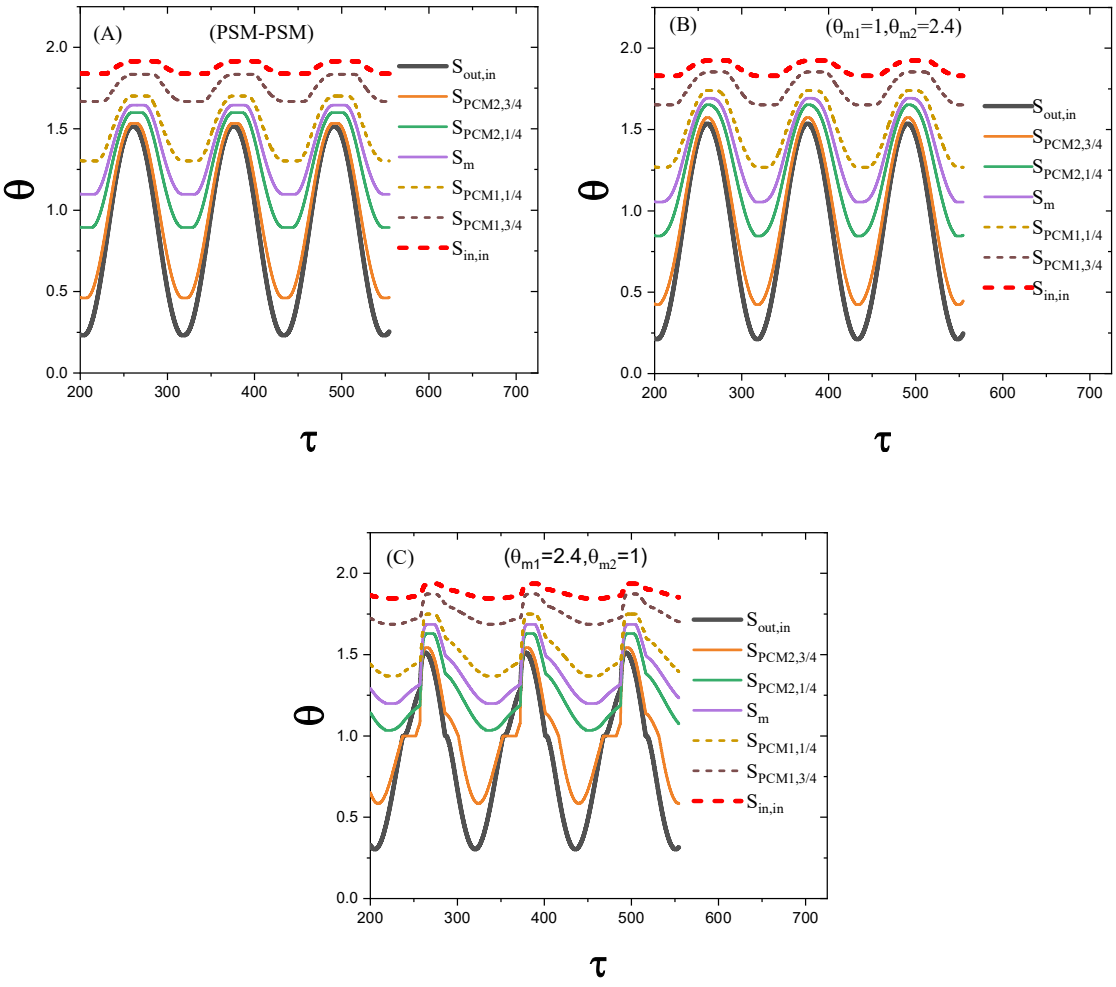

Figure 5.6 Dimensionless temperature evolution in winter for the combinations: (A) $(\boldsymbol{PSM, PSM})$, (B) $(\boldsymbol{\theta_{m1} = 1, \theta_{m2} = 2.4})$, (C) $(\boldsymbol{\theta_{m1} = 2.4, \theta_{m2} = 1})$.

Furthermore, the combination $(\theta_{m1} = 2.4, \theta_{m2} = 1)$ exhibits a significant reduction of approximately 86% in temperature fluctuation amplitude compared to the combination $(\theta_{m1} = 1, \theta_{m2} = 2.4)$, where the reduction is approximately only 1.5%. This difference arises due to the positioning of the layer with an appropriate phase change temperature $(\theta_m = 2.4)$, in relation to the summer excitation, which is closer to the outer side in the first combination $(\theta_{m1} = 2.4, \theta_{m2} = 1)$. Additionally, the occurrence of phase change moments is observed, where the temperature stays consistent for a specific period as time progresses.

These instances align with either solidification, signifying the PCM's charging phase, or fusion, denoting the PCM's operational phase. The specific phase change moments depend on the instantaneous outdoor stimulus as well as the phase change temperatures of the two layers.

As mentioned earlier in the "summer" section, Figure 5.6 illustrates the dimensionless temperature progression over time across the various building envelope layers for many combinations. The figure also highlights the instances of phase transition occurring at various locations within the building wall for combinations $(\theta_{m1} = 1, \theta_{m2} = 2.4)$ and $(\theta_{m1} = 2.4, \theta_{m2} = 1)$, where the temperature stays steady at the phase transition point. At these times, the phase change material either stores or releases energy via latent heat. Conversely, in other time intervals, the accumulated heat or cold is reflected by a noticeable increase or decrease in the material's temperature in a sensible manner.

Moreover, the temperature variations by the combination involving phase change points $(\theta_{m1} = 2.4, \theta_{m2} = 1)$ demonstrates a significant reduction in temperature fluctuation throughout the wall, minimizing it to approximately 6% in comparison to the baseline scenario (PSM-PSM). In contrast, the combination featuring phase change material layers $(\theta_{m1} = 1, \theta_{m2} = 2.4)$ and the case without PCM layers (*PSM, PSM*) do not exhibit a reduction in temperature fluctuation. Additionally, the combination $(\theta_{m1} = 2.4, \theta_{m2} = 1)$ demonstrates distinctive instances of phase transition, with temperature remaining constant for specific durations within the time progression. These instances of phase change occur during the fusion period, representing the PCM charging phase, and the solidification period, representing the phase change material operational phase. The presence of these instances relies on the instantaneous outdoor stimuli and the phase change points of the two phase change material layers. In contrast, the combination $(\theta_{m1} = 1, \theta_{m2} = 2.4)$ does not display any moments of phase transition because of the distant location of the phase change material layer with a melting temperature of $(\theta_m = 1)$, which is appropriate for the outdoor ambiance in winter, in comparison to the combination $(\theta_{m1} = 2.4, \theta_{m2} = 1)$ that is closer to the outside excitation.

5.6.2 Phase change front kinetic

Based on Figure 5.7, it can be observed that in combinations where $(\theta_{m2} = 2.4)$ or $(\theta_{m2} = 3)$, the second phase change material layer (PCM 2) exhibits the two phase change

operations, namely freezing and melting, according to the immediate outdoor environment. For ($\theta_{m2} = 2.4$), two phase transition interfaces are depicted. The initial one commences at the surface ($S_{out,in}$), which is in close proximity to the outdoor ambiance, and progresses towards the center of the phase change material over the charging phase through a freezing operation. Alternatively, throughout the operational phase, it undergoes melting due to the outdoor environment influence. The combined effects of external and internal stimuli create a secondary phase transition interface at the boundary (S_m), which progresses towards the core of the phase change material layer PCM 2 throughout the charging (solidification) phase, and conversely, moving away during the operational phase (fusion).

Within the scenario of ($\theta_{m2} = 3$), a single phase transition interface is noticeable within the second phase change material layer. This front progresses from the surface in proximity to the outside towards the center. The phase change includes both freezing and melting, according to the external environment. Unlike the scenario ($\theta_{m2} = 2.4$), the combined effect of external and internal excitations prevents the zone of the second phase change material layer PCM 2 in proximity to the interface from reaching the phase change point ($\theta_m = 3$). In the first phase change material layer PCM 1, the phase transition operation is only observed for ($\theta_{m2} = 2.4$) since it is closest to the inside ambient temperature ($\theta_{in} = 2$). The interface of the phase change operation initiates at the boundary and progresses towards the center of the phase change material layer PCM 1, undergoing charging and discharging processes accordingly.

During winter, as shown in Figure 5.8, the phase transition operation is exclusively seen within the second phase change material layer PCM 2, which is positioned closer to the outdoor environment. No phase transition interface is observed in the first phase change material layer PCM 1 as a result of the temperature gradient caused by both external and internal stimuli, hindering it from achieving the phase transition point at any of the suggested phase change temperatures in the previous combinations. Nonetheless, in the second phase change material layer PCM 2, only the combinations where ($\theta_{m2} = 1$) or ($\theta_{m2} = 0.4$) permit reaching the phase transition point. In these situations, A solitary phase transition interface appears and progresses from the surface ($S_{out,in}$), located close to the outdoor, toward the

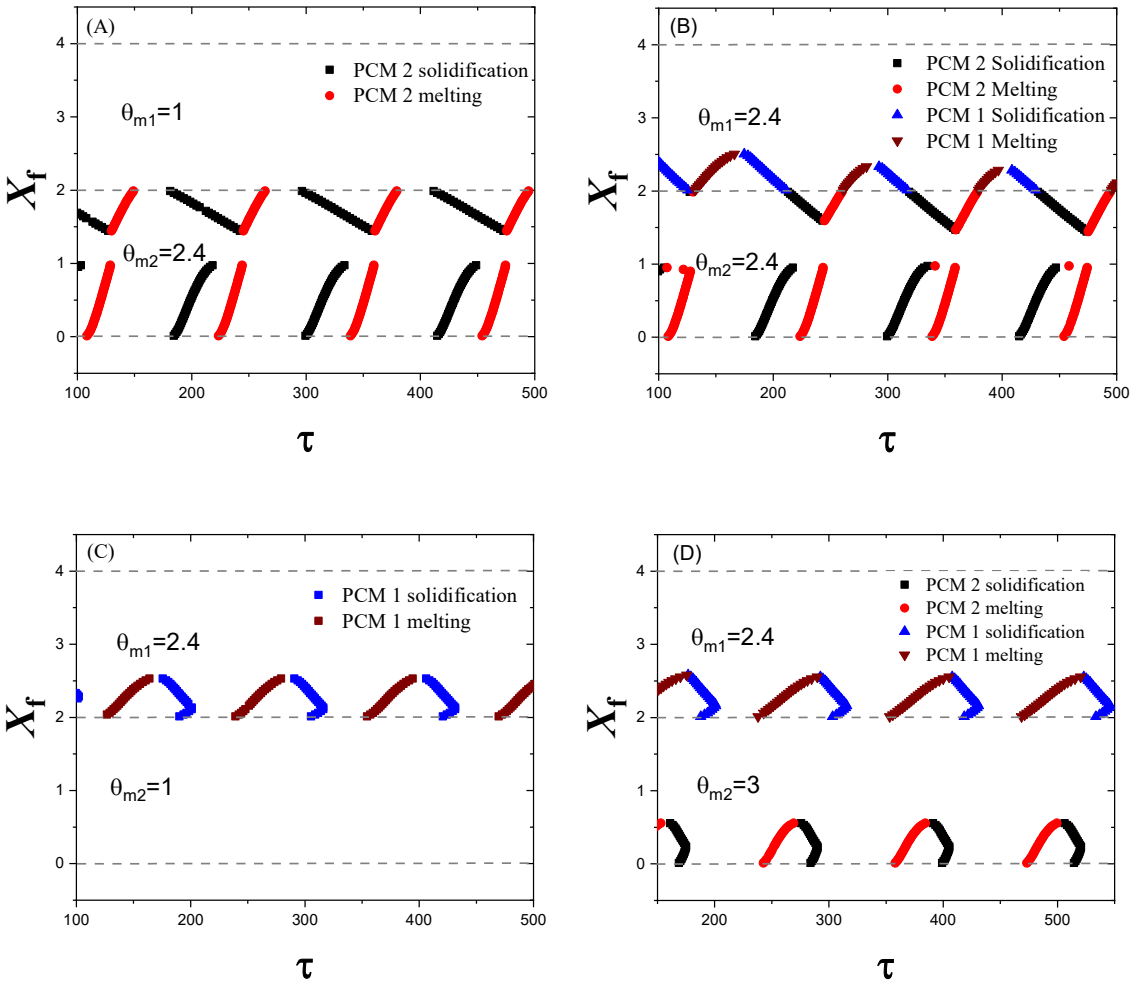

Figure 5.7 Front position evolution of melting temperatures in summer for different combinations: (A) $(\boldsymbol{\theta_{m1} = 1, \theta_{m2} = 2.4})$, (B) $(\boldsymbol{\theta_{m1} = 2.4, \theta_{m2} = 2.4})$, (C) $(\boldsymbol{\theta_{m1} = 2.4, \theta_{m2} = 1})$, $(\boldsymbol{D})(\boldsymbol{\theta_{m1} = 2.4, \theta_{m2} = 3})$.

middle of the layer. This takes place in the charging phase through the melting operation and in the discharging phase through the freezing phase.

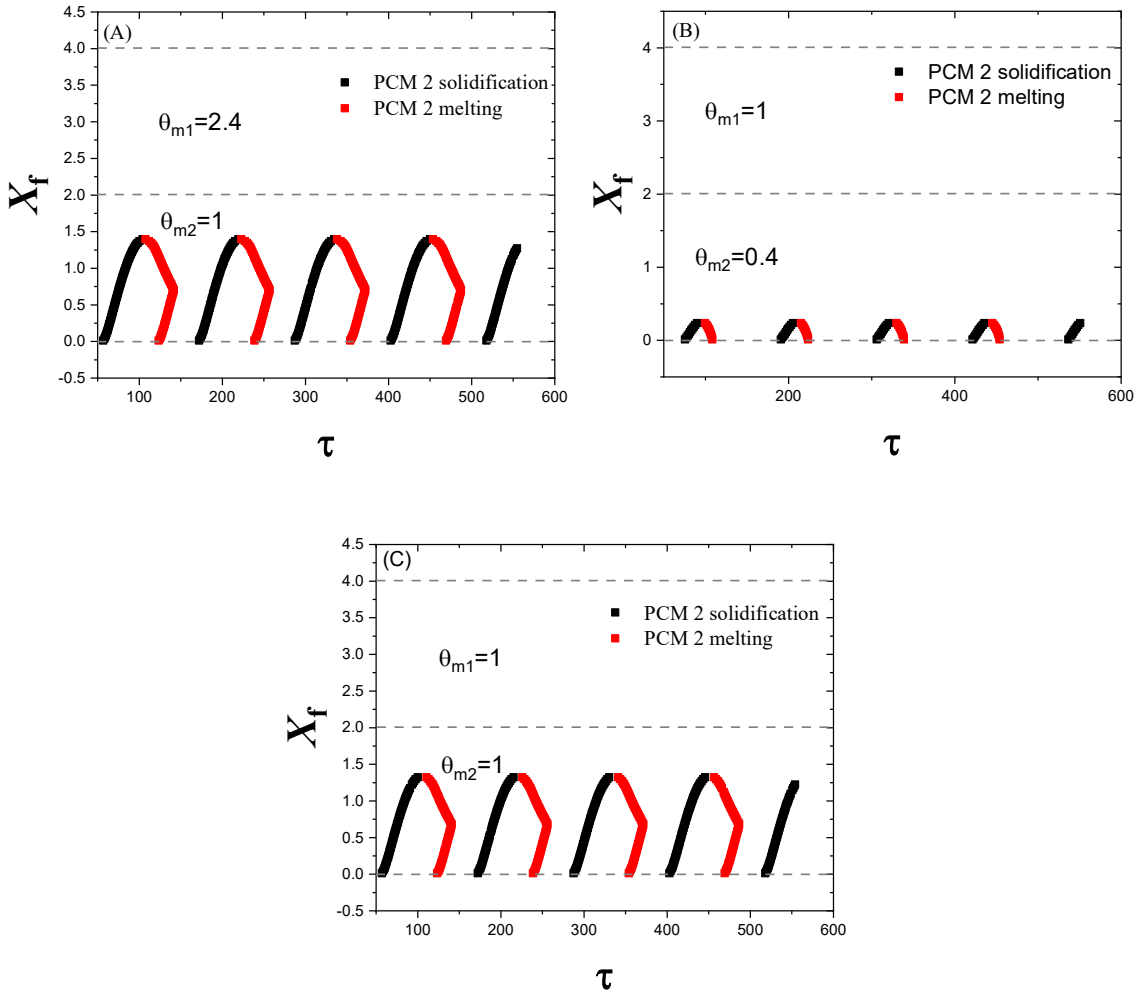

Figure 5.8 Front position evolution of melting temperatures in winter for different combinations: (A) $(\boldsymbol{\theta_{m1} = 2.4, \theta_{m2} = 1})$, (B) $(\boldsymbol{\theta_{m1} = 1, \theta_{m2} = 0.4})$, (C) $(\boldsymbol{\theta_{m1} = 1, \theta_{m2} = 1})$

5.6.3 Operating PCM fraction

Figure 5.9(A) illustrates that regardless of the combination $(\theta_{m1}, \theta_{m2})$, the second phase change material layer PCM 2 makes a greater contribution to the operating PCM fraction in comparison to the first phase change material layer PCM 1. The second phase change material layer PCM 2, with melting temperatures $(\theta_{m2} = 2.4)\ and\ (\theta_{m2} = 3)$, reaches the phase change point and exhibits a greater operational quantity when the first phase change material layer PCM 1 does not achieve the phase transition. Notably, the combination with $(\theta_{m2} = 2.4)$ demonstrates the largest portion of active PCM (in operation), reaching up to 77%,

indicating its suitability for responding to outdoor stimuli within the summer season. In contrast, the first PCM layer attains the phase transition temperature only when ($\theta_{m1} = 2.4$), resulting in a reduced fraction of the PCM in operation of about 26%, in comparison to situations where the second layer is the one that has ($\theta_{m2} = 2.4$) (located closer to the external environment). In terms of the overall operating PCM quantity (taking in consideration the two PCM layers), the combination ($\theta_{m1} = 2.4, \theta_{m2} = 2.4$) displays the maximum value of 46.75%, indicating that the two phase change material layers undergo the phase transition process. Similarly, the combination ($\theta_{m1} = 2.4, \theta_{m2} = 3$) exhibits an operating PCM fraction of 28.5%. For the combinations ($\theta_{m1} = 2.4, \theta_{m2} = 3$) and ($\theta_{m1} = 1, \theta_{m2} = 2.4$), a satisfactory active PCM portion of 38.5% is observed, taking into account that in these situations, solely the second phase change material layer experiences the phase transition operation. In the remaining combinations, a reduced proportion of operating PCM is noted.

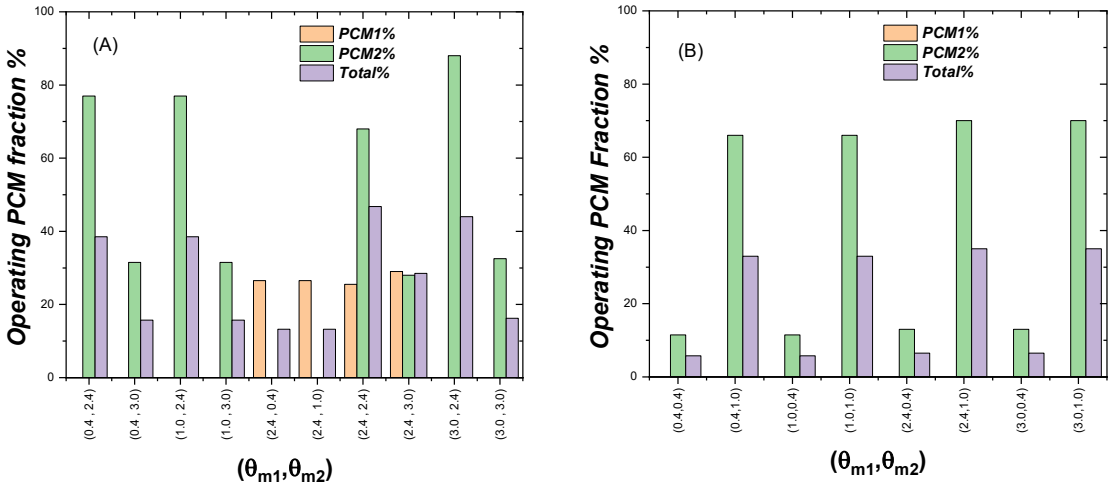

Figure 5.9 Operating PCM fraction for different combination: (A) in summer, (B) in winter.

Based on Figure 5.9(B), when exposed to winter external conditions, In every (θ_{m1}, θ_{m2}) combination, the first phase change material layer PCM 1 remains unaffected by any phase transition. Nonetheless, the second PCM layer can attain the phase transition temperature in situations where ($\theta_{m2} = 1$) and ($\theta_{m2} = 0.4$). Among these, the fraction of the PCM in operation is greater for ($\theta_{m2} = 1$), which is better suited for winter outdoor environment, achieving a fraction of 35%. On the contrary, the faction of the PCM in operation is only

approximately 6% for $\theta_{m2} = 0.4$. As the second phase change material layer PCM 2 is the only layer undergoing the phase transition, the total operating PCM portion is determined by it. Consequently, the combinations with ($\theta_{m2} = 1$) demonstrate the highest fraction due to their compatibility with the winter outdoor ambiance.

5.6.4 Phase change dimensionless duration for charging /discharging cycles

In Figure 5.10(A), the charging and discharging phases of the two phase change material layers are depicted, with the freezing phase representing the charging period and the melting phase representing the discharging period, during the summer. As mentioned in [92], a longer discharging duration indicates higher efficiency of the PCM. It is seen that combinations with ($\theta_{m2} = 2.4$) show a longer discharging duration (40≤ τ_{cycle} ≤58) because of the effective phase change operation in these combinations.

On the contrary, in situations where the phase transition is weak, like ($\theta_{m1} = 0.4, \theta_{m2} = 3$), the discharging time is short (τ_{cycle} =28). This case demonstrates that when the operational PCM portion is substantial, the duration of discharge is longer, conversely, the discharge duration is shorter. Additionally, the combination ($\theta_{m1} = 2.4, \theta_{m2} = 2.4$) exhibits the longest duration of operation in comparison to all other scenarios, with a τ_{cycle} of 58. Observations indicate that combinations where the phase change operation is effectively realized require a longer period for full discharge in contrast to the charging period. On the other hand, in situations with weak phase transition operations, the time required for charging is longer than the discharging duration.

Figure 5.10(B) illustrates the charging and discharging cycles of the phase change material layers, where the melting operation represents the charging duration and the solidification operation represents the discharging period, during the winter season. It is evident that combinations like ($\theta_{m1} = 2.4, \theta_{m2} = 1$) and ($\theta_{m1} = 3, \theta_{m2} = 1$) exhibit longer discharging durations, with a τ_{cycle} of 48. Similarly, combinations like ($\theta_{m1} = 1, \theta_{m2} = 1$), and ($\theta_{m1} = 0.4, \theta_{m2} = 1$) also require a considerable amount of time for complete discharge, with a τ_{cycle} of 26, in comparison to other combinations. However, the charging duration is relatively longer in these cases, with a τ_{cycle} of 30. Additionally, it is noteworthy that for ($\theta_{m1} = 1, \theta_{m2} = 1$) *and* ($\theta_{m1} = 0.4, \theta_{m2} = 1$), the time required for charging is greater than the

time needed for discharging. On the contrary, in all other scenarios, the time required for charging is less than the time needed for discharging.

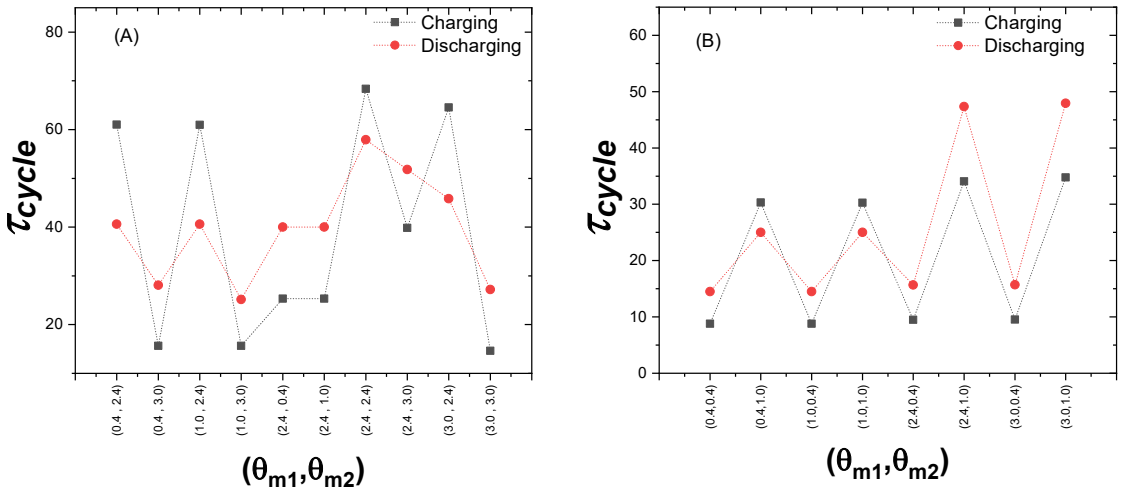

Figure 5.10 Phase change dimensionless operating duration for charging / discharging cycles in summer (A), in winter (B), for different combinations $(\boldsymbol{\theta_{m1}, \theta_{m2}})$

5.6.5 Heat flux evolution

Figure. 11, presents the evolution of the dimensionless heat flux over time. In the case of the combination (*PSM-PSM*), it can be observed that the influence of summer outdoor environment reaches the inner side of the wall ($S_{in,out}$), resulting in fluctuating heat flux. Nonetheless, in combinations where the phase transition operation is successfully realized, like in the case of $(\theta_{m1} = 2.4, \theta_{m2} = 2.4)$ and $(\theta_{m1} = 1, \theta_{m2} = 2.4)$, a reduction in the amplitude of heat flux oscillation is noticeable, with a decrease of 13% and 6.5% respectively. This reduction varies across different combinations $(\theta_{m1}, \theta_{m2})$. Thus, the impact of outdoor environment at the inner side of the wall ($S_{in,out}$) is damped. The highest reduction is observed in the combination $(\theta_{m1} = 2.4, \theta_{m2} = 2.4)$. Furthermore, certain combinations perform well in terms of amplitude damping, even if their phase transition operation is moderate, like the scenario $(\theta_{m1} = 2.4, \theta_{m2} = 3)$, with an amplitude damping ratio of 11%.

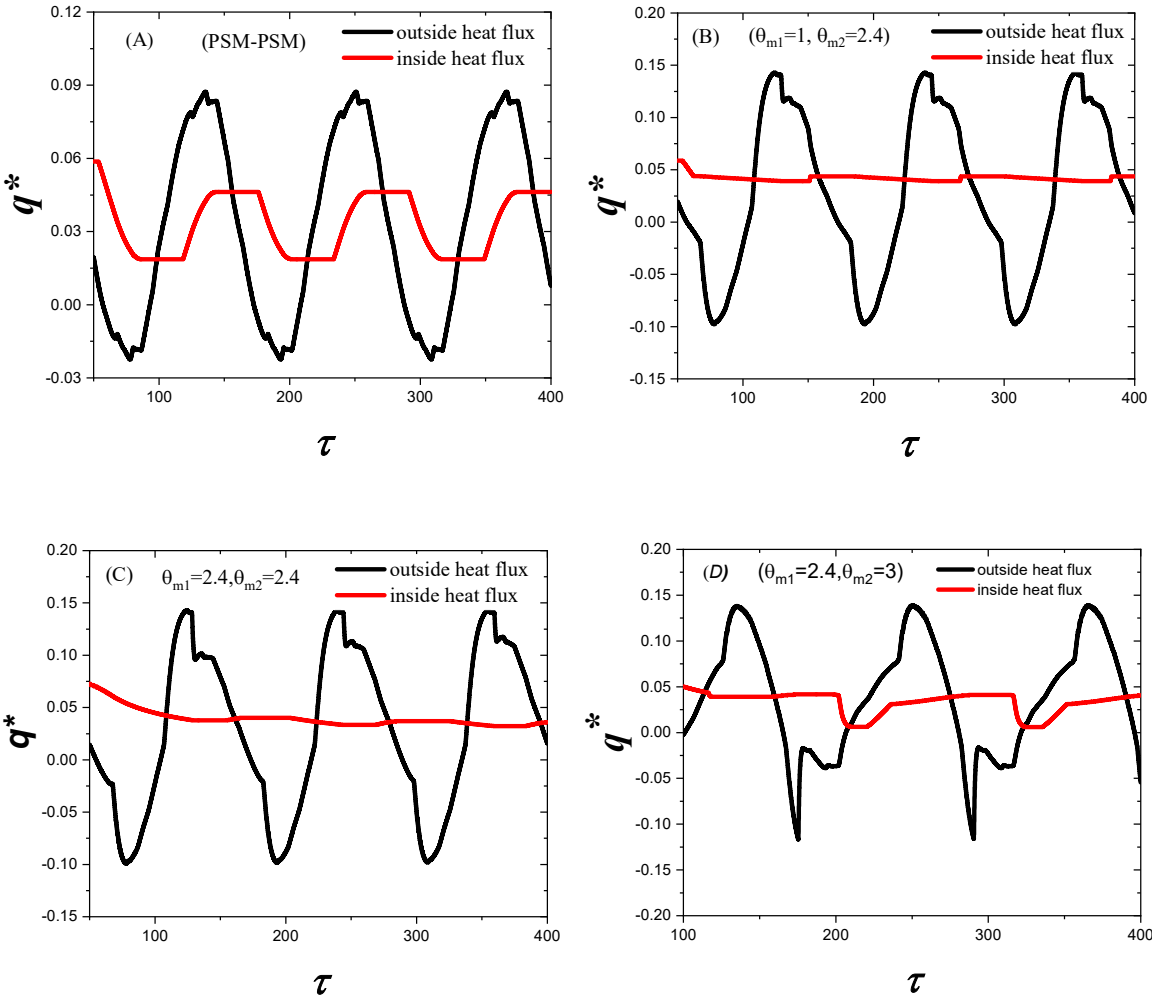

Figure 5.11 Heat flux evolution in summer for the combinations: (A) $(\boldsymbol{PSM, PSM})$, (B) $(\boldsymbol{\theta_{m1} = 1, \theta_{m2} = 2.4})$, (C) $(\boldsymbol{\theta_{m1} = 2.4, \theta_{m2} = 2.4})$.(D) $(\boldsymbol{\theta_{m1} = 2.4, \theta_{m2} = 3})$.

The reduction of the heat flux amplitude relates to changes in the fraction of PCM in operation. Combinations with a high fraction of operating PCM exhibit a notable reduction in the amplitude of heat flux fluctuation, while combinations with a low fraction of PCM in operation experience less reduction. Furthermore, it is worth noting that the combination $(\theta_{m1} = 2.4, \theta_{m2} = 3)$ demonstrates moderate smoothing of the heat flux, but it also exhibits a noticeable shift in peak load in comparison to the baseline scenario (PSM-PSM). However, combinations $(\theta_{m1} = 1, \theta_{m2} = 2.4)$ and $(\theta_{m1} = 2.4, \theta_{m2} = 2.4)$ not only showcase heat

flux homogenization (smoothing) but additionally exhibit a substantial shift in peak load in comparison to the case of building envelope without phase change (*PSM-PSM*).

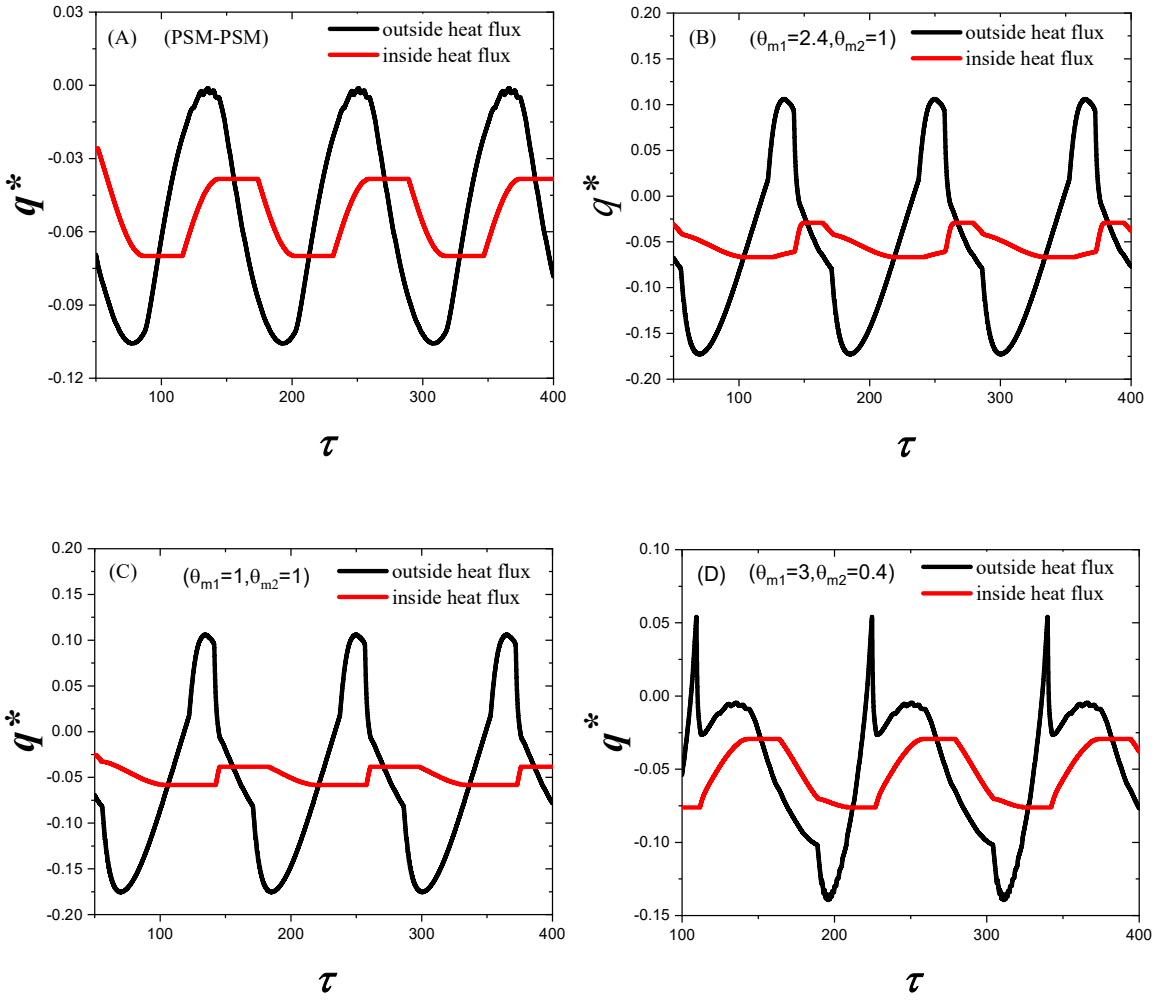

Figure 5.12 Heat flux evolution in winter for the combinations: (A) $(\boldsymbol{PSM}, \boldsymbol{PSM})$, (B) $(\theta_{m1} = 2.4, \theta_{m2} = 1)$, (C) $(\theta_{m1} = 1, \theta_{m2} = 1)$.(D) $(\theta_{m1} = 3, \theta_{m2} = 0.4)$

Similarly, to the summer case, Figure 5.12 presents the evolution of the dimensionless heat flux over time during the winter season. It is observed that for the reference case (*PSM-PSM*) and certain combinations with weak phase transition, like $(\theta_{m1} = 3, \theta_{m2} = 0.4)$, the influence of outside excitation extends to the inner side of the wall $(S_{in,out})$, resulting in unaltered heat flux fluctuation amplitude. Conversely, in combinations where the phase transition operation is effectively achieved, like in the scenario of $(\theta_{m1} = 1, \theta_{m2} = 1)$, a

reduction in amplitude of up to 15% is achieved in comparison to the baseline scenario, indicating a significant decrease in fluctuation. Additionally, within the combination ($\theta_{m1} = 2.4, \theta_{m2} = 1$), the amplitude experiences a notable reduction in comparison to cases of limited phase transition, with a proportion of 3%.

Furthermore, in line with the variation in operating PCM fraction, combinations with a higher fraction of operating PCM experience a more significant reduction in heat flux amplitude, and vice versa. However, unlike the summer season, in this case, besides the limited heat flux regularization (smoothing) observed, significant peak load shifting in contrast to the baseline scenario (*PSM-PSM*) is only evident in the combination ($\theta_{m1} = 1, \theta_{m2} = 1$).

5.6.6 Heat and average heat flux gained/lost over one day

Figure 5.13 (A) illustrates the daily average of dimensionless heat flux within the summer season, taking into account the daytime (discharging) and nighttime (charging) periods. Surprising results are observed, where scenarios with a limited phase transition operation exhibit the greatest reduction in the average heat flux in comparison to the baseline scenario (*PSM-PSM*), particularly in the case of ($\theta_{m1} = 2.4, \theta_{m2} = 0.4$) with a reduction ratio of 22%.

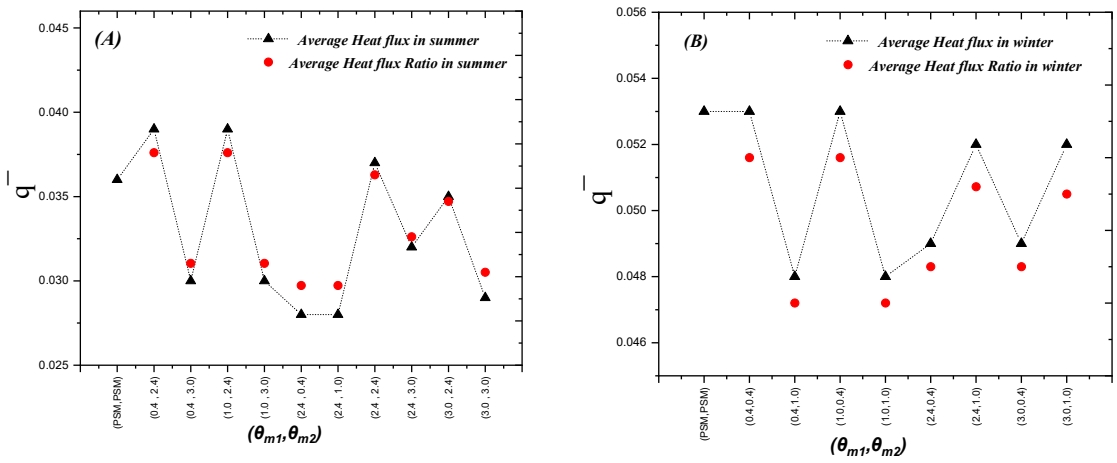

Figure 5.13 Average heat flux over one day for different combination: (A) in summer, (B) in winter.

However, the combination with a strong phase change process achievement ($\theta_{m1} = 2.4, \theta_{m2} = 2.4$) does not exhibit a substantial reduction; instead, the average heat flux delivered to the interior environment rises by 3%. This can be attributed to the liberated heat from the building envelope, especially from the phase change material layers, to the interior during the charging period, because of storing a substantial quantity of heat during the period of operating. This leads to a greater average of transferred heat to the indoor ambiance with smoother instantaneous temperature and heat flux. Conversely, combinations with an ineffective phase change operation do not store as much heat during the operating cycle, resulting in lower average of transferred heat to the indoor ambiance during the period of charging.

Based on Figure 5.13(B), contrary to the results observed in the summer period, combinations with a great fraction of operational PCM (indicating that the phase change operation is effectively established), such as ($\theta_{m1} = 0.4, \theta_{m2} = 1$), and ($\theta_{m1} = 1, \theta_{m2} = 1$), exhibit the greatest reduction in the daily average lost heat flux in contrast to the baseline scenario (*PSM-PSM*), with a reduction ratio of about 10%. Combinations ($\theta_{m1} = 2.4, \theta_{m2} = 0.4$) and ($\theta_{m1} = 3, \theta_{m2} = 0.4$) also exhibit a substantial reduction in average lost heat flux over a day, with a reduction ratio of 7.5%. However, combinations ($\theta_{m1} = 2.4, \theta_{m2} = 1$) ($\theta_{m1} = 3, \theta_{m2} = 1$) show a weaker reduction, with ratios of 2% and 2.5%, respectively. In contrary, combinations ($\theta_{m1} = 0.4, \theta_{m2} = 0.4$) and ($\theta_{m1} = 1, \theta_{m2} = 0.4$), where the phase transition operation is not well achieved, do not exhibit any reduction in average lost heat flux.

It can be concluded that the phase transition operation during the winter season is not effectively accomplished in comparison to the summer season. Therefore, a lower amount of heat is needed for charging the phase change material layers. In contrast, during the summer season, where the phase transition operation is effectively accomplished, a greater quantity of heat is required to be liberated for charging the phase change material layers.

5.6.7 Annual study

As mentioned earlier, the central concept of this study revolves around the use of two PCM layers, which can interchange their positions based on the season, whether it is summer or winter. [(combination for summer), (reverse combination for winter)] according to the

performance of each combination in its suitable season. Within this part, the annual parameters are characterized by the mean performance, which considers the thermal performance of the building envelope across both the summer and winter seasons.

Considering the behavior of all combinations throughout both seasons, the annual mean fraction of operating PCM is presented in Figure 5.14(A). It is observed that combinations where $(\theta_{m1} = \theta_{m2})$ operate in only one season, such as cases $(\theta_{m1} = 0.4, \theta_{m2} = 0.4)$ and $(\theta_{m1} = 3, \theta_{m2} = 3)$, resulting in a minimal operational PCM portion of 5% and 8%, respectively. Conversely, combinations like $(\theta_{m1} = 2.4, \theta_{m2} = 2.4)$ in summer season and $(\theta_{m1} = 1, \theta_{m2} = 1)$ in winter season exhibit a higher operating PCM fraction compared to other scenarios since every combination is well-suited for a particular season. For these scenarios, the yearly average operating PCM fraction is significantly higher, reaching ratios of 23% and 18%, respectively.

Additionally, combinations featuring distinct phase change temperatures $(\theta_{m1} \neq \theta_{m2})$ can perform well across the two seasons, in case of each phase change point is appropriate for its corresponding season. Based on the above observations, it is evident that the combination $[(\theta_{m1} = 1, \theta_{m2} = 2.4)$ for summer, $(\theta_{m1} = 2.4, \theta_{m2} = 1)$ for winter] achieves the greatest yearly average operating PCM fraction of 35%. However, other combinations, such as $[(\theta_{m1} = 1, \theta_{m2} = 3)$ for summer, $(\theta_{m1} = 3, \theta_{m2} = 1)$ for winter] and $[(\theta_{m1} = 0.4, \theta_{m2} = 2.4)$ for summer, $(\theta_{m1} = 2.4, \theta_{m2} = 0.4)$ for winter] also perform well with an operating PCM fraction ratio of 25% in both cases, as their melting temperatures are close to the suitable values for each respective season.

Based on the previous studies examining the variation of heat flux over time in both seasons, it is evident that the combination $(\theta_{m1} = 2.4, \theta_{m2} = 2.4)$ exhibits the highest effectiveness in mitigating the impact of external excitation by minimizing the amplitude of heat flux fluctuations during summer (by 13%). However, this particular combination does not function optimally during the winter season. Conversely, for winter, the combination $(\theta_{m1} = 1, \theta_{m2} = 1)$ demonstrates the greatest minimizing in the amplitude of heat flux fluctuations (up to 15%), but in summer season it does not operates effectively. However, certain combinations may not yield the highest level of amplitude reduction in their respective suitable seasons. For example, the combination $(\theta_{m1} = 1, \theta_{m2} = 2.4)$ in summer, and

$(\theta_{m1} = 2.4, \theta_{m2} = 1)$ in winter do not exhibit the most significant decrease in the amplitude of the heat flux fluctuation. However, considering the advantage of utilizing mobile layers, the combination $[(\theta_{m1} = 1, \theta_{m2} = 2.4)$ for summer, $(\theta_{m1} = 2.4, \theta_{m2} = 1)$ for winter] showcases the best overall performance in comparison to all other scenarios (achieving a reduction of 6.5% in heat flux fluctuation amplitude).

5.6.7.1 Phase change dimensionless operating duration for charging / discharging cycles

In Figure 5.14(B), it is evident that the combination $[(\theta_{m1} = 1, \theta_{m2} = 2.4)$ for summer,$(\theta_{m1} = 2.4, \theta_{m2} = 1)$ for winter] exhibits the longest average annual discharging duration (τ_{annual} = 43). This combination operates effectively in both seasons, maintaining a great fraction of operational PCM throughout. Similarly, other scenarios, like $[(\theta_{m1} = 1, \theta_{m2} = 3)$ for summer, $(\theta_{m1} = 3, \theta_{m2} = 1)$for winter] , and $[(\theta_{m1} = 0.4, \theta_{m2} = 2.4)$ for summer, $(\theta_{m1} = 2.4, \theta_{m2} = 0.4)$ for winter], can also achieve longer yearly average discharging durations of τ_{annual} = 38 and τ_{annual} = 28, respectively. The latter is longer than the discharging durations observed in cases where $(\theta_{m1} = \theta_{m2})$ since those combinations only operate during their respective suitable seasons. Moreover, it is noteworthy that combinations with higher annual average operating PCM fractions tend to have longer annual average charging durations. Among them, the combination $[(\theta_{m1} = 1, \theta_{m2} = 2.4)$ for summer, $(\theta_{m1} = 2.4, \theta_{m2} = 1)$ for winter] shows the longest charging duration, reaching τ_{annual} = 48.

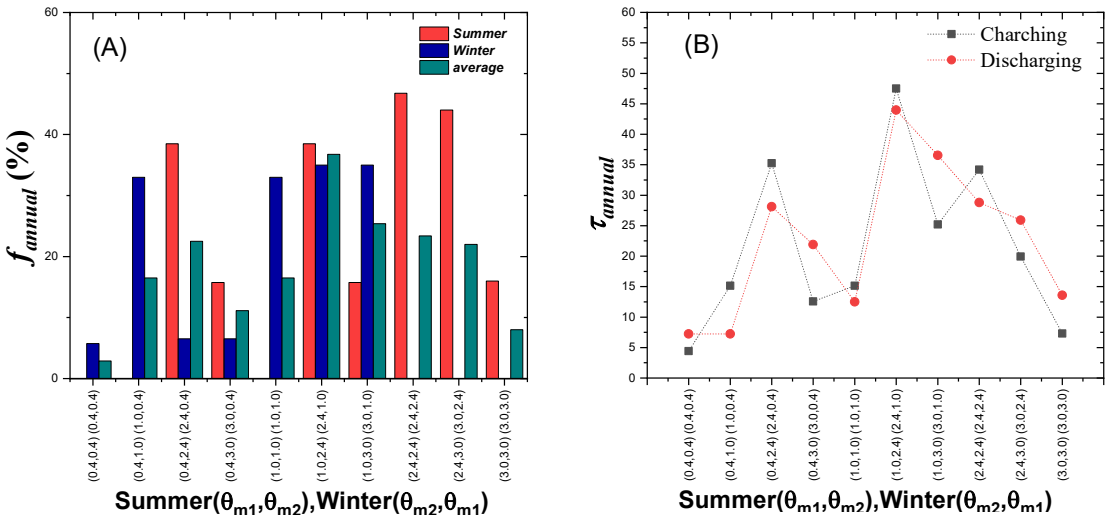

Figure 5.14 Annual average operating PCM fraction (A) and duration of charging/discharging (B)

5.6.7.2 Annual average heat flux gained/lost over one day

Taking into account the utilizing of the concept of dynamic phase change material layers, we determine the yearly average heat flux gained or lost within a single day, which represents the average energy consumed by HVAC system in order to maintain thermal comfort. Figure 5.15 demonstrates that the combination [$(\theta_{m1} = 0.4, \theta_{m2} = 3)$ for summer, $(\theta_{m1} = 3, \theta_{m2} = 0.4)$ for winter] exhibits the greatest minimizing in the yearly average heat flux gained/lost in comparison to the baseline scenario (PSM-PSM), with a potential diminution ratio of 12%. Moreover, certain combinations where $(\theta_{m1} = \theta_{m2})$, such as $(\theta_{m1} = 3, \theta_{m2} = 3)$ and $(\theta_{m1} = 1, \theta_{m2} = 1)$, show a noteworthy reduction in the annual average heat flux, with reduction ratios of 7% and 6% respectively. In similar manner, scenarios [$(\theta_{m1} = 2.4, \theta_{m2} = 3)$ for summer, $(\theta_{m1} = 3, \theta_{m2} = 2.4)$ for winter] demonstrate a decrease ratio of 4%, while [$(\theta_{m1} = 1, \theta_{m2} = 3)$ for summer, $(\theta_{m1} = 3, \theta_{m2} = 1)$ for winter] show a reduction ratio of 8%. However, all other combinations result in only marginal reductions. Consequently, the combination [$(\theta_{m1} = 0.4, \theta_{m2} = 3)$ for summer, $(\theta_{m1} = 3, \theta_{m2} = 0.4)$ for winter] proves to be the most effective in minimizing the annual average energy consumed by the HVAC system.

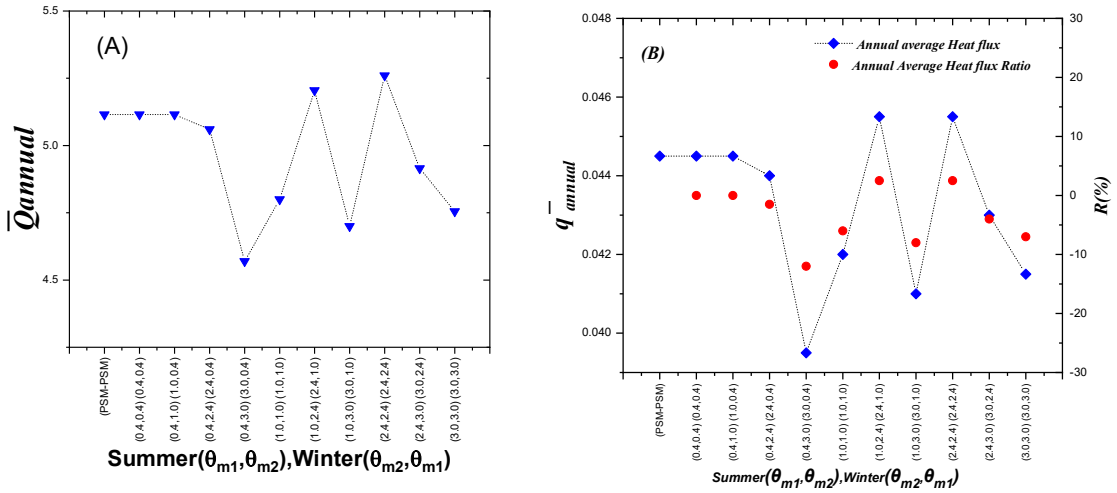

Figure 5.15 Annual average heat (A) and average heat flux (B) gained/lost over one day

5.7 Conclusion

The investigation of mobile PCM layers in the building envelope's performance for different seasons (summer and winter) has yielded the following conclusions:

Among the combinations, the operating PCM fraction is higher for $(\theta_{m1} = 2.4, \theta_{m2} = 2.4)$ in summer season and $(\theta_{m1} = 1, \theta_{m2} = 1)$ in the winter season, with ratios of 46.75% and 33% respectively. This is because each combination is appropriate with one season. However, when considering the performance of all combinations throughout both seasons, it becomes evident that the combination [$(\theta_{m1} = 1, \theta_{m2} = 2.4)$ for summer, $(\theta_{m1} = 2.4, \theta_{m2} = 1)$ for winter] achieves the greatest annual average operating PCM fraction, with a ratio of 35%.

Due to its operation in both seasons and the provision of a high operating PCM fraction in each, the combination [$(\theta_{m1} = 1, \theta_{m2} = 2.4)$ for summer, $(\theta_{m1} = 2.4, \theta_{m2} = 1)$ for winter] exhibits the longest yearly average duration of discharge. Several other combinations, such as [$(\theta_{m1} = 1, \theta_{m2} = 3)$ for summer, $(\theta_{m1} = 3, \theta_{m2} = 1)$ for winter] and [$(\theta_{m1} = 0.4, \theta_{m2} = 2.4)$ for summer, $(\theta_{m1} = 2.4, \theta_{m2} = 0.4)$ for winter] have longer annual average discharge durations compared to cases where $(\theta_{m1} = \theta_{m2})$, as the latter only operate during the appropriate seasons.

The combination $(\theta_{m1} = 2.4, \theta_{m2} = 2.4)$ proves to be the most efficient at reducing the impact of external excitation by reducing the amplitude of heat flux fluctuations during the summer season by 13%. However, its performance is not favorable during the winter season. Similarly, the combination $(\theta_{m1} = 1, \theta_{m2} = 1)$ demonstrates the greatest reduction in the amplitude of heat flux fluctuation during winter (15%), but it is not operational during the summer season. Moreover, considering the utilization of mobile layers, the combination [$(\theta_{m1} = 1, \theta_{m2} = 2.4)$ for summer, $(\theta_{m1} = 2.4, \theta_{m2} = 1)$ for winter] outperforms all other combinations. It exhibits superior performance in terms of minimizing the effects of external excitation when compared to alternative configurations.

The combination [$(\theta_{m1} = 0.4, \theta_{m2} = 3)$ for summer, $(\theta_{m1} = 3, \theta_{m2} = 0.4)$ for winter] demonstrates the most significant reduction in the annual average heat flux gained/lost in comparison to the baseline scenario (PSM-PSM), with a reduction ratio reaching 12%.

By employing the proposed design in this study, it has been discovered that combinations of melting temperatures aligned with the range of outside temperature fluctuations, where one is close to the maximum temperature in summer and the other is close to the minimum temperature in winter, effectively minimize energy consumption by the HVAC system (reducing it by up to 6.5%). On the other hand, combinations that have melting temperatures within the range of the outside fluctuating temperature and are in close proximity to the desired indoor comfort temperature for each season, coupled with the capability to adjust the position of each PCM layer to align with the outside environment during the corresponding suitable season, ensure the best annual performance of the double-layer PCM wall in terms of minimizing fluctuations and reducing the amplitude of the instantaneous heat flux. This effect leads to a substantial reduction in the power requirements of the HVAC system (up to 12%).

Perspective: For improved energy efficiency, the system presented in this work, may require an addition tool or technology that ensures the heat releasing within charging cycle to the outdoor instead of the interior ambient during summer season.

General Conclusion

The primary objective of this thesis was to demonstrate the diverse impacts of various parameters on the phase change phenomena occurring within a multi-layered building envelope. This exploration encompassed a wide array of interior and exterior conditions, all with the intention of addressing scenarios in which the performance of PCM walls might fall short. This comprehensive analysis included the examination of both single and double PCM layer building envelopes. Additionally, the study delved into the potential benefits of mobile PCM layers in enhancing the building envelope's effectiveness during distinct seasons, such as summer and winter. By considering the points elucidated below, the efficiency of the PCM-integrated building envelope could be enhanced:

Examining a single PCM layer building envelope during charging cycle illustrates how the PCM layer impacts the whole building envelope behavior under several conditions (building type and climate zone) during charging cycle, where it is found:

Heat released ratio study shows that:

• As the melting temperature (θ_m) increases, the heat loss also increases. For instance, at a melting temperature of θ_m=0.8, the wall released an additional heat ratio of 20% compared to the reference case PSM. Conversely, at θ_m=0.4, this ratio reaches 11%.

• Furthermore, reducing the latent heat of the PCM layer results in a decrease in both the released heat amount and the solid fraction. For example, when the latent heat is high (Ste=0.01), an additional heat released ratio of 120% is observed compared to the reference case PSM. On the other hand, cases with lower latent heat in the PCM layer (Ste=0.25, 0.5) generally exhibit a reduced amount of released heat during a half-day charging cycle compared to the high latent heat case (Ste=0.01), with additional heat released ratios of 10% and 5%, respectively.

Furthermore, the study examined the performance of a building envelope incorporating a PCM layer during various seasons, including summer and winter, indicate that:

• The cases where the melting temperatures are situated within the range of outside temperature fluctuations and are in proximity to the indoor comfort temperature (depending on the season) result in optimal yearly performance of the PCM wall. This optimal

performance is manifested in the smoothing of instantaneous heat flux and the reduction of its amplitude. Specifically, melting temperatures of θ_m=2.4 for summer and θ_m=1 for winter are prime examples. This trend, as supported by previous research, brings about a significant reduction in the maximum and amplitude of the instantaneous heat flux, enabling the efficient use of a low-power HVAC system.

• Conversely, instances where melting temperatures are aligned with the farthest temperature values from the outside fluctuations (one near the maximum temperature in summer and the other close to the minimum temperature in winter) contribute to minimizing energy consumption by the HVAC system. For instance, in the case of θ_m=3 during summer, energy consumption could be curtailed by 19.71%. In winter, a melting temperature of θ_m=1, positioned within the range of outside temperature fluctuations and close to the indoor comfort temperature, results in a reduction of energy consumption by 10.29%.

Investigating a double PCM layer building envelope during charging cycle illustrate how both PCM layers (inner and outer) impact each other, as well as the whole building envelope behavior under several conditions (building type and climate zone). Then, taking into account the following illustrated points, it could be shown when PCMs with different melting temperatures or latent heat are able to improve the building envelope's performance or not:

The analysis of the heat released ratio uncovers the following patterns:

• The primary factor governing the amount of heat lost is the melting temperature of the outer PCM layer. This is mainly due to its proximity to external influences. An increasing in θ_{m1} corresponds to an elevated heat loss. For instance, the combination $(\theta_{m1} = 0.7, \theta_{m2} = 0.5)$ yields an additional heat ratio of 18% compared to the reference case (PSM, PSM), while the combination $(\theta_{m1} = 0.5, \theta_{m2} = 0.7)$ achieves a 13% increase.

• On the other hand, the melting temperature of the inner PCM layer does not significantly affect the amount of heat released, as it is commonly chosen to align with the opposite season. Combinations featuring the same θ_{m1} exhibit an identical extra heat release ratio. For instance, both $(\theta_{m1} = 0.6, \theta_{m2} = 0.5)$ and $(\theta_{m1} = 0.6, \theta_{m2} = 0.7)$ combinations lead to a 15% rise in heat release.

Consequently, for effective charging of the PCM layer with a melting temperature suitable for the specific season, placing it in close proximity to external influences is recommended.

• To optimize the efficient charging of PCM layers, it's advisable for the latent heat of the inner PCM layer, situated farthest from external influences, to be lower than that of the outer PCM layer, which is in closer proximity to the external environment. This can be accomplished by assigning a higher Stefan number to the inner layer (Ste_2) compared to the outer layer (Ste_1). This arrangement promotes a more robust solidification process, yielding a higher solid fraction and consequently releasing a greater amount of heat. For instance, in the case of the combination ($Ste_1 = 0.1, Ste_2 = 0.01$), the heat released ratio was 15%, while for ($Ste_1 = 0.1, Ste_2 = 0.5$), it reached 25%. Furthermore, increasing the latent heat of the outer PCM layer augments the heat release ratio.

Nonetheless, when optimizing both melting temperatures and latent heats, it's imperative to account for the overall performance of the wall and the heat accumulated during operational cycles. This comprehensive approach ensures that the chosen parameters harmoniously align with the desired objectives, yielding an effective and balanced outcome.

The performance of mobile PCM layers in the building envelope has been investigated for different seasons (summer and winter). The findings are summarized as follows:

• The combination ($\theta_{m1} = 2.4, \theta_{m2} = 2.4$) emerges as the most effective in mitigating the influence of external factors by reducing the amplitude of heat flux fluctuations during the summer season by 13%. However, its performance is less favorable during the winter season. Similarly, the combination ($\theta_{m1} = 1, \theta_{m2} = 1$) showcases the highest reduction in amplitude of heat flux fluctuations during winter (15%), but it is not well-suited for the summer season.

• Furthermore, when considering the integration of mobile layers, the combination [($\theta_{m1} = 1, \theta_{m2} = 2.4$) for summer, ($\theta_{m1} = 2.4, \theta_{m2} = 1$) for winter] surpasses all other configurations. It demonstrates superior performance in minimizing the impacts of external excitation compared to alternative configurations.

• The combination [($\theta_{m1} = 0.4, \theta_{m2} = 3$) for summer, ($\theta_{m1} = 3, \theta_{m2} = 0.4$) for winter] demonstrates the most significant reduction in the annual average heat flux gained/lost compared to the reference case (PSM-PSM), with a reduction ratio reaching 12%.

By employing the proposed design in this study, it has been discovered that combinations of melting temperatures aligned with the range of outside temperature fluctuations, where one is close to the maximum temperature in summer and the other is close to the minimum

temperature in winter, effectively minimize energy consumption by the HVAC system (reducing it by up to 6.5%). On the other hand, combinations that have melting temperatures within the range of the outside fluctuating temperature and are in close proximity to the desired indoor comfort temperature for each season, coupled with the capability to adjust the position of each PCM layer to align with the outside environment during the corresponding suitable season, ensure the best annual performance of the double-layer PCM wall in terms of minimizing fluctuations and reducing the amplitude of the instantaneous heat flux. This effect leads to a substantial reduction in the power requirements of the HVAC system (up to 12%).

References

[1] "Yan H., Shen Q., Fan L.C.H., Wang Y., Zhang L. Greenhouse gas emissions in building construction: A case study of One Peking in Hong Kong. Build. Environ. 2010;45:949–955. doi: 10.1016/j.buildenv.2009.09.014.

[2] A. H. Abedin, "A Critical Review of Thermochemical Energy Storage Systems," *Open Renew. Energy J.*, vol. 4, no. 1, pp. 42–46, Aug. 2011, doi: 10.2174/1876387101004010042.

[3] B. Zalba, J. M. Marín, L. F. Cabeza, and H. Mehling, "Review on thermal energy storage with phase change: materials, heat transfer analysis and applications," *Appl. Therm. Eng.*, vol. 23, no. 3, pp. 251–283, Feb. 2003, doi: 10.1016/S1359-4311(02)00192-8.

[4] K. Pielichowska and K. Pielichowski, "Phase change materials for thermal energy storage," *Prog. Mater. Sci.*, vol. 65, pp. 67–123, Aug. 2014, doi: 10.1016/J.PMATSCI.2014.03.005.

[5] K. E. Min, "A Study of Thermal Energy Storage of Phase Change Materials: Thermophysical Properties and Numerical Simulations," *Thesis*, 2019, [Online]. Available: https://archives.pdx.edu/ds/psu/28090.

[6] A. Sharma, V. V. Tyagi, C. R. Chen, and D. Buddhi, "Review on thermal energy storage with phase change materials and applications," *Renew. Sustain. Energy Rev.*, vol. 13, no. 2, pp. 318–345, Feb. 2009, doi: 10.1016/J.RSER.2007.10.005.

[7] Y. B. Tao, C. H. Lin, and Y. L. He, "Preparation and thermal properties characterization of carbonate salt/carbon nanomaterial composite phase change material," *Energy Convers. Manag.*, vol. 97, pp. 103–110, Jun. 2015, doi: 10.1016/J.ENCONMAN.2015.03.051.

[8] M. M. Kenisarin, "High-temperature phase change materials for thermal energy storage," *Renew. Sustain. Energy Rev.*, vol. 14, no. 3, pp. 955–970, Apr. 2010, doi: 10.1016/J.RSER.2009.11.011.

[9] C. Veerakumar and A. Sreekumar, "Phase change material based cold thermal energy storage: Materials, techniques and applications – A review," *Int. J. Refrig.*, vol. 67, pp. 271–289, Jul. 2016, doi: 10.1016/J.IJREFRIG.2015.12.005.

[10] G. Zsembinszki, C. Prieto, G. Ziskind, and L. F. Cabeza, "Advances in thermal energy storage for renewable energies integration in the energy system," *Renew. Energy*, vol. 176, pp. 635–636, Oct. 2021, doi: 10.1016/J.RENENE.2021.05.140.

[11] M. Teggar, S.S.M. Ajarostaghi, Ç. Yıldız, M. Arıcı, K.A.R. Ismail, H. Niyas, F.A.
M. Lino, M.S. Mert, M. Khalid, "Performance enhancement of latent heat storage systems by using extended surfaces and porous materials: A state-of-the-art review," *J. Energy Storage*, vol. 44, p. 103340, Dec. 2021, doi: 10.1016/J.EST.2021.103340.

[12] R. Thaib, S. R. Hamdani, T. M. I. Mahlia, and N. A. Pambudi, "Experimental analysis of using

beeswax as phase change materials for limiting temperature rise in building integrated photovoltaics," *Case Stud. Therm. Eng.*, vol. 12, pp. 223–227, Sep. 2018, doi: 10.1016/J.CSITE.2017.12.005.

[13] A. Waqas and J. Ji, "Thermal management of conventional PV panel using PCM with movable shutters – A numerical study," *Sol. Energy*, vol. 158, pp. 797–807, Dec. 2017, doi: 10.1016/J.SOLENER.2017.10.050.

[14] F. L. Tan and C. P. Tso, "Cooling of mobile electronic devices using phase change materials," *Appl. Therm. Eng.*, vol. 24, no. 2–3, pp. 159–169, Feb. 2004, doi: 10.1016/J.APPLTHERMALENG.2003.09.005.

[15] R. Kandasamy, X. Q. Wang, and A. S. Mujumdar, "Transient cooling of electronics using phase change material (PCM)-based heat sinks," *Appl. Therm. Eng.*, vol. 28, no. 8–9, pp. 1047–1057, Jun. 2008, doi: 10.1016/J.APPLTHERMALENG.2007.06.010.

[16] L. F. Cabeza, L. Navarro, A.L. Pisello, L. Olivieri, C. Bartolome, J. S anchez, S. Alvarez, J.A. Tenorio, "Behaviour of a concrete wall containing micro-encapsulated PCM after a decade of its construction," *Sol. Energy*, vol. 200, pp. 108–113, Apr. 2020, doi: 10.1016/J.SOLENER.2019.12.003.

[17] A. De Gracia and L. F. Cabeza, "Phase change materials and thermal energy storage for buildings," *Energy Build.*, vol. 103, pp. 414–419, Sep. 2015, doi: 10.1016/J.ENBUILD.2015.06.007.

[18] V. Bianco, M. De Rosa, and K. Vafai, "Phase-change materials for thermal management of electronic devices," *Appl. Therm. Eng.*, vol. 214, no. June, 2022, doi: 10.1016/j.applthermaleng.2022.118839.

[19] T. Markandeyulu, J. Krishna Devanuri, and K. Kiran Kumar, "On the Suitability of Phase Change Material (PCM) for Thermal Management of Electronic Components," *Indian J. Sci. Technol.*, vol. 9, no. Special Issue 1, pp. 1–4, May 2016, doi: 10.17485/IJST/2016/V9IS1/107939.

[20] M. S. Lori and K. Vafai, "Heat transfer and fluid flow analysis of microchannel heat sinks with periodic vertical porous ribs," *Appl. Therm. Eng.*, vol. 205, p. 118059, Mar. 2022, doi: 10.1016/J.APPLTHERMALENG.2022.118059.

[21] M. Shafahi, V. Bianco, K. Vafai, and O. Manca, "Thermal performance of flat-shaped heat pipes using nanofluids," *Int. J. Heat Mass Transf.*, vol. 53, no. 7–8, pp. 1438–1445, Mar. 2010, doi: 10.1016/J.IJHEATMASSTRANSFER.2009.12.007.

[22] S. Lu and K. Vafai, "A comparative analysis of innovative microchannel heat sinks for electronic cooling," *Int. Commun. Heat Mass Transf.*, vol. 76, pp. 271–284, Aug. 2016, doi: 10.1016/J.ICHEATMASSTRANSFER.2016.04.024.

[23] P. J. Shamberger and N. M. Bruno, “Review of metallic phase change materials for high heat flux transient thermal management applications,” *Appl. Energy*, vol. 258, p. 113955, Jan. 2020, doi: 10.1016/J.APENERGY.2019.113955.

[24] L. Ianniciello, P. H. Biwolé, and P. Achard, “Electric vehicles batteries thermal management systems employing phase change materials,” *J. Power Sources*, vol. 378, pp. 383–403, Feb. 2018, doi: 10.1016/J.JPOWSOUR.2017.12.071.

[25] S. D. Chitta, C. Akkaldevi, J. Jaidi, S. Panchal, M. Fowler, and R. Fraser, “Comparison of lumped and 1D electrochemical models for prismatic 20Ah LiFePO4 battery sandwiched between minichannel cold-plates,” *Appl. Therm. Eng.*, vol. 199, p. 117586, Nov. 2021, doi: 10.1016/J.APPLTHERMALENG.2021.117586.

[26] A. Arshad, H. M. Ali, W. M. Yan, A. K. Hussein, and M. Ahmadlouydarab, “An experimental study of enhanced heat sinks for thermal management using n-eicosane as phase change material,” *Appl. Therm. Eng.*, vol. 132, pp. 52–66, Mar. 2018, doi: 10.1016/J.APPLTHERMALENG.2017.12.066.

[27] M. Sivashankar, C. Selvam, and S. Manikandan, “A review on the selection of phase change materials for photovoltaic thermal management,” *IOP Conf. Ser. Mater. Sci. Eng.*, vol. 1130, no. 1, p. 012026, Apr. 2021, doi: 10.1088/1757-899X/1130/1/012026.

[28] A. Naseer, F. Jamil, H.M. Ali, A. Ejaz, S. Khushnood, T. Ambreen, W.M. Yan, “Role of phase change materials thickness for photovoltaic thermal management,” *Sustain. Energy Technol. Assessments*, vol. 49, p. 101719, Feb. 2022, doi: 10.1016/J.SETA.2021.101719.

[29] H. Mahamudu, M. M. Rahman, H. S. C. Metselaar, S. Mekhilef, S. A. Shezan, R. Sohel, S. Bin Abu Karim, W. N. I. Badiuzaman, “Temperature Regulation of Photovoltaic Module Using Phase Change Material: A Numerical Analysis and Experimental Investigation,” *Int. J. Photoenergy*, vol. 2016, 2016, doi: 10.1155/2016/5917028.

[30] E. Borri, G. Zsembinszki, and L. F. Cabeza, “Recent developments of thermal energy storage applications in the built environment: A bibliometric analysis and systematic review,” *Appl. Therm. Eng.*, vol. 189, p. 116666, May 2021, doi: 10.1016/J.APPLTHERMALENG.2021.116666.

[31] D. Vérez, E. Borri, A. Crespo, B. D. Mselle, Á. de Gracia, G. Zsembinszki, L. F. Cabeza, “Experimental Study on Two PCM Macro-Encapsulation Designs in a Thermal Energy Storage Tank,” *Appl. Sci. 2021, Vol. 11, Page 6171*, vol. 11, no. 13, p. 6171, Jul. 2021, doi: 10.3390/APP11136171.

[32] M. Arıcı, E. Tütüncü, M. Kan, and H. Karabay, “Melting of nanoparticle-enhanced paraffin wax in a rectangular enclosure with partially active walls,” *Int. J. Heat Mass Transf.*, vol. 104, pp. 7–17, Jan. 2017, doi: 10.1016/J.IJHEATMASSTRANSFER.2016.08.017.

[33] M.E. Tiji, H.I. Mohammed, R.K. Ibrahem, A. Dulaimi, J. M. Mahdi, H. Sh. Majdi, M.M. Keshtkar, P. Talebizadehsardari, "Evaluation of T-Shaped Fins With a Novel Layout for Improved Melting in a Triple-Tube Heat Storage System," *Front. Energy Res.*, vol. 10, p. 1063, Aug. 2022, doi: 10.3389/FENRG.2022.947391/BIBTEX.

[34] X. Sun, J. M. Mahdi, H. I. Mohammed, H. S. Majdi, W. Zixiong, and P. Talebizadehsardari, "Solidification Enhancement in a Triple-Tube Latent Heat Energy Storage System Using Twisted Fins," *Energies 2021, Vol. 14, Page 7179*, vol. 14, no. 21, p. 7179, Nov. 2021, doi: 10.3390/EN14217179.

[35] I. Shojaeinasab Chatroudi, M. Atashafrooz, H. I. Mohammed, A. M. Abed, and P. Talebizadehsardari, "Heat transfer enhancement and free convection assessment in a double-tube latent heat storage unit equipped with optimally spaced circular fins: Evaluation of the melting process," *Front. Energy Res.*, vol. 11, p. 11, Jan. 2023, doi: 10.3389/FENRG.2023.1097382/BIBTEX.

[36] M. Sheikholeslami, "Numerical analysis of solar energy storage within a double pipe utilizing nanoparticles for expedition of melting," *Sol. Energy Mater. Sol. Cells*, vol. 245, p. 111856, Sep. 2022, doi: 10.1016/J.SOLMAT.2022.111856.

[37] M. Sheikholeslami, "Efficacy of porous foam on discharging of phase change material with inclusion of hybrid nanomaterial," *J. Energy Storage*, vol. 62, p. 106925, Jun. 2023, doi: 10.1016/J.EST.2023.106925.

[38] Z. A. Al-Absi, M. H. M. Isa, and M. Ismail, "Phase change materials (PCMs) and their optimum position in building walls," *Sustain.*, vol. 12, no. 4, 2020, doi: 10.3390/su12041294.

[39] O. Imghoure, N. Belouaggadia, M. Ezzine, R. Lbibb, and Z. Younsi, "Performance evaluation of phase change materials for thermal comfort in a hot climate region," *Appl. Therm. Eng.*, vol. 186, Mar. 2021, doi: 10.1016/J.APPLTHERMALENG.2020.116509.

[40] D. Li, Z. Li, Y. Zheng, C. Liu, A. K. Hussein, and X. Liu, "Thermal performance of a PCM-filled double-glazing unit with different thermophysical parameters of PCM," *Sol. Energy*, vol. 133, pp. 207–220, Aug. 2016, doi: 10.1016/J.SOLENER.2016.03.039.

[41] C. Liu, Y. Wu, D. Li, T. Ma, A. K. Hussein, and Y. Zhou, "Investigation of thermal and optical performance of a phase change material–filled double-glazing unit," *https://doi.org/10.1177/1744259117708734*, vol. 42, no. 2, pp. 99–119, Jun. 2017, doi: 10.1177/1744259117708734.

[42] M. Sheikholeslami, "Modeling investigation for energy storage system including mixture of paraffin and ZnO nano-powders considering porous media," *J. Pet. Sci. Eng.*, vol. 219, p. 111066, Dec. 2022, doi: 10.1016/J.PETROL.2022.111066.

[43] A. Fateh, F. Klinker, M. Brütting, H. Weinläder, and F. Devia, "Numerical and experimental

investigation of an insulation layer with phase change materials (PCMs)," *Energy Build.*, vol. 153, pp. 231–240, Oct. 2017, doi: 10.1016/J.ENBUILD.2017.08.007.

[44] S. D. Zwanzig, Y. Lian, and E. G. Brehob, "Numerical simulation of phase change material composite wallboard in a multi-layered building envelope," *Energy Convers. Manag.*, vol. 69, pp. 27–40, May 2013, doi: 10.1016/J.ENCONMAN.2013.02.003.

[45] X. Kong, S. Lu, J. Huang, Z. Cai, and S. Wei, "Experimental research on the use of phase change materials in perforated brick rooms for cooling storage," *Energy Build.*, vol. 62, pp. 597–604, Jul. 2013, doi: 10.1016/J.ENBUILD.2013.03.048.

[46] L. Zhu, Y. Yang, S. Chen, and Y. Sun, "Numerical study on the thermal performance of lightweight temporary building integrated with phase change materials," *Appl. Therm. Eng.*, vol. 138, pp. 35–47, Jun. 2018, doi: 10.1016/J.APPLTHERMALENG.2018.03.103.

[47] J. Lei, J. Yang, and E. H. Yang, "Energy performance of building envelopes integrated with phase change materials for cooling load reduction in tropical Singapore," *Appl. Energy*, vol. 162, pp. 207–217, Jan. 2016, doi: 10.1016/J.APENERGY.2015.10.031.

[48] A. Gounni and M. El Alami, "The optimal allocation of the PCM within a composite wall for surface temperature and heat flux reduction: An experimental Approach," *Appl. Therm. Eng.*, vol. 127, pp. 1488–1494, Dec. 2017, doi: 10.1016/J.APPLTHERMALENG.2017.08.168.

[49] X. Shi, S. A. Memon, W. Tang, H. Cui, and F. Xing, "Experimental assessment of position of macro encapsulated phase change material in concrete walls on indoor temperatures and humidity levels," *Energy Build.*, vol. 71, pp. 80–87, Mar. 2014, doi: 10.1016/J.ENBUILD.2013.12.001.

[50] X. Sun, Y. Zhang, K. Xie, and M. A. Medina, "A parametric study on the thermal response of a building wall with a phase change material (PCM) layer for passive space cooling," *J. Energy Storage*, vol. 47, p. 103548, Mar. 2022, doi: 10.1016/J.EST.2021.103548.

[51] A. Lagou, A. Kylili, J. Šadauskienė, and P. A. Fokaides, "Numerical investigation of phase change materials (PCM) optimal melting properties and position in building elements under diverse conditions," *Constr. Build. Mater.*, vol. 225, pp. 452–464, Nov. 2019, doi: 10.1016/J.CONBUILDMAT.2019.07.199.

[52] Z. Liu, J. Hou, X. Meng, and B. J. Dewancker, "A numerical study on the effect of phase-change material (PCM) parameters on the thermal performance of lightweight building walls," *Case Stud. Constr. Mater.*, vol. 15, p. e00758, Dec. 2021, doi: 10.1016/J.CSCM.2021.E00758.

[53] A. Bozzhigitov, S. A. Memon, and I. Adilkhanova, "Sensitivity of energy performance to the selection of PCM melting temperature for the building located in Cfb climate zone," *Energy Reports*, vol. 8, pp. 6301–6320, Nov. 2022, doi: 10.1016/J.EGYR.2022.04.059.

[54] D. Zhou and P. Eames, "Phase Change Material Wallboard (PCMW) melting temperature

optimisation for passive indoor temperature control," *Renew. Energy*, vol. 139, pp. 507–514, Aug. 2019, doi: 10.1016/J.RENENE.2019.02.109.

[55] E. Tunçbilek, M. Arıcı, M. Krajčík, Y. Li, M. Jurčević, and S. Nižetić, "Impact of nano-enhanced phase change material on thermal performance of building envelope and energy consumption," *Int. J. Energy Res.*, vol. 46, no. 14, pp. 20249–20264, Nov. 2022, doi: 10.1002/ER.8200.

[56] M. Li, Q. Cao, H. Pan, X. Wang, and Z. Lin, "Effect of melting point on thermodynamics of thin PCM reinforced residential frame walls in different climate zones," *Appl. Therm. Eng.*, vol. 188, p. 116615, Apr. 2021, doi: 10.1016/J.APPLTHERMALENG.2021.116615.

[57] R. A. Kishore, M. V. A. Bianchi, C. Booten, J. Vidal, and R. Jackson, "Parametric and sensitivity analysis of a PCM-integrated wall for optimal thermal load modulation in lightweight buildings," *Appl. Therm. Eng.*, vol. 187, p. 116568, Mar. 2021, doi: 10.1016/J.APPLTHERMALENG.2021.116568.

[58] M. Arıcı, F. Bilgin, S. Nižetić, and H. Karabay, "PCM integrated to external building walls: An optimization study on maximum activation of latent heat," *Appl. Therm. Eng.*, vol. 165, p. 114560, Jan. 2020, doi: 10.1016/J.APPLTHERMALENG.2019.114560.

[59] M. Prabhakar, M. Saffari, A. de Gracia, and L. F. Cabeza, "Improving the energy efficiency of passive PCM system using controlled natural ventilation," *Energy Build.*, vol. 228, p. 110483, Dec. 2020, doi: 10.1016/J.ENBUILD.2020.110483.

[60] G. Zhou, Y. Yang, and H. Xu, "Energy performance of a hybrid space-cooling system in an office building using SSPCM thermal storage and night ventilation," *Sol. Energy*, vol. 85, no. 3, pp. 477–485, Mar. 2011, doi: 10.1016/J.SOLENER.2010.12.028.

[61] A. Louanate, R. El Otmani, K. Kandoussi, and M. Boutaous, "Dynamic modeling and performance assessment of single and double phase change material layer–integrated buildings in Mediterranean climate zone," *https://doi.org/10.1177/1744259120945361*, vol. 44, no. 5, pp. 461–478, Aug. 2020, doi: 10.1177/1744259120945361.

[62] X. Kong, J. Li, M. Fan, W. Li, and H. Li, "Study on the thermal performance of a new double layer PCM trombe wall with multiple phase change points," *Sol. Energy Mater. Sol. Cells*, vol. 240, p. 111685, Jun. 2022, doi: 10.1016/J.SOLMAT.2022.111685.

[63] M. Arıcı, F. Bilgin, M. Krajčík, S. Nižetić, and H. Karabay, "Energy saving and CO2 reduction potential of external building walls containing two layers of phase change material," *Energy*, vol. 252, p. 124010, Aug. 2022, doi: 10.1016/J.ENERGY.2022.124010.

[64] K. S. Reddy, V. Mudgal, and T. K. Mallick, "Thermal performance analysis of multi-phase change material layer-integrated building roofs for energy efficiency in built-environment," *Energies*, vol. 10, no. 9, 2017, doi: 10.3390/en10091367.

[65] X. Jin and X. Zhang, “Thermal analysis of a double layer phase change material floor,” *Appl. Therm. Eng.*, vol. 31, no. 10, pp. 1576–1581, Jul. 2011, doi: 10.1016/J.APPLTHERMALENG.2011.01.023.

[66] N. Zhu, P. Hu, and L. Xu, “A simplified dynamic model of double layers shape-stabilized phase change materials wallboards,” *Energy Build.*, vol. 67, pp. 508–516, Dec. 2013, doi: 10.1016/J.ENBUILD.2013.08.043.

[67] N. Zhu, P. Liu, P. Hu, F. Liu, and Z. Jiang, “Modeling and simulation on the performance of a novel double shape-stabilized phase change materials wallboard,” *Energy Build.*, vol. 107, pp. 181–190, Nov. 2015, doi: 10.1016/J.ENBUILD.2015.07.051.

[68] A. U. Rehman, S. R. Sheikh, Z. Kausar, and S. J. McCormack, “Numerical Simulation of a Novel Dual Layered Phase Change,” *Energies*, vol. 14, no. 13, 2021.

[69] F. Almeida, Z. Dahai, A. S. Fung, and W. H. Leong, “Investigation of Multilayered Phase-Change-Material Modeling in ESP-r,” *Int. High Perform. Build. Conf. Purdue*, no. January, 2010.

[70] W. Sun, Y. Zhang, Z. Ling, X. Fang, and Z. Zhang, “Experimental investigation on the thermal performance of double-layer PCM radiant floor system containing two types of inorganic composite PCMs,” *Energy Build.*, vol. 211, 2020, doi: 10.1016/j.enbuild.2020.109806.

[71] A. Pasupathy and R. Velraj, “Effect of double layer phase change material in building roof for year round thermal management,” *Energy Build.*, vol. 40, no. 3, pp. 193–203, 2008, doi: 10.1016/j.enbuild.2007.02.016.

[72] N. Zhu, F. Liu, P. Liu, P. Hu, and M. Wu, “Energy saving potential of a novel phase change material wallboard in typical climate regions of China,” *Energy Build.*, vol. 128, pp. 360–369, 2016, doi: 10.1016/j.enbuild.2016.06.093.

[73] A. Zastawna-Rumin and K. Nowak, “Experimental Research of a Partition Composed of Two Layers of Different Types of PCM,” *Energy Procedia*, vol. 91, pp. 259–268, 2016, doi: 10.1016/j.egypro.2016.06.216.

[74] B. P. Jelle, A. Gustavsen, and R. Baetens, “The path to the high performance thermal building insulation materials and solutions of tomorrow,” *https://doi.org/10.1177/1744259110372782*, vol. 34, no. 2, pp. 99–123, Jul. 2010, doi: 10.1177/1744259110372782.

[75] M. Fawaier and B. Bokor, “Dynamic insulation systems of building envelopes: A review,” *Energy Build.*, vol. 270, p. 112268, Sep. 2022, doi: 10.1016/J.ENBUILD.2022.112268.

[76] G. Gan, “Numerical evaluation of thermal comfort in rooms with dynamic insulation,” *Build. Environ.*, vol. 35, no. 5, pp. 445–453, Jul. 2000, doi: 10.1016/S0360-1323(99)00034-7.

[77] M. S. E. Imbabi, “Modular breathing panels for energy efficient, healthy building construction,” *Renew. Energy*, vol. 31, no. 5, pp. 729–738, Apr. 2006, doi:

10.1016/J.RENENE.2005.08.009.

[78] A. Alongi, A. Angelotti, and L. Mazzarella, “A numerical model to simulate the dynamic performance of Breathing Walls,” *https://doi.org/10.1080/19401493.2020.1868578*, vol. 14, no. 2, pp. 155–180, 2021, doi: 10.1080/19401493.2020.1868578.

[79] T. Pflug, T. E. Kuhn, R. Nörenberg, A. Glück, N. Nestle, and C. Maurer, “Closed translucent façade elements with switchable U-value—A novel option for energy management via the facade,” *Energy Build.*, vol. 86, pp. 66–73, Jan. 2015, doi: 10.1016/J.ENBUILD.2014.09.082.

[80] A. de Gracia, “Dynamic building envelope with PCM for cooling purposes – Proof of concept,” *Appl. Energy*, vol. 235, no. November 2018, pp. 1245–1253, 2019, doi: 10.1016/j.apenergy.2018.11.061.

[81] O. Arfi and E. Mezaache, “TRANSFERT THERMIQUE INSTATIONNAIRE DANS UN MUR TRICOUCHES SUBISSANT UN CHANGEMENT DE PHASE PAR SOLIDIFICATION.,” *Sci. Technol. A, exactes Sci.*, vol. 0, no. 40, pp. 17–25, May 2016, Accessed: Jan. 09, 2023. [Online]. Available: http://revue.umc.edu.dz/index.php/a/article/view/1579.

[82] M. Bouteldja, E. H. Mezaache, and A. Laouer, “Numerical study of the solidification of phase change materials in a rectangular cavity: Effects of convection and aspect ratio,” *Ann. Chim. Sci. des Mater.*, vol. 43, no. 1, pp. 1–9, 2019, doi: 10.18280/ACSM.430101.

[83] L. Bilir and Z. Ilken, “Total solidification time of a liquid phase change material enclosed in cylindrical/spherical containers,” *Appl. Therm. Eng.*, vol. 25, no. 10, pp. 1488–1502, Jul. 2005, doi: 10.1016/J.APPLTHERMALENG.2004.10.005.

[84] M. Teggar and E. H. Mezaache, “Numerical Investigation of a PCM Heat Exchanger for Latent Cool Storage,” *Energy Procedia*, vol. 36, pp. 1310–1319, Jan. 2013, doi: 10.1016/J.EGYPRO.2013.07.149.

[85] N. Boulaktout, E. H. Mezaache, M. Teggar, M. Arıcı, K. A. R. Ismail, and Ç. Yıldız, “Effect of Fin Orientation on Melting Process in Horizontal Double Pipe Thermal Energy Storage Systems,” *J. Energy Resour. Technol.*, vol. 143, no. 7, Jul. 2021, doi: 10.1115/1.4050904.

[86] S. V. Patankar, “Numerical Heat Transfer and Fluid Flow,” Oct. 2018, doi: 10.1201/9781482234213.

[87] E. H. Mezaache and M. Daguenet, “Etude numérique de l’influence de l’inclinaison sur l’évaporation d’un film liquide s’écoulant sur une paroi plane isotherme ou à flux de chaleur imposé,” *Can. J. Chem. Eng.*, vol. 76, no. 2, pp. 203–210, Apr. 1998, doi: 10.1002/CJCE.5450760207.

[88] R. Chebah, A. Laouer, and E. H. Mezaache, “Passive control and stability of the indoor temperature of a closed cavity based on the process of integrating phase change materials,”

Energy, Ecol. Environ., pp. 1–11, Sep. 2022, doi: 10.1007/S40974-022-00260-7/METRICS.

[89] V. Alexiades and A. D. Solomon, "Mathematical Modeling Of Melting And Freezing Processes," *Math. Model. Melting Freez. Process.*, May 2018, doi: 10.1201/9780203749449.

[90] N. Vitorino, J. C. C. Abrantes, and J. R. Frade, "Numerical solutions for mixed controlled solidification of phase change materials," *Int. J. Heat Mass Transf.*, vol. 53, no. 23–24, pp. 5335–5342, Nov. 2010, doi: 10.1016/J.IJHEATMASSTRANSFER.2010.07.023.

[91] M. A. Izquierdo-Barrientos, J. F. Belmonte, D. Rodríguez-Sánchez, A. E. Molina, and J. A. Almendros-Ibáñez, "A numerical study of external building walls containing phase change materials (PCM)," *Appl. Therm. Eng.*, vol. 47, pp. 73–85, Dec. 2012, doi: 10.1016/J.APPLTHERMALENG.2012.02.038.

[92] A. J. Hamad, "Energy saving and charging discharging characteristics of multiple pcms subjected to internal air flow," *Fluids*, vol. 6, no. 8, 2021, doi: 10.3390/fluids6080275.

[93] K. Zhong, S. Li, G. Sun, S. Li, and X. Zhang, "Simulation study on dynamic heat transfer performance of PCM-filled glass window with different thermophysical parameters of phase change material," *Energy Build.*, vol. 106, pp. 87–95, Nov. 2015, doi: 10.1016/J.ENBUILD.2015.05.014.

[94] L. Yang, Y. Liu, Y. Qiao, J. Liu, and M. Wang, "Building Envelope with Phase Change Materials," *Zero Net Zero Energy*, pp. 1–24, 2019, doi: 10.5772/intechopen.85012.

[95] C. Barreneche, A. I. Fernández, M. Niubó, J. M. Chimenos, F. Espiell, M. Segarra, C. Solé, L. F. Cabeza, "Development and characterization of new shape-stabilized phase change material (PCM) - Polymer including electrical arc furnace dust (EAFD), for acoustic and thermal comfort in buildings," *Energy Build.*, vol. 61, pp. 210–214, 2013, doi: 10.1016/j.enbuild.2013.02.026.

[96] M. Teggar and E. H. Mezaache, "STUDY OF HEAT TRANSFER DURING SOLIDIFICATION OF PHASE CHANGE MATERIAL INSIDE CAPSULES," *Proc. CHT-08 ICHMT Int. Symp. Adv. Comput. Heat Transf.*, pp. 1–13, Aug. 2008, doi: 10.1615/ICHMT.2008.CHT.1360.

[97] G. Strang, E. Herman, OpenStax College, Open Textbook Library, and OpenStax (Nonprofit organization), "Calculus. Volume 2."